Institute of Physics
Faculty of Mathematics, Physics and Chemistry
University of Silesia

Jakub Spiechowicz

Ph.D. Thesis

Anomalous transport phenomena in driven periodic systems

Doctoral Supervisor:
Prof. Dr. Jerzy Łuczka

Katowice, 2015

Abstract

This thesis is a mini-review of anomalous transport processes occurring in driven periodic systems. Josephson junctions are used as a convenient example which provides a physical motivation for Brownian motion in a periodic potential and may be employed for experimental corroboration of the presented results. Multiple intriguing phenomena were identified, ratchet effect, negative mobility and anomalous diffusion, to name but a few. In this mini-review the constructive role of Brownian motion is illustrated to show how fluctuations, either thermal or extrinsic, can be used to control degrees of freedom of differing nature. Much emphasis is given to author's own contribution to this field, however, the presented approach is universal and has multifaceted applications in variety of physical systems.

Streszczenie

Praca zawiera przegląd procesów anomalnego transportu zachodzących w czasowo i przestrzennie periodycznych układach fizycznych. Złącza Josephsona są używane jako wygodna motywacja fizyczna ruchu Browna w periodycznym potencjale, która może zostać wykorzystana w celu doświadczalnej weryfikacji otrzymanych rezultatów. Zidentyfikowano wiele intrygujących zjawisk, wśród nich efekt zębatkowy, ujemną mobilność czy anomalną dyfuzję. W pracy zaprezentowano konstruktywny wpływ ruchu Browna ilustrując w jaki sposób fluktuacje pochodzenia termicznego lub nierównowagowego mogą zostać wykorzystane w celu kontroli stopni swobody rozmaitej natury. Nacisk położono na wkład własny autora w ten obszar badawczy, niemniej jednak, użyta metodyka jest uniwersalna i ma wiele zastosowań w różnorodnych układach fizycznych.

This doctoral dissertation has been prepared as a mono-thematic collection of the following scientific papers:

[D1] J. Spiechowicz, J. Łuczka and P. Hänggi, *Absolute negative mobility induced by white Poissonian noise*, J. Stat. Mech., P02044 (2013)

[D2] J. Spiechowicz, P. Hänggi and J. Łuczka, *Brownian motors in the microscale domain: Enhancement of efficiency by noise*, Phys. Rev. E **90**, 032104 (2014)

[D3] J. Spiechowicz and J. Łuczka, *Poissonian noise assisted transport in periodic systems*, in press in Phys. Scr. (2015)

[D4] J. Spiechowicz, P. Hänggi and J. Łuczka, *Josephson junction ratchet: The impact of finite capacitances*, Phys. Rev. B **90**, 054520 (2014)

[D5] J. Spiechowicz and J. Łuczka, *Efficiency of a SQUID Ratchet Driven by External Current*, New. J. Phys. **17**, 023054 (2015)

[D6] J. Spiechowicz and J. Łuczka, *Josephson phase diffusion in the SQUID ratchet*, Chaos **25**, 053110 (2015)

[D7] J. Spiechowicz and J. Łuczka, *Diffusion anomalies in ac-driven Brownian ratchets*, Phys. Rev. E **91**, 062104 (2015)

accompanied by the Guidebook on their contents.

Acknowledgments

This thesis grew out of my PhD studies at the University of Silesia where I had the privilege to work in the group of Jerzy Łuczka. It is a state of the art mini-review of a rapidly developing field. My contribution to this area has been done in close collaboration with Jerzy Łuczka. I would like to thank him for many discussions and his scientific guidance over the last years as well as for critical reading the manuscript. I also want to express my gratitude to Łukasz Machura who served as an assistant advisor in a doctoral degree conferral procedure.

Guidebook

Table of contents

1. Introduction

The importance of periodic systems in physics, chemistry, biology and engineering science has become evident in the last decades. It is mainly due to their ubiquitous presence in Nature. Prominent examples include pendulums [1], super-ionic conductors [2], Josephson junctions [3], dipoles rotating in external fields [4], phase-locked loops [5], dislocations in solid state physics [6], solitons described by the Sine-Gordon equation [7], the Frenkel-Kontorova lattices [8], fluxon motion in superconductors [9], dynamics of adatoms subjected to a time-periodic force [10], charge density waves [11] and cold atoms in optical lattices [12], to name but a few. No less important is their fundamental and practical significance. The latter is especially true from the point of view of their *transport properties* which we will be particularly interested in throughout this thesis.

All the systems mentioned above possess at least one common feature which, because of their diversity, may be difficult to notice at first glance. They are *isomorphic* with Brownian motion in a periodic potential [13]. The Brownian particle description is commonly used as it provides a simple interpretation of the underlying equations - one that is easy to understand and visualize, and which refers to objects described by the intuitive laws of classical mechanics. Therefore in the following thesis we will discuss the analysed systems primarily using this approach.

In such systems, the *transport phenomenon*, that is, a directed movement of a certain physical quantity can be trivially induced by applying a macroscopic gradient, like a force or a temperature difference. However, under many practical circumstances this is not a viable option: (i) currents induced by macroscopic gradients are rarely selective, (ii) a target particle that carries no charge or dipole can hardly be manipulated by means of any perturbation, (iii) external control drastically complicates the design of a small system. For these reasons the optimal solution seems to be a self-propelled system that operates by rectifying environmental signals using its characteristic properties. This is indeed the case in systems possessing *spatial or dynamical symmetry breaking*, where Brownian motion combined with unbiased external input signals, deterministic or random, can assist directed transport of particles at nano scales. Then we speak of *"Brownian motors"*.

Important hallmarks of any genuine Brownian motor are the following [14]: the presence of some amount of (not necessarily thermal) noise and sort of symmetry breaking supplemented by temporal periodicity, typically via an unbiased, non-equilibrium perturbation. There are examples of experimentally accessible physical systems that can be classified as the Brownian motors. An important representative that comes to mind is transport of ions through nanopores [19], cold atoms in optical lattices [12, 20], type II superconducting devices based on the motion of Abrikosov vortices [21, 22], Josephson vortices [23, 24] and the Josephson phase in SQUIDs [25, 26], see also [14] and Refs. therein.

The subtle interplay between non-linearity, noise-assisted escape dynamics and non-equilibrium driving implies that, generally, not even the direction of transport can be

predicted *a priori* in such systems. Moreover it often gives rise to emergence of unusual or even counter-intuitive phenomena, in the sense that they might seem at first glance to contradict our everyday experience. Examples are stochastic resonance [15], ratchet effects [16], negative mobility [17], anomalous diffusion [18], enhancement of diffusion [D6] or efficiency [D2, D5]. Brownian motors despite their apparent simplicity exhibit a plethora of *anomalous transport phenomena*.

Among experimentally accessible physical systems that constitute the above paradigms those built of Josephson junctions are particularly promising. It is due to the fact that they offer some advantages over other setups: (i) precise experimental control of applied driving forces here in the form of external currents, (ii) easy detection of directed motion manifested in a non-zero long-time dc voltage, (iii) access to studies over a wide frequency range of adiabatic and non-adiabatic external perturbations and finally (iv) both under-damped and over-damped dynamics can be investigated by proper junction fabrication and variation of system parameters. Therefore Josephson junctions will be used as a convenient system which provides a physical motivation for the Brownian particle model and can be used to experimentally verify our results.

The goal of this thesis is to give a mini-review of anomalous transport phenomena in driven periodic systems with particular emphasis on the author's own contribution to this field.

1.1. Outline and scope

This thesis is organized as follows. In Section 2 we introduce by means of the Newton-Langevin equation a general model of a driven periodic system which will be of particular importance until the end of this dissertation. We continue looking at this topic in Section 3 where we present conditions that are necessary to observe the directed transport in our system taking into account its symmetry property. There we also detail on the physical realization of the studied model and introduce anomalous phenomena related to the directed transport. In Section 4 we briefly discuss quantities characterizing performance of Brownian motors. The next part is devoted to description of diffusive transport which together with its directed variant and the discussion of energetic issues completes the specification of transport properties of the studied system. Section 6 shows technical details of comprehensive numerical simulations which were indispensable in order to obtain relevant transport characteristics. Finally, in Section 7 the meticulous discussion on anomalous transport phenomena in driven periodic systems is presented. The last part provides concluding remarks.

2. Driven periodic system

Modelling systems and understanding their generic properties discloses components of the setup which are crucial or may be sub-relevant. Here we demonstrate it with a model of a driven periodic system built of the following parts [27]

- A classical inertial particle of mass m
- Moving in a spatially periodic potential $U(x) = U(x + L)$ of period L
- Driven by an *unbiased* time-periodic force $G(t) = G(t + \mathsf{T})$ of period T
- Affected by thermal noise of temperature T

which can be compactly written as the Newton-Langevin equation [28]

$$m\ddot{x} + \gamma\dot{x} = -U'(x) + G(t) + F(t) + \sqrt{2D_T}\,\xi(t). \tag{1}$$

Here, the dot and prime denote differentiation with respect to time t and the Brownian particle's space coordinate x, respectively. The parameter γ characterizes the friction coefficient. Due to the periodicity of the potential $U(x)$ a mean value of the conservative force corresponding to it is zero, namely

$$\langle -U'(x)\rangle = \frac{1}{L}\int_0^L dx\,[-U'(x)] = 0. \tag{2}$$

The driving $G(t)$ is assumed to be *unbiased*, i.e.

$$\langle G(t)\rangle = \frac{1}{\mathsf{T}}\int_0^{\mathsf{T}} dt\,G(t) = 0. \tag{3}$$

Thermal equilibrium fluctuations due to the coupling of the particle with thermostat is modelled by symmetric and unbiased δ-correlated Gaussian white noise $\xi(t)$,

$$\langle \xi(t)\rangle = 0, \quad \langle \xi(t)\xi(s)\rangle = \delta(t-s), \tag{4}$$

where $\langle\cdot\rangle$ indicates an average over its realizations. The noise intensity factor D_T obeys the fluctuation-dissipation theorem [29]

$$D_T = \gamma k_B T \tag{5}$$

with k_B noting the famous Boltzmann constant. We assume that the particle may be additionally exposed to a biased or unbiased force $F(t)$ of either deterministic or stochastic origin. When $F(t) = G(t) = 0$ then the equilibrium character of thermal fluctuations implies the canonical Gibbs state [30].

3. Directed transport

Single particle transport may have either directed or diffusive nature. In the former case the stochastic dynamics in (1) sustains a non-zero long time asymptotic stationary velocity, i.e.

$$\langle v\rangle \neq 0. \tag{6}$$

Due to the presence of the time-periodic force $G(t)$ in the long time limit the Brownian particle's velocity $v = \dot{x}$ is also periodic and can be expressed as the Fourier series [27]

$$\lim_{t\to\infty}\langle \dot{x}(t)\rangle = \langle v\rangle + v_{\mathsf{T}}(t) + v_{2\mathsf{T}}(t) + ... \tag{7}$$

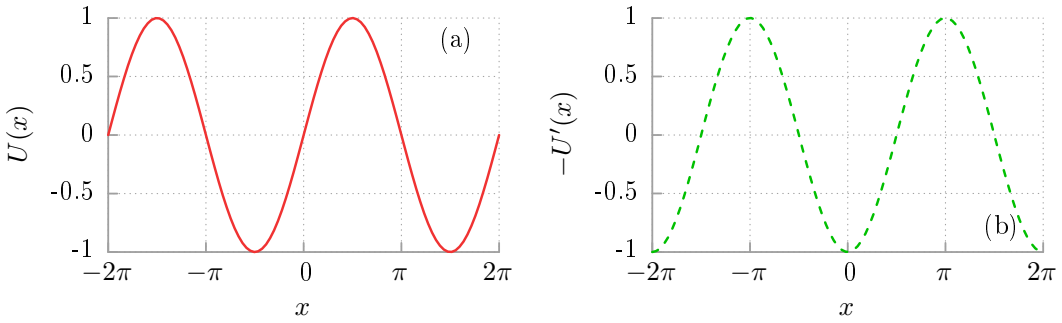

Figure 1: Panel (a): the paradigmatic model of a *symmetric* substrate, namely the periodic potential $U(x)$ (13) with $L = 2\pi$ and $\Delta U = 1$. Panel (b): the conservative potential force $-U'(x)$.

Under these circumstances the relevant time-independent component $\langle v \rangle$ indicating the directed transport may be obtained after an additional temporal averaging

$$\langle v \rangle = \lim_{t\to\infty} \frac{1}{\mathsf{T}} \int_t^{t+\mathsf{T}} ds \, \langle \dot{x}(s) \rangle. \tag{8}$$

It should be clarified that here $\langle \cdot \rangle$ means an average over both realizations of thermal noise as well as initial conditions. The latter is mandatory because for some parameter regimes the system may be non-ergodic and obtained results strongly depend on the choice of initial conditions.

Such transport can be observed in this system only when at least one of the following components is *asymmetric* [12]

- The force $F(t)$
- The potential $U(x)$
- The driving $G(t)$

The last one is *symmetric* if there exists $0 \leq t_0 < \mathsf{T}$ such that

$$G(t_0 + t) = G(t_0 - t). \tag{9}$$

Note that the assumption of the unbiased $G(t)$, namely $\langle G(t) \rangle = 0$ does not solely imply that it is symmetric. A perfect illustration may be a biharmonic driving

$$G(t) = A \left[\cos(\Omega t) + \epsilon \cos(2\Omega t + \phi) \right] \tag{10}$$

which although unbiased is generally asymmetric [12]. In this thesis as the time-periodic force $G(t)$ we pick possibly the simplest *symmetric* form, namely the harmonic driving of amplitude A and angular frequency Ω,

$$G(t) = A \cos(\Omega t). \tag{11}$$

In the next two subsections we separately discuss each of the remaining conditions for the occurrence of the directed transport.

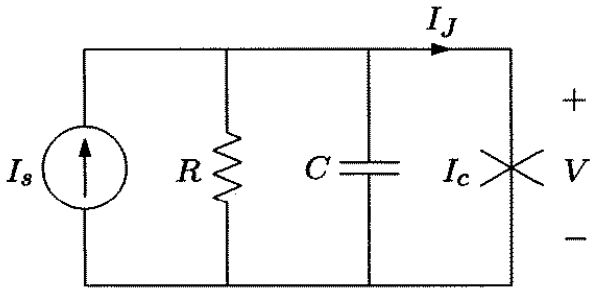

Figure 2: The Stewart-McCumber model of the Josephson junction [34].

3.1. Symmetric substrate

We first consider the case when the periodic substrate described by the potential $U(x)$ is *symmetric* under reflection, to be specific

$$U(x_0 + x) = U(x_0 - x) \tag{12}$$

for certain x_0 with $0 \leq x_0 < L$. An example may be the potential [13], see Fig. 1,

$$U(x) = \Delta U \sin\left(\frac{2\pi}{L}x\right). \tag{13}$$

Under such a choice the only way to obtain the directed transport of the Brownian particle is to drive it by means of the *asymmetric* force $F(t)$ of either deterministic or stochastic origin [31]. If $F(t)$ is periodic in time and fulfils the condition analogous to (9) we call it *symmetric*. When $F(t)$ is a stationary stochastic process then the adjective *symmetric* means that all of its *odd* higher order cumulants vanish completely

$$C_{2n+1}(t_1, ..., t_{2n+1}) = \langle F(t_1)...F(t_{2n+1})\rangle = 0 \tag{14}$$

with $n = 1, 2, ...$ The statistics of the process $F(t)$, as defined by all (not just by $C_1(t) = \langle F(t)\rangle$ and $C_2(t-s) = \langle F(t)F(s)\rangle$) cumulant averages is then clearly symmetric [32]. Examples are the symmetric dichotomous noise [33] or the symmetric white Poissonian noise [D1, D3].

3.1.1. Josephson junction As an example of the symmetric substrate we consider a Josephson junction consisting of two weakly coupled superconducting films. Such coupling can be realized as an oxide barrier thin enough for electrons to tunnel between the electrodes. This prediction is the content of the original Josephson work published in 1962 [3]. It is useful to consider a circuit representation of the Josephson junction. In this model, conduction through the device includes three independent components: a superconducting current due to the tunnelling of Cooper pairs, a normal current due to the tunnelling of quasi-particles and a displacement current associated with the junction capacitance [34], see Fig. 2. Consequently, the current balance equation for the above circuit can be written as

$$I_s = I_c \sin\varphi + \frac{V}{R} + C\frac{dV}{dt} + \sqrt{\frac{2k_BT}{R}}\,\xi(t), \tag{15}$$

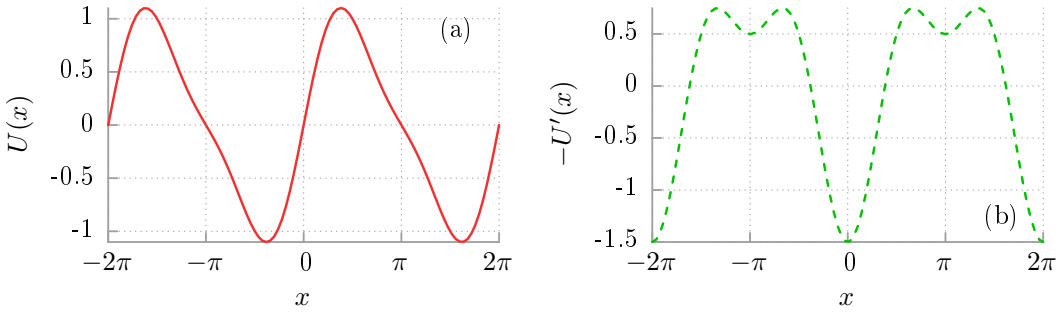

Figure 3: Panel (a): the archetypal model of a *ratchet* substrate, namely the *double-sine potential* (18) with $L = 2\pi$ and $\Delta U = 1$. Panel (b): the conservative potential force $-U'(x)$.

where φ is the difference in phase between the macroscopic wave functions that describe the paired electrons in the two superconducting layers. The term $I_J = I_c \sin\varphi$ characterizes the super-current flowing through the device which maximally takes critical value I_c and the last component in the right hand side is due to the Johnson-Nyquist [35] δ-correlated thermal noise of vanishing mean. Using the Josephson relation $V = (\hbar/2e)\dot{\varphi}$ [3] one obtains the *Stewart-McCumber model* [36, 37]

$$\frac{\hbar}{2e} C\ddot{\varphi} + \frac{\hbar}{2e}\frac{1}{R}\dot{\varphi} = -U'(\varphi) + I_s + \sqrt{\frac{2k_BT}{R}}\,\xi(t) \tag{16}$$

with

$$U(\varphi) = -I_c \cos\varphi. \tag{17}$$

The above equality multiplied by the factor $\hbar/2e$ and provided that the time periodic part can be extracted from the current I_s applied to the device, has exactly the same form as the driven periodic system described by the Newton-Langevin equation (1). In this mechanical analogue, the voltage drop across the junction V becomes the particle velocity $v = \dot{x}$, the current $I_s = I_s(t)$ applied to the device represents the external force $F(t) + G(t)$, the junction capacitance C and the conductance $1/R$ corresponds to the particle mass m and the viscous damping γ, respectively. The Stewart-McCumber model is quite simple and it is important to be aware of the limitations of its applicability. Although adequate for many purposes it neglects both the spatial distribution of the phase φ over the junction and the complex frequency dependence of the tunnelling currents [34].

3.2. Asymmetric substrate

On the contrary, when the Brownian particle moves in the *asymmetric* substrate, i.e. there is no such x_0 that the condition (12) is fulfilled, the directed transport may emerge even when the perturbing force $F(t)$ is *absent* or *symmetric* [38]. The archetypal model

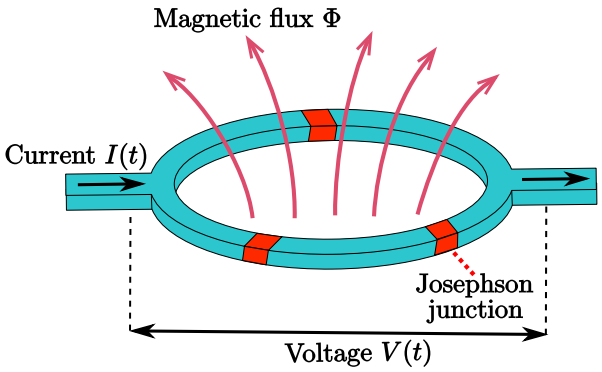

Figure 4: The asymmetric SQUID composed of three Josephson junctions and driven by the external current $I(t)$ [D4]. The external constant magnetic flux is Φ and the instantaneous voltage across the SQUID is $V(t)$.

of the asymmetric structure is the double-sine potential [39], see also Fig. 3,

$$U(x) = \Delta U \left[\sin\left(\frac{2\pi}{L}x\right) + \frac{1}{4}\sin\left(\frac{4\pi}{L}x\right) \right]. \tag{18}$$

However, it should be clarified that there is no directed transport at thermal equilibrium, i.e. when $F(t) = G(t) = 0$, regardless of the symmetry property of the substrate $U(x)$. In particular, then no preferential direction of the stochastic dynamics (1) arises in spite of the broken spatial symmetry of the system. This *a priori* quite counter-intuitive observation is a consequence of the second law of thermodynamics. It was first argued by Smoluchowski [40] and later popularized by Feynman [41].

It no longer holds true when the periodic driving $G(t)$ often termed as the *rocking mechanism* is present and takes the system away from a thermal equilibrium state. In the absence of any such prohibitive obvious reason, and in view of the fact that, after all, the spatial symmetry of the system is broken, the manifestation of a preferential direction for the particle motion appears to be an almost unavoidable educated guess, through a rigorous proof can rarely be given. This very postulate, namely that if *a certain phenomenon is not ruled out by symmetries then it will occur*, is called *Curie's principle* [42]. It is worth to note that the absence of the directed transport at thermal equilibrium regardless of the broken spatial symmetry of the substrate $U(x)$ does not undermine Curie's principle since the necessary condition for the system to be at such a state can also be expressed in the form of a symmetry condition, namely the so called *detailed balance symmetry* [28].

Regarding nomenclature, such a substrate is often termed a *ratchet* [16], whereas generally the dynamics described by (1) is called a *Brownian motor* [43] not only if the potential $U(x)$ is asymmetric but also in the opposite case when additionally the force $F(t)$ is asymmetric. Strictly speaking, due to the presence of the periodic perturbation $G(t)$ which serves as the rocking mechanism which drives the system out of equilibrium these scenarios should be referred to as a *rocking* ratchet or Brownian motor, respectively [39].

3.2.1. SQUID ratchet At sufficiently high temperatures quantum effects such as coherence and tunnelling events can be safely neglected. In this regime the description of the Josephson junction can be well approximated by the Newton-Langevin equation in the framework of the Stewart-McCumber model. Then an artificial Brownian motor can be experimentally realized in a setup of the asymmetric superconducting quantum interference device (SQUID) illustrated in Fig. 4 and originally proposed by Zapata et al. in 1996 [45]. This device maps precisely onto the rocking ratchet concept. The evolution of the effective Josephson phase across this device is governed by the following equation [D4]

$$\frac{\hbar}{2e}C\ddot{\varphi} + \frac{\hbar}{2e}\frac{1}{R}\dot{\varphi} = -U'(\varphi) + I(t) + \sqrt{\frac{2k_BT}{R}}\,\xi(t), \tag{19}$$

with

$$U(\varphi) = -2J_1\cos\left(\frac{\varphi}{2}\right) - J_2\cos\left(\varphi + \tilde{\Phi}_e\right) \tag{20}$$

where J_1 and J_2 are the critical Josephson currents for the junctions in the lower and upper arm, respectively. The dimensionless external magnetic flux is $\tilde{\Phi}_e$ whereas $I(t)$ models the current applied to the device.

3.3. Anomalous transport

The term *anomalous transport* is often used to describe non-equilibrium processes that cannot be explained with the help of standard methods of statistical physics [44]. In the following we introduce these which relate to the directed transport in driven periodic systems.

3.3.1. Ratchet effect We already realized that particles in the asymmetric substrate can drift on average in preferred direction even when all perturbing forces or gradients are absent or symmetric. Breaking of thermal equilibrium and of spatial inversion symmetry of the potential is generally sufficient for occurrence of the so called *ratchet effect* [46, 47], i.e. the emergence of the directed transport in a spatially periodic system that lacks reflection symmetry. For a qualitative analysis it is adequate to consider the case of the absence of any external force $F(t) = 0$ apart from the driving $G(t)$ which takes the system out of thermal equilibrium. Then the occurrence of the ratchet effect is equivalent to a finite velocity, c.f. Fig. 5,

$$\langle v\rangle \neq 0, \quad \text{for } F(t) = 0. \tag{21}$$

This property is the distinguishing feature between the ratchet effect and the somewhat related *absolute negative mobility* effect which we will encounter later in this chapter.

3.3.2. Negative mobility In this section we assume for definiteness that the force $F(t)$ is equivalent to a static constant bias $F(t) = F$. This presumption is not restrictive as it is shown by author of this thesis and his co-workers in [D1, D2].

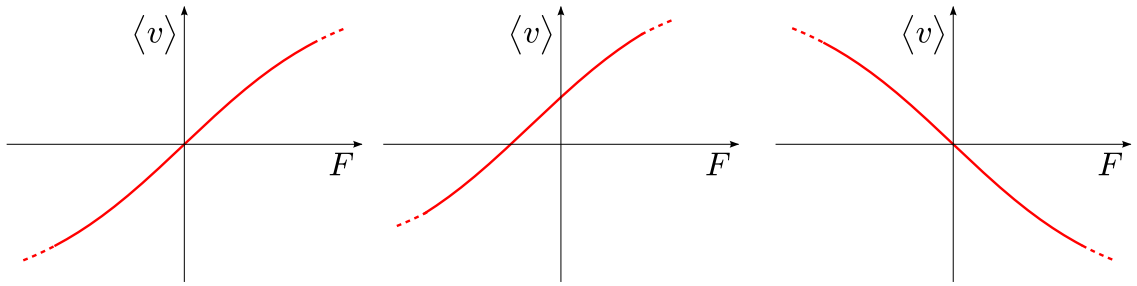

(a) Typical response (b) Ratchet effect (c) Absolute negative mobility

Figure 5: Response of a Brownian particle to a constant load force F.

One of the central results of thermodynamics is due to Le Chatèlier [44] and states that *if a system is at thermal equilibrium its reaction to an applied bias is so that the response is in the same direction of this applied force towards a new equilibrium.* For small values of F one can expect a linear response regime to be present and $\langle v \rangle$ assumes a form

$$\langle v \rangle = \mu F \tag{22}$$

where the coefficient μ is the *mobility* of the particle. In the normal transport regime it is positive $\mu > 0$ meaning that the particle should on average move in the direction pointed to by the load F. If it travels in the opposite way the mobility becomes negative $\mu < 0$. In the neighbourhood of $F = 0$ this counter-intuitive phenomenon is termed *absolute negative mobility* [17, 48].

The negative mobility effect at first glance might appear to violate the Le Chatèlier principle which manifests the laws of thermodynamics. However, the key ingredient for the occurrence of absolute negative mobility is that the system is driven far away from thermal equilibrium into a time-dependent non-equilibrium state and the resulting dynamics is such that it is exhibiting a vanishing, unbiased average response. In the presence of a finite bias F, the absolute negative mobility response in a *symmetric* periodic potential $U(x)$ is such that an average, anti-symmetric transport velocity $\langle v(F) \rangle$, obeying $\langle v(F) \rangle = -\langle v(-F) \rangle$, occurs around the zero load $F = 0$. This situation must be contrasted with the anomalous transport generated by the ratchet mechanism: there, a non-vanishing velocity occurs even for the vanishing bias $F = 0$, and thus no anti-symmetric mobility behaviour takes place around the zero bias regime, c.f. Fig. 5.

4. Performance of Brownian motors

The asymptotic long time stationary velocity $\langle v \rangle$ given by (8) is the most important transport characteristic of the system (1). However, alone it does not provide any information on the quality of the transport process. Is it effective or ineffective? To answer the question about the performance of Brownian motors we need to consider its other attributes. One of them are *fluctuations* of the velocity around its average value

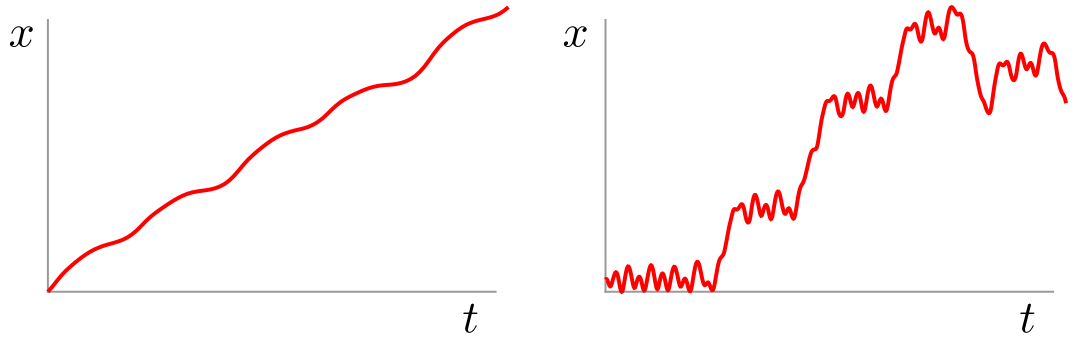

Figure 6: Typical trajectories of an inertial, rocking Brownian motor, both assumes the same average velocity but differing velocity fluctuations.

which in the asymptotic long time stationary regime can be represented as

$$\sigma_v^2 = \langle v^2 \rangle - \langle v \rangle^2. \tag{23}$$

Then, typically the instantaneous velocity $v(t)$ takes values within the interval of standard deviation

$$v(t) \in \left[\langle v \rangle - \sigma_v, \langle v \rangle + \sigma_v \right]. \tag{24}$$

Note that if fluctuations are large, i.e. if $\sigma_v > |\langle v \rangle|$, then it is possible that the particle moves for some time in the direction opposite to its average velocity $\langle v \rangle$, the spread of velocities is large and overall transport is not effective.

The next feature which is important in answering the question about the quality of the transport phenomenon is related to the ratio of energy input into the system and its energetic output. How much of the energy input is converted into the directed motion of the particle and how much of it is wasted by spreading out into the environment and dissipated as heat? A proper quantifier to characterize this aspect of transport is the *efficiency* of the system. A generic definition of the efficiency of a device which converts energy is the ratio between the output and the input energy (power)

$$\varepsilon = \frac{P_{out}}{P_{in}}. \tag{25}$$

Unfortunately, there is no overall consensus on the numerator P_{out} [49, 50, 51, D5]. Depending on a choice of the output power different definitions of the efficiency characterize various aspects of the energy conversion by the Brownian motor. If the particle is working against a constant load $\mathcal{F}$ then in the steady state the efficiency is given as follows

$$\varepsilon_e = \frac{\mathcal{F}\langle v \rangle}{P_{in}}. \tag{26}$$

This definition is not always adequate to determine the optimal performance of the Brownian motor since it assumes that work is being done against a load $\mathcal{F}$ which is clearly not always the case. A load-independent efficiency has been introduced by Wang

and Oster [49] and then analysed in [50, 51]. It was computed using the dissipated power associated with the directed motion of the Brownian motor against the friction force

$$\varepsilon_s = \frac{F_\gamma \langle v \rangle}{P_{in}} = \frac{\gamma \langle v \rangle^2}{P_{in}}. \tag{27}$$

This quantity is called the *Stokes efficiency* [49, D2, D5]. It should be mentioned that the numerator in the above definition is not an average power to overcome the friction force which correct form reads

$$P_\gamma = \langle F_\gamma v \rangle = \gamma \langle v^2 \rangle. \tag{28}$$

However, this expression should not be plugged into the efficiency because there are operating regimes when the mean velocity is extremely small $\langle v \rangle \approx 0$ but at the same time $\langle v^2 \rangle \neq 0$ and the Brownian motor efficiency would be large even though the particle does not move on average in one direction.

In the case of the driven periodic system (1) the input power P_{in} was first calculated by Machura and co-workers in 2004 [51, D5]. It follows from an energy balance of the underlying inertial Newton-Langevin dynamics and reads

$$P_{in} = \gamma(\langle v^2 \rangle - \langle v^2 \rangle_{eq}) = \gamma(\langle v \rangle^2 + \sigma_v^2 - \langle v^2 \rangle_{eq}) \tag{29}$$

where in accordance to the equipartition theorem the relation

$$\left\langle \frac{mv^2}{2} \right\rangle_{eq} = \frac{k_B T}{2} \tag{30}$$

holds true in thermodynamic equilibrium [44]. The Stokes efficiency is consistent with our intuition: a decrease of fluctuations σ_v^2 leads to a smaller input power and hence to an increase of the efficiency. Consequently, the transport is optimized in regimes that *maximize* the directed velocity and *minimize* its fluctuations.

5. Diffusive transport

Apart from quantities characterizing quality of transport processes that relate directly to the asymptotic long time stationary velocity $\langle v \rangle$ like its variance or the Stokes efficiency there are also those connected with the realization of stochastic motion of the Brownian particle's space coordinate x. The most fundamental measure to describe it is the *mean square displacement* [52]

$$\langle \Delta x^2(t) \rangle = \langle [x(t) - \langle x(t) \rangle]^2 \rangle \tag{31}$$

which in many cases is expected to behave in the power law form [18]

$$\langle \Delta x^2(t) \rangle \sim t^\alpha. \tag{32}$$

When the power exponent α is non-zero then the motion is *diffusive*. In contrast to the directed transport the diffusive regime may not necessarily carry a long time asymptotic stationary velocity $\langle v \rangle \neq 0$. Its special case is *coherent* or *dispersionless* regime which occurs when $\alpha = 0$ [53]. It is a rather unique situation since the diffusive transport of

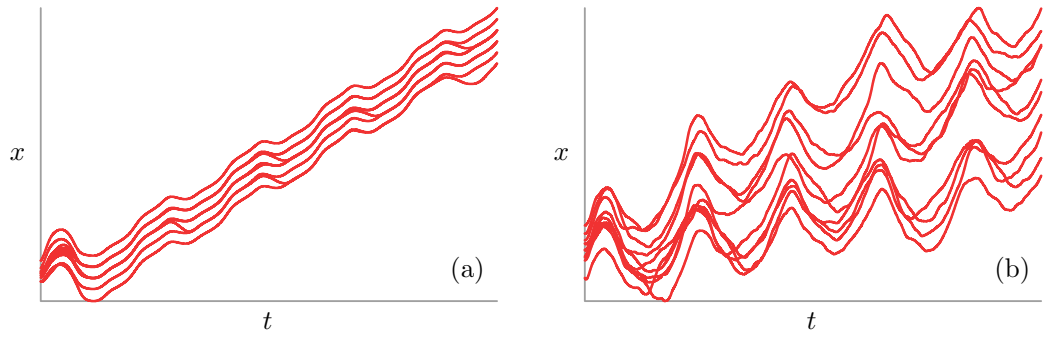

Figure 7: Two sets of illustrative trajectories of an inertial, rocking Brownian motor. A distinct different diffusion behaviour is observed [D6].

particles or generally speaking small objects is a widespread feature of physical systems [54]. For instance, even when the Brownian particle described by (1) drifts with finite directed velocity $\langle v \rangle$, the random switches between locked states of vanishing temporally averaged velocity $\langle v \rangle_{\mathsf{T}} = (1/\mathsf{T}) \int_t^{t+\mathsf{T}} ds\, \dot{x}(s) = 0$ and running ones with $\langle v \rangle_{\mathsf{T}} \neq 0$ cause a spatial dispersion around its mean position [55]. Normal diffusive transport is characterized by the power exponent which is equal to unity $\alpha = 1$. In such a case one can define a time-independent diffusion coefficient [13, 55]

$$D = \lim_{t \to \infty} \frac{\langle \Delta x^2(t) \rangle}{2t}. \tag{33}$$

It measures the spreading of trajectories $x(t)$ around its mean value $\langle x(t) \rangle$. Intuitively, when the dispersion is small then the transport is more optimal, see Fig. 7. The ratio of the diffusion coefficient D and the period L of the substrate $U(x)$ can be considered as a velocity describing the normal diffusion over one period of the potential. Its relation to the asymptotic long time stationary average velocity $\langle v \rangle$ determines the dimensionless Pèclet number [56, D6]

$$Pe = \frac{L|\langle v \rangle|}{D}. \tag{34}$$

A large Pèclet number indicates motion of mainly regular nature. If it is small then random or chaotic contribution dominates the dynamics.

5.1. Anomalous diffusion

More than a century ago Einstein studied motion of non-interacting Brownian particles and derived his famous relation connecting transport and diffusion [52]

$$D = \mu k_B T \tag{35}$$

giving a link between the diffusion coefficient D, a property of unperturbed system, and the mobility μ which quantifies the reaction of system to a small perturbation. Einstein's relation is generally not fulfilled when particles move in a non-linear potential landscape.

Then the subtle interplay between the substrate and equilibrium thermal fluctuations gives rise to a very rich new phenomenology [57].

A remarkable example may be two distinct regimes of *anomalous diffusion* [18]: *sub-diffusion* for $0 < \alpha < 1$ and *super-diffusion* for $\alpha > 1$. Anomalous diffusion may not occur indefinitely into the asymptotic long time stationary regime nevertheless persistence over several time decades has been predicted theoretically and validated experimentally [58, 59]. Therefore even if the ultimate behaviour can be precisely normal, the experimentally relevant evolution may be the anomalous one.

6. GPU accelerated Monte Carlo simulation of Brownian motors

Unfortunately, neither the Newton-Langevin equation (1) describing a driven periodic system nor the corresponding Fokker-Planck variant cannot be solved by use of any known analytical methods. Therefore, in order to obtain the relevant transport characteristics we have to resort to comprehensive numerical simulations of driven random dynamics. We integrated it by employing a weak version of the stochastic second-order predictor-corrector algorithm with a time step typically set to about $10^{-3} \cdot \mathsf{T}$. Since (1) is a second-order differential equation, we have to specify two initial conditions, $x(0)$ and $\dot{x}(0)$. Moreover, because for some regimes of the parameter space the system may be non-ergodic to avoid the dependence of the presented results on the specific selection of initial conditions, we have chosen $x(0)$ and $\dot{x}(0)$ equally distributed over the intervals $[0, L]$ and $[-2, 2]$, respectively. All quantities of interest were ensemble averaged over $10^3 - 10^4$ different trajectories which evolved over $10^3 - 10^6$ periods of the external ac driving.

Numerical calculations were done by use of a CUDA environment implemented on a modern desktop GPU. This scheme allowed for a speed-up of a factor of the order 10^3 times as compared to common present-day CPU method. However, in order to achieve such astonishing performance gain one has to carefully redesign the applied algorithms. With the help of recent review by author of this thesis [60] this task is probably much easier. There all technical details of our comprehensive numerical simulations can be found. The huge leap in speed using the above approach makes it possible to interactively investigate problems that previously required lengthy calculations and to explore much larger areas of the parameter space of various stochastic dynamical systems, in particular, those with spatial and temporal periodicity.

7. Anomalous transport phenomena in driven periodic systems

Despite its simplicity the archetypal model of a driven periodic system presented in (1) exhibits an extremely rich dynamics and variety of *anomalous transport* features like the ratchet effect, the phenomenon of negative mobility as well as the anomalous diffusion. In this section a mini-review of these fascinating processes is presented with particular emphasis on the author's own contribution to this field.

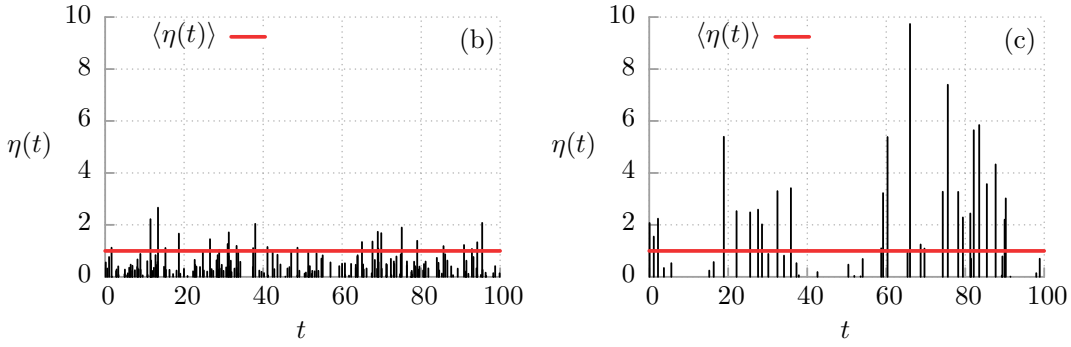

Figure 8: Two illustrative realizations of white Poissonian noise $\eta(t)$ with the amplitudes $\{z_i\}$ of the δ-spikes distributed according to the exponential probability density $\rho(z) = \zeta^{-1}\theta(z)e^{-z/\zeta}$ [D1]. In panel (b): $\lambda = 2$, $D_P = 0.5$, in (c): $\lambda = 0.5$, $D_P = 2$.

7.1. Josephson Brownian motor

The effect of absolute negative mobility, see Fig. 5, was first reported in 2007 by Machura et al. [17] in the system described by the following dimensionless equation (1)

$$\ddot{x} + \gamma\dot{x} = -U'(x) + a\cos(\omega t) + F + \sqrt{2\gamma\mathcal{D}}\,\xi(t) \tag{36}$$

with the *symmetric* periodic potential $U(x) = \sin(2\pi x)$, the harmonic driving $G(t) = a\cos(\omega t)$ and the external perturbation in the form of the constant static bias $F(t) = F$. It is known that this system is minimal for absolute negative mobility to appear [61]. Within a year of initial discovery, the presence of absolute negative mobility was confirmed experimentally in an experiment involving the determination of current-voltage characteristics of the microwave-driven Josephson junction [62]. The original analysis was further extended by the same group who reported the emergence of negative non-linear mobility as well as negative differential mobility [63]. Yet further examples of absolute negative mobility have been described theoretically in the same system but in companionship of coloured noise [64], for over-damped and under-damped non-linear Brownian motion with presence of time-delayed feedback [65, 66], non-uniform space-dependent damping [67] and for vibrational motor [68].

In contrast to the original work by Machura et al. [17] in [D1] we study the transport properties of the same Brownian particle, however, instead of the constant static force $F(t) = F$ it is subjected to a biased non-equilibrium noise $F(t) = \eta(t)$. Such a case is important because it could help to explain and clarify the understanding of unusual transport properties not only in physical but also in biological systems such as, e.g., the bi-directionality of the net cargo movement inside living cells, where there are no a systematic deterministic load but rather random collisions in the form of kicks and impulses. In order to make a comparison with the primary scenario of the deterministic load F, the mean value of the biased non-equilibrium noise is set equal to F; i.e. $\langle\eta(t)\rangle = F$. As a model for such forcing we proposed a random sequence of δ-shaped

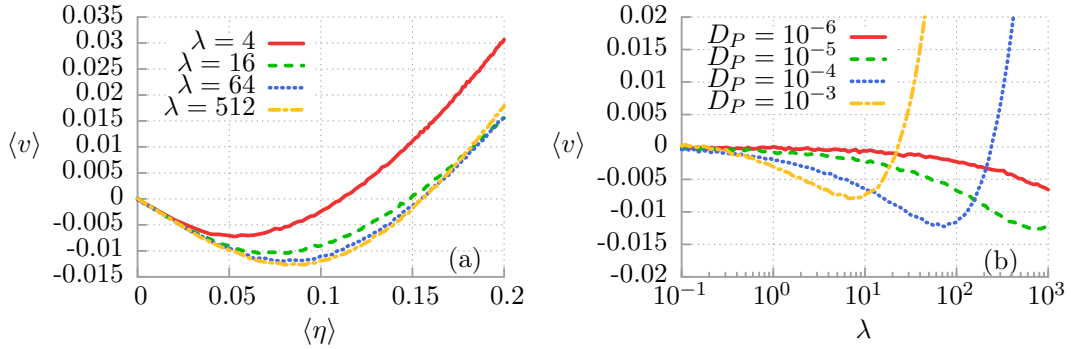

Figure 9: Panel (a): absolute negative mobility, the asymptotic time-averaged velocity $\langle v\rangle$ of the driven inertial Brownian particle as a function of the mean value of the white Poissonian noise $\langle\eta(t)\rangle$ for various spiking frequencies λ. Panel (c): transport control, the same characteristic but depicted versus the spiking rate λ for several values of the white Poissonian noise intensity D_P, for details see [D1].

pulses with stochastic amplitudes defined in terms of generalized *white Poissonian noise*

$$\eta(t) = \sum_{i=1}^{n(t)} z_i \delta(t - t_i), \tag{37}$$

where t_i are the arrival times of a Poissonian counting process $n(t)$ with parameter λ, see Fig. 8. It means that the probability for occurrence of k impulses in the time interval $[0, t]$ is governed by the Poisson distribution

$$\Pr\{n(t) = k\} = \frac{(\lambda t)^k}{k!} e^{-\lambda t}. \tag{38}$$

The amplitudes $\{z_i\}$ of the δ-pulses denote independent random variables distributed according to a common probability density $\rho(z)$. The process $\eta(t)$ presents white noise of finite mean and a covariance given by

$$\langle\eta(t)\rangle = \lambda\langle z_i\rangle, \quad \langle\eta(t)\eta(s)\rangle - \langle\eta(t)\rangle\langle\eta(s)\rangle = 2D_P\delta(t - s), \tag{39}$$

here D_P is the white Poissonian noise intensity which reads

$$D_P = \frac{\lambda\langle z_i^2\rangle}{2}. \tag{40}$$

In particular, in [D1] we demonstrated the possibility of manipulating the direction of transport in the system by adjusting the parameters of the white Poissonian noise λ and D_P, see Fig. 9 (b). The former determines the mean number of δ-pulses per unit time while the latter describes their largeness. Moreover, we have generalized the theoretical concept behind the phenomenon of absolute negative mobility to the case of the biased non-equilibrium noise and showed that such dynamics is able to exhibit this anomaly, cf. Fig. 9 (a). The effect of absolute negative mobility has its roots in a purely stochastic dynamics of the system. In some regions of the multidimensional parameter space, one can find an impact of the white Poissonian noise similar to that of the deterministic bias. However, in general the exact equivalence of these two sources

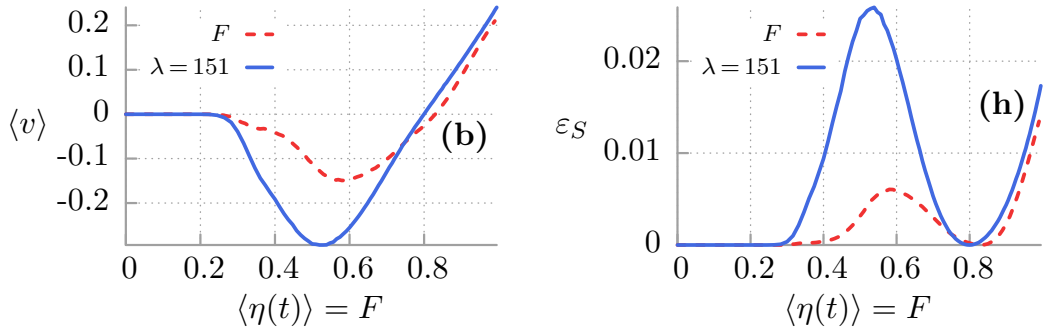

Figure 10: The asymptotic average velocity $\langle v \rangle$ and the Stokes efficiency ε_S as a function of the deterministic constant bias F and the random force $\eta(t)$ in the form of white Poissonian noise of the mean value $\langle \eta(t) \rangle = F$ [D2].

of symmetry-breaking mechanism does not hold true. It is observed only in the *limiting case* of a spiking rate $\lambda \to \infty$ and with the fixed mean value $\langle \eta(t) \rangle = F$. Moreover, the results presented in [D1] are robust with respect to the distribution of the random amplitudes of δ-pulses.

The above findings were confirmed and greatly extended in our subsequent paper [D2]. We showed that within selected parameter regimes, noise $\eta(t)$ of the mean value $\langle \eta(t) \rangle = F$ and exponentially distributed amplitudes $\{z_i\}$ of the δ-pulses can be significantly more effective than the deterministic force F: the Brownian motor can move *much faster*, its velocity fluctuations are *much smaller* and the motor Stokes efficiency increases *several times*. These features hold true in both normal and absolute negative mobility regimes, see Fig. 10. Specific results are detailed for generalized white Poissonian noise. The main conclusion remain valid, however, as well for other models of random perturbations. Thus the idea that stochastic biased forces can be beneficial over deterministic load carries potential for practical realization in physics of Brownian motors. Exploiting the analogy between the Brownian particle and the Josephson junction, it can be validated by use of a setup consisting of this device operating in experimentally accessible regimes. We provide an exemplary set of physical parameters in the absolute negative mobility regime: for operational temperature $T = 4\text{K}$, the critical Josephson current $I_c \approx 170\mu\text{A}$. For a realistic capacitance $C = 20\text{pF}$, the plasma frequency $\omega_p \approx 160\text{GHz}$. The amplitude of the ac current is $I_a \approx 240\mu\text{A}$, the ac-angular frequency is $\Omega \approx 96\text{GHz}$ and the dc current or the mean value of the Poisson noise is $I_d \approx 15.5\mu\text{A}$. Under these conditions, the negative-valued absolute negative mobility voltage is $V \approx -15.7\mu\text{V}$ for the Poissonian noise case and $V \approx -7.9\mu\text{V}$ for the deterministic force. The proposed mechanism of a "reduction of noise by noise" may explain exotic transport phenomena not only in physical but also in biological settings and, additionally, can be implemented in enhancing the working efficiency of synthetic molecular motors, all of which *in situ* operate in strongly fluctuating environments.

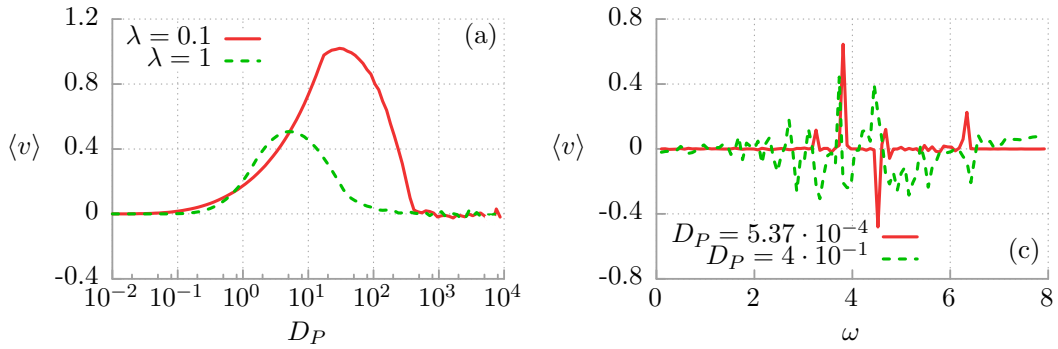

Figure 11: Panel (a): the asymptotic long time average velocity $\langle v \rangle$ as a function of the white Poissonian noise intensity D_P in the absence of the harmonic driving. Panel (b): the same transport characteristic $\langle v \rangle$ but depicted versus the frequency ω of the harmonic driving, for details see [D3].

Finally, in [D3] we revisited the problem of transport of a harmonically driven inertial particle moving in a *symmetric* periodic potential, but subjected to *unbiased* generalized white Poissonian noise $\Gamma(t) = \eta(t) - \langle \eta(t) \rangle$ and coupled to thermal bath. Such noise is characterized by *temporal asymmetry*, i.e. sharp δ-pulses of zero duration followed by a constant negative bias which lasts over an exponentially distributed waiting time. In [31] it has been demonstrated that the white noise nature of such additive, temporally asymmetric fluctuations is sufficient to induce directed transport in periodic structures, in the presence and in the absence of an internal asymmetry. We independently confirmed this result but for the case of the inertial Brownian particle. Moreover, under presence of external harmonic driving this system exhibits a phenomenon of *multiple velocity reversals* [69], see Fig. 11. Consequently, it is possible to manipulate the direction of transport by tuning of the parameters of the driving and the white Poissonian noise.

7.2. SQUID rocking ratchet

Zapata et al. in their inspiring work [45] argued that the phase across the asymmetric SQUID threaded by the magnetic flux, see Fig. 4, can experience the effective ratchet potential. They showed that under the external ac current, the rocking ratchet mechanism operates whereby one sign of the time derivative of the phase is favoured. A few years later, these results have been experimentally validated by the Tübingen group [25, 26]. However, in the first attempt the over-damped regime, where capacitative effects can be ignored, was considered. In contrast to over-damped Brownian motors, rocking ratchets with massive particles exhibit strong inertial effects and are capable of reversing their rectified velocity. Moreover, in the noiseless case they are naturally undergoing chaotic dynamics with consequences of extremal sensitivity to the initial conditions [69, 70]. Nevertheless, an appropriate amount of noise stabilize their rectification properties and makes them a promising device with potential applications

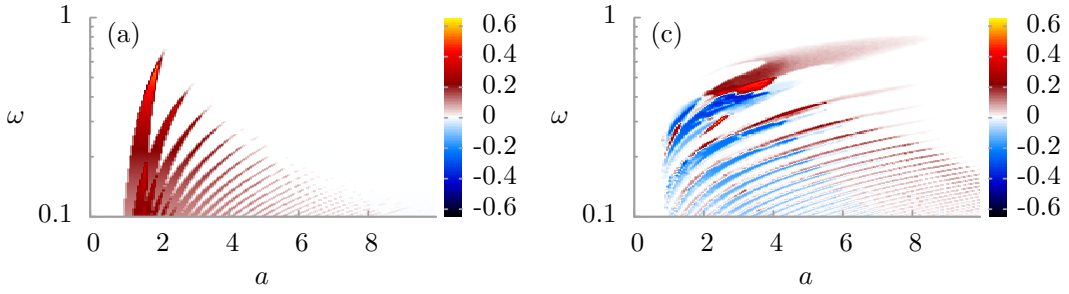

Figure 12: The deterministic transport behaviour of the capacitive SQUID ratchet as a function of ac driving amplitude a and its angular frequency ω with distinct regimes: (a) over-damped and (c) under-damped. The average voltage drop $\langle v \rangle$ is presented [D4].

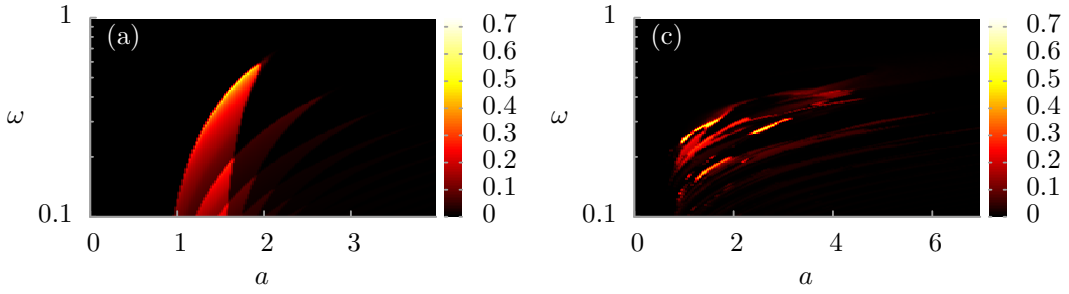

Figure 13: The Stokes efficiency ε_s in the parameter plane $\{a, \omega\}$ of the ac current for two distinct regimes: (a) over-damped and (c) under-damped [D5].

in science and technology.

After nearly 20 years we revisited the problem of the SQUID ratchet [D4] to reveal many overlooked intriguing features including *negative conductance* [63], *multiple voltage reversals* [69], *thermal noise-induced voltage reversals* and solely *thermal noise-induced ratchet voltage*. In doing so, we extended and generalized an earlier study by Zapata et al. [45] and analyse directed transport in wide parameter regimes: covering the over-damped to the moderate damping up to its fully under-damped regime, see Fig. 12. This extension is non-trivial since in this case the system allows for classical chaos. Then the effective Josephson phase undergoes the dimensionless dynamics given by the following equation [D4]

$$C\ddot{x}(t) + \dot{x}(t) = -U'(x) + F + a\cos(\omega t) + \sqrt{2\mathcal{D}}\,\xi(t) \tag{41}$$

with the spatially periodic potential $U(x)$ of the ratchet form

$$U(x) = -\sin(x) - \frac{j}{2}\sin(2x + \tilde{\Phi}_e - \pi/2). \tag{42}$$

As a consequence, the resulting ratchet dynamics becomes rather rich, giving rise to features which are absent in the over-damped limit. We have been able to detect the

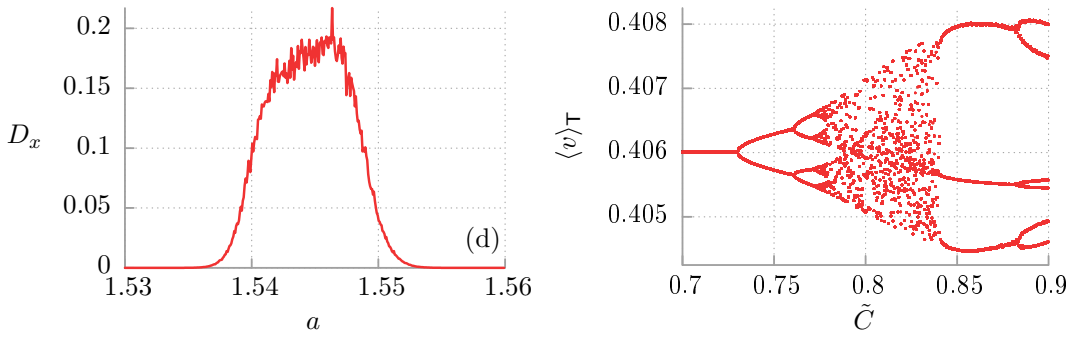

Figure 14: Impact of the ac current amplitude a on the diffusion coefficient D_x and the dc voltage $\langle v \rangle_{\mathsf{T}}$ bifurcation diagram in the deterministic limit as a function of the capacitance $\tilde{C}$ of the SQUID. Other parameters correspond to the regime for which the rectification efficiency takes its globally maximal value [D6].

set of parameters for which ratchet effect is *globally maximal* and demonstrated how the direction of transport can be manipulated by tailoring the threading external magnetic flux.

In the next paper [D5] we studied the quality of transport processes occurring in the inertial SQUID ratchet. We focused on the connection between the directed transport characterized by the dc voltage drop across the SQUID and its efficiency, see Fig. 13. In particular, we examined voltage fluctuations and energetic performance of the device. We derived the expression for the power delivered by externally applied current. Surprisingly it depends not only on the current parameters itself but also on properties and parameters of the device like its temperature, the resistance or the capacitance. It turned out that the device operates best in the over-damped or close to damped regimes. We have been able to identify the tailored set of parameters for which the Stokes efficiency is *globally maximal*. Thermal fluctuations usually have destructive impact on the energetic performance of the device, however, we demonstrated the regime for which *thermal noise enhances the efficiency* by inducing the large average voltage and minimizing its variance. Finally, we showed how the effectiveness of the device can be tuned by tailoring the external magnetic flux.

Apart from quantities characterizing quality of transport processes that relate directly to the asymptotic long time stationary average voltage drop like its variance or the Stokes efficiency of the SQUID there are also those connected with the realization of stochastic motion of the Josephson phase like its mean square displacement and the diffusion coefficient. Surprisingly, despite the great overall interest which Brownian motors have attracted since the early 90s, this subject has not been intensively analysed. There are only several papers loosely related to this problem [71, 72, 73, 74, 75]. However, they are all focused on *symmetric* periodic structures. Very recently, we addressed a relation between the phase diffusion and the quality of transport characterized by the dc voltage drop across the SQUID ratchet and the efficiency of

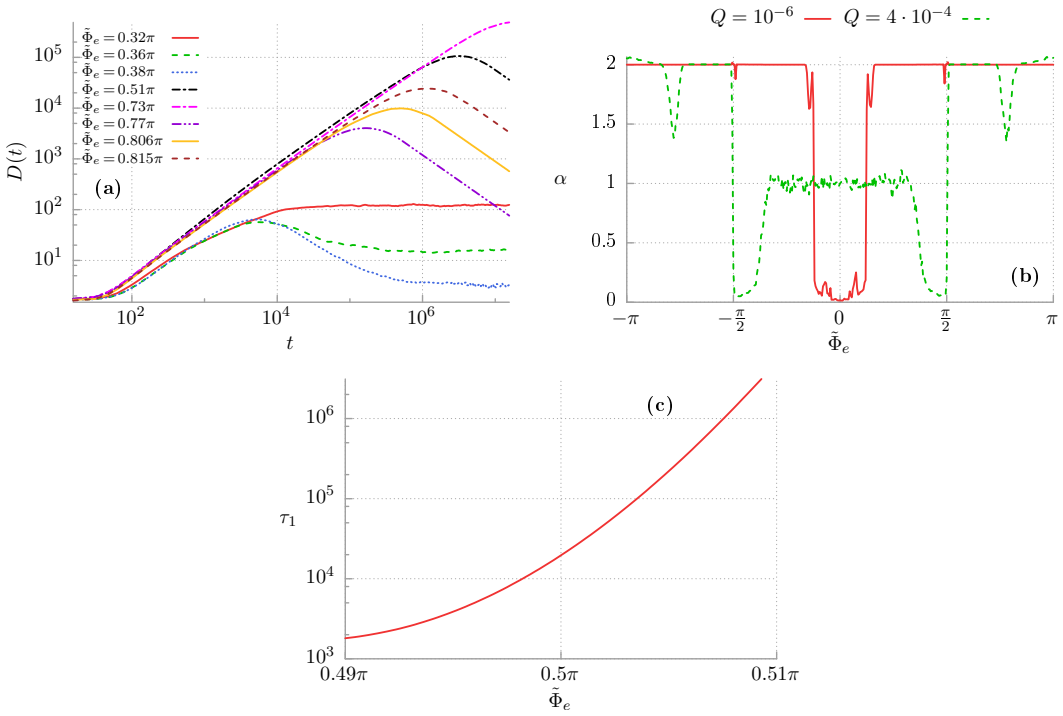

Figure 15: Control of diffusion by the external magnetic flux $\tilde{\Phi}_e$. Panel (a): the diffusion coefficient $D(t)$ for selected values of the flux $\tilde{\Phi}_e$. Panel (b): the power exponent α in dependence of the same quantity. Panel (c): The crossover time τ_1 of super-diffusive motion as a function of $\tilde{\Phi}_e$, for details see [D7].

this device [D6]. In doing so, we concentrated on the previously reported regime [D5] for which efficiency of the SQUID attains a global maximum. For asymptotic long times, the mean square displacement of the Josephson phase is a linear function of time, meaning that diffusion is normal. Nevertheless, its coefficient is small indicating rather regular phase evolution. It can be magnified several times by tailoring experimentally accessible parameters like amplitudes of the ac current or external magnetic flux leading to the phenomenon of *diffusion enhancement* [55, 76], see Fig. 14 (d). We also showed that in the deterministic limit of vanishing thermal noise this regime is essentially *non-chaotic* and possesses an unexpected simplicity of attractors. However, there are also regions where due to the coexistence of several disjoint attractors the *deterministic diffusion* can be observed [72, 73, 74], c.f. the right panel of Fig. 14.

An interesting question concerns a possibility of emergence of the anomalous phase diffusion in this setup. We answered this in the positive [D7]. In this work we investigated diffusion processes in the archetypal model of an inertial Brownian ratchet. As a particular realization we picked the asymmetric SQUID device driven by the time-periodic current and pierced by the external constant magnetic flux. Within selected parameter regimes the Josephson phase evolves in three distinct regimes: initially as *super-diffusion*, next as *sub-diffusion* and finally as normal diffusion in the asymptotic long-time limit, c.f. Fig. 15 (a). The crossover times separating these stages *can*

be controlled by temperature and an external magnetic flux. The first two anomalous periods can last many orders longer than characteristic time scales of the system, thus being comfortably detectable experimentally, see Fig. 15 (c). Most notably, the origin of abnormal behaviour is clearly related to the ratchet form of the potential revealing an *entirely new mechanism of emergence of anomalous diffusion.* This effect is particularly evident for low temperature regimes, see Fig. 15 (b) and should be clearly contrasted with the one that operates in disordered systems [77, 78]. In the opposite limiting scenario of high thermal noise intensity new manifest of the fascinating interplay between non-linearity and thermal fluctuations was detected, namely the phenomenon of *noise suppressed diffusion.*

Due to good experimental control of the SQUID ratchet as well as easy detection of the discussed diffusion behaviour in the power spectrum of the voltage fluctuations it is one of the most promising setup for verification of these findings and can provide a completely new *testing ground* for investigating anomalies in diffusion phenomena.

8. Concluding remarks

With this thesis we have taken a tour through the many intriguing and often counter-intuitive *anomalous transport phenomena* occurring in driven periodic systems. Due to the universality of presented approach our results have multifaceted applications in the most diverse areas of physics outlined in the introduction.

In particular, in the previous sections we demonstrated the existence of different kinds of anomalous transport processes in a Josephson Brownian motor as well as in a SQUID rocking ratchet. These include ratchet effect, multiple velocity reversals, absolute negative mobility, non-equilibrium noise induced transport, non-equilibrium noise enhanced efficiency, diffusion amplification, deterministic diffusion, anomalous diffusion and numerous thermal noise induced phenomena like velocity reversals, ratchet effect, efficiency enhancement and suppression of diffusion. In the author's opinion the most important results are

- Demonstration that stochastic forcing can be significantly more effective than the deterministic load of equal mean value, in both normal and negative mobility regime [D2]
- Discovery of diffusion anomalies in driven Brownian ratchets together with the detection of an entirely new mechanism of emergence of anomalous diffusion which is based on breaking of the reflection symmetry of the potential [D7]

The former may provide a new operating principle in which micro- and nanomotors could be powered by biased noise while the latter sheds an essentially new light on the role of symmetry breaking in diffusion anomalies.

It seems that anomalous transport phenomena, while quite surprising at first glance are actually fairly common and robust, given the multiple areas of the parameter spaces where we were able to detect their presence. Regardless of their practical applications,

they are quite interesting in their own right, as they increase our understanding of dynamical systems and challenge commonly held intuitions. It is very possible that further intriguing transport effects remain to be discovered even in simple one-dimensional classical systems, since it seems our knowledge is never as complete as we think it to be.

Above all, the main conclusion to be drawn from this thesis is as follows: rather than fighting (not necessarily thermal) noise we should put it to work to our advantage. Periodic systems, combined with spatiotemporal symmetry breaking and non-linearity serve as a blueprint for this purpose, using this ceaseless noise source to direct and steer degrees of freedom of differing nature reliably and effectively.

References

[1] M. Gitterman, *The Chaotic Pendulum (World Scientific, 2010)*

[2] P. Fulde, L. Pietronero, W. Schneider, and S. Strässler, *Problem of Brownian Motion in a Periodic Potential*, Phys. Rev. Lett. **35**, 1776 (1975)

[3] B. Josephson, *Possible new effects in superconductive tunnelling*, Phys. Lett. **1**, 251 (1962)

[4] W. Coffey, Y. Kalmykov and J. Waldron, *The Langevin Equation* (World Scientific, 2012)

[5] A. Viterbi, *Principles of Coherent Communication* (McGraw-Hill, 1966)

[6] A. Seeger, in *Continuum Models of Discrete Systems* (ed. E. Kröner and K. Anthony, University of Waterloo Press, 1980)

[7] G. Lamb, *Elements of Soliton Theory* (Wiley, 1980)

[8] O. Braun and Y. Kivshar, *Nonlinear dynamics of the Frenkel-Kontorova model*, Phys. Rep. **306**, 1 (1998)

[9] B. Shapiro, M. Gitterman, I. Dayan and G. Weiss, *Exact calculation of Shapiro step sizes for pulse-driven Josephson junctions*, Phys. Rev. B **46**, 8349 (1992)

[10] R. Guantes, J. Vega and S. Miret-Artés, *Chaos and anomalous diffusion of adatoms on solid surfaces*, Phys. Rev. B **64**, 245415 (2001)

[11] G. Grüner, A. Zawadowski and P. Chaikin, *Nonlinear Conductivity and Noise due to Charge-Density-Wave Depinning in $NbSe_3$*, Phys. Rev. Lett. **46**, 511 (1981)

[12] S. Denisov, S. Flach and P. Hänggi, *Tunable transport with broken space-time symmetries*, Phys. Rep. **538**, 77 (2014)

[13] H. Risken, *The Fokker-Planck Equation* (Springer, Berlin, 1984)

[14] P. Hänggi and F. Marchesoni, *Artificial Brownian motors: Controlling transport on the nanoscale*, Rev. Mod. Phys. **81**, 387 (2009)

[15] L. Gammaitoni, P. Hänggi, P. Jung, and F. Marchesoni, *Stochastic Resonance*, Rev. Mod. Phys. **70**, 223 (1998)

[16] P. Reimann, *Brownian motors: noisy transport far from equilibrium*, Phys. Rep. **361**, 57 (2002)

[17] Ł. Machura, M. Kostur, P. Talkner, J. Łuczka and P. Hänggi, *Absolute negative mobility induced by thermal equilibrium fluctuation*s, Phys. Rev. Lett. **98**, 40601 (2007)

[18] R. Metzler and J. Klafter, *The random walk's guide to anomalous diffusion: a fractional dynamics approach*, Phys. Rep. **339**, 1 (2000)

[19] R. Karnik, C. Duan, K. Castelino, H. Dalguji and A. Majumdar, *Rectification of ionic current in a nanofluidic diode*, Nano Lett. **7**, 547 (2007)

[20] R. Gommers, S. Bergamini and F. Renzoni, *Dissipation-induced symmetry breaking in a driven optical lattice*, Phys. Rev. Lett. **95**, 073003 (2005)

[21] C. S. Lee, B. Jankó, I. Derényi and A. L. Barabási, *Reducing vortex density in superconductors using the 'ratchet effect'*, Nature **400**, 337 (1999)

[22] J. E. Villegas, S. Savel'ev, F. Nori, E. M. Gonzalez, J. V. Anguita, R. Arcia and J. L. Vincent, *A superconducting reversible rectifier that controls the motion of magnetic flux quanta*, Science **302**, 1188 (2003)

[23] A. V. Ustinov, C. Coqul, A. Kemp, Y. Zolotaryuk and M. Salerno, *Ratchetlike dynamics of fluxons in annular Josephson junctions driven by biharmonic microwave fields*, Phys. Rev. Lett. **93**, 087001 (2004)

[24] M. Beck, E. Goldobin, M. Neuhaus, M. Siegel, R. Kleiner and D. Koelle, *High-efficiency deterministic Josephson vortex ratchet*, Phys. Rev. Lett. **95**, 090603 (2005)

[25] S. Weiss, D. Koelle, J. Müller, R. Gross and K. Barthel, *Ratchet effect in dc SQUIDs*, Europhys. Lett. **51**, 499 (2000)

[26] A. Sterck, R. Kleiner and D. Koelle, *Three-junction SQUID rocking ratchet*, Phys. Rev. Lett. **95**, 177006 (2005)

[27] P. Jung, *Periodically driven stochastic systems*, Phys. Rep. **234**, 175 (1993)

[28] P. Hänggi and H. Thomas, *Stochastic Processes: Time-Evolution, Symmetries and Linear*

Response, Phys. Rep. **88**, 207 (1982)
[29] U. Marconi, A. Puglisi, L. Rondoni and A. Vulpiani, *Fluctuation-dissipation: Response theory in statistical physics*, Phys. Rep. **461**, 111 (2008).
[30] A. Khinchin, *Mathematical Foundations of Statistical Mechanics* (Dover, 1949)
[31] J. Łuczka, R. Bartussek, P. Hänggi, *White-Noise-Induced Transport in Periodic Structure*, Europhys. Lett. **31**, 431 (1995)
[32] P. Hänggi, R. Bartussek, P. Talkner and J. Łuczka, *Noise-Induced Transport in Symmetric Periodic Potentials: White Shot Noise versus Deterministic Noise*, Europhys. Lett. **35**, 315 (1996)
[33] J. Kula, T. Czernik and J. Łuczka, *Transport Generated by Dichotomous Fluctuations*, Phys. Lett. A **214**, 14 (1996)
[34] R. Kautz, *Noise, chaos, and the Josephson voltage standard*, Rep. Prog. Phys. **59**, 935 (1996)
[35] H. Nyquist, *Thermal agitation of electric charge in conductors*, Phys. Rev. **32**, 110 (1928)
[36] W. Stewart, *Current-voltage characteristics of Josephson junctions*, Appl. Phys. Lett. **12**, 277 (1968)
[37] D. McCumber, *Effect of ac Impedance on dc Voltage-Current Characteristics of Superconductor Weak-Link Junctions*, J. Appl. Phys. **39**, 3113 (1968)
[38] J. Łuczka, T. Czernik and P. Hänggi, *Symmetric White Noise Can Induce Directed Current in Ratchets*, Phys. Rev. E **56**, 3968 (1997)
[39] R. Bartussek, P. Hänggi, and J. G. Kissner, *Periodically Rocked Thermal Ratchets*, Europhys. Lett. **28**, 459 (1994)
[40] M. von Smoluchowski, *Experimentell nachweisbare, der üblichen Thermodynamik widersprechende Molekularphänomene*, Physik. Zeitschr. **13** 1069 (1912)
[41] R. P. Feynman, R. B. Leighton, M. Sands, *The Feynman Lectures on Physics, Vol. I* (Addison Wesley, 1963)
[42] P. Curie, *Sur la symétrie dans les phénomenes physiques, symétrie d'un champ électrique et d'un champ magnétique*, J. Phys. (Paris) 3 Série (théorique et appliqué) **III**, 393 (1894)
[43] R. Bartussek and P. Hänggi, *Brownsche Motoren: Wie aus Brownscher Bewegung makroskopischer Transport wird*, Phys. Bl. **51**, 506 (1995)
[44] L. D. Landau, E. M. Lifshitz, *Statistical Physics, Part 1 (Course of Theoretical Physics, Volume 5)* (Butterworth-Heinemann, 1980)
[45] I. Zapata, R. Bartussek, F. Sols and P. Hänggi, *Voltage rectification by a SQUID ratchet*, Phys. Rev. Lett. **77**, 2292 (1996)
[46] A. Ajdari, J. Prost, *Mouvement induit par un potentiel periodique de basse symmetrie: dielectrophorese pulsee*, C. R. Acad. Sci. Paris **315**, Série II, 1635 (1992)
[47] M. Magnasco, *Forced thermal ratchets*, Phys. Rev. Lett. **71**, 1477 (1993)
[48] D. Speer, R. Eichhorn and P. Reimann, *Brownian motion: Anomalous response due to noisy chaos*, Europhys. Lett. **79**, 10005 (2007)
[49] H. Wang and G. Oster, *The Stokes efficiency for molecular motors and its applications*, Europhys. Lett. **57**, 134 (2002)
[50] D. Suzuki and T. Munakata, *Rectification efficiency of a Brownian motor*, Phys. Rev. E **68**, 021906 (2003)
[51] Ł. Machura, M. Kostur, P. Talkner, J. Łuczka, F. Marchesoni and P. Hänggi, *Brownian motors: current fluctuations and rectification efficiency*, Phys. Rev. E **70**, 061105 (2004)
[52] A. Einstein, in *Investigations on the theory of the Brownian movements*, (ed. R. Fürth, Dover, New York, 1956)
[53] K. Lindenberg, J. M. Sancho, A. M. Lacasta and I. M. Sokolov, *Dispersionless Transport in a Washboard Potential*, Phys. Rev. Lett. **98**, 020602 (2007)
[54] P. S. Burada, P. Hänggi, F. Marchesoni, G. Schmid and P. Talkner, *Diffusion in confined geometries*, ChemPhysChem **10**, 45 (2009)
[55] G. Costantini and F. Marchesoni, *Threshold diffusion in a tilted washboard potential*, Europhys.

Lett. **48**, 491 (1999)

[56] Ł. Machura, M. Kostur, F. Marchesoni, P. Talkner, P. Hänggi and J. Łuczka, *Optimal strategy for controlling transport in inertial Brownian motors*, J. Phys.: Condens. Matter **17**, S3741 (2005)

[57] J. Sancho, A. Lacasta, *The rich phenomenology of Brownian particles in nonlinear potential landscapes*, Eur. Phys. J. ST **187**, 49 (2010)

[58] I. Bronstein, Y. Israel, E. Kepten, S. Mal, Y. Shav-Tai, E. Barkai and Y. Garini, *Transient Anomalous Diffusion of Telomeres in the Nucleus of Mammalian Cells*, Phys. Rev. Lett. **103**, 018102 (2009)

[59] R. D. L. Hanes, M. Schmiedeberg and S. U. Egelhaaf, *Brownian particles on rough substrates: Relation between intermediate subdiffusion and asymptotic long-time diffusion*, Phys. Rev. E **88**, 062133 (2013)

[60] J. Spiechowicz, M. Kostur and Ł. Machura, *GPU accelerated Monte Carlo simulation of Brownian motors dynamics with CUDA*, Comput. Phys. Commun. **191**, 140 (2015)

[61] D. Speer, R. Eichhorn and P. Reimann, *Transient chaos induces anomalous transport properties of an underdamped Brownian particle* , Phys. Rev. E **76**, 051110 (2007)

[62] J. Nagel, D. Speer, T. Gaber, A. Sterck, R. Eichhorn, P. Reimann, K. Ilin, M. Siegel, D. Koelle, and R. Kleiner, *Observation of Negative Absolute Resistance in a Josephson Junction*, Phys. Rev. Lett. **100**, 217001 (2008)

[63] M. Kostur, Ł. Machura, P. Talkner, P. Hänggi and J. Łuczka, *Anomalous transport in biased ac-driven Josephson junctions: Negative conductances*, Phys. Rev. B **77**, 104509 (2008)

[64] M. Kostur, J. Łuczka, and P. Hänggi, *Negative Mobility induced by Colored Thermal Fluctuations*, Phys. Rev. E **80**, 051121 (2009)

[65] D. Hennig, *Current control in a tilted washboard potential via time-delayed feedback*, Phys. Rev. E **79**, 041114 (2009)

[66] L. Du and D. Mei, *Time delay control of absolute negative mobility and multiple current reversals in an inertial Brownian motor*, J. Stat. Mech., P11016 (2011)

[67] C. Mulhern, *Persistence of uphill anomalous transport in inhomogeneous media*, Phys. Rev. E **88**, 022906 (2013)

[68] L. Du and D. Mei, *Absolute negative mobility in a vibrational motor*, Phys. Rev. E **85**, 011148 (2012)

[69] P. Jung, J. Kissner and P. Hänggi, *Regular and chaotic transport in asymmetric periodic potentials: Inertia ratchets*, Phys. Rev. Lett. **76**, 3436 (1996)

[70] J. Mateos, *Chaotic Transport and Current Reversal in Deterministic Ratchets*, Phys. Rev. Lett. **84**, 258 (2000)

[71] H. Gang, A. Daffertshofer and H. Haken, *Diffusion of Periodically Forced Brownian Particles Moving in Space-Periodic Potentials*, Phys. Rev. Lett. **76**, 4874 (1996)

[72] J. Blackburn and N. Gronbech-Jensen, *Phase diffusion in a chaotic pendulum*, Phys. Rev. E **53**, 3068 (1996)

[73] R. Harish, S. Rajasekar and K. Murphy, *Diffusion in a periodically driven damped and undamped pendulum*, Phys. Rev. E **65**, 046214 (2002)

[74] K. Tanimoto, K. Kato and K. Nakamura, *Phase dynamics in SQUID's: Anomalous diffusion and irregular energy dependence of diffusion coefficients*, Phys. Rev. B **66**, 012507 (2002)

[75] W. Guo, L. Du and D. Mei, *Anomalous diffusion and enhancement of diffusion in a vibrational motor*, J. Stat. Mech., P04025 (2014)

[76] P. Reimann, Ch. van der Broeck, H. Linke, P. Hänggi, J. Rubi and A. Pérez-Madrid, *Giant Acceleration of Free Diffusion by Use of Tilted Periodic Potentials*, Phys. Rev. Lett. **87**, 010602 (2001)

[77] R. D. L. Hanes and S. U. Egelhaaf, *Dynamics of individual collodidal particles in one-dimensional random potentials: a simulation study*, J. Phys.: Condens. Matter **24**, 464116 (2012)

[78] M. S. Simon, J. M. Sancho and K. Lindenberg, *Transport and diffusion of underdamped Brownian particles in random potentials*, Eur. Phys. J. B **87**, 201 (2014)

Jakub Spiechowicz

Personal info

Date of birth	16 July 1990
Place of birth	Chrzanów, Poland
Nationality	Polish
Status	Single

Education

2013-2015	Ph.D., Physics, University of Silesia, Katowice, Poland
2012-2013	M.Sc., Theoretical Physics, University of Silesia, Katowice, Poland, summa cum laude
2009-2012	B.Sc., General Physics, University of Silesia, Katowice, Poland, summa cum laude
2006-2009	3rd High School, Jaworzno, Poland

Achievements

2013-2015	European Social Fund Human Capital Programme Ph.D. Scholarship FORSZT
2013	Laureate of the Ministry of Science and Higher Education program "Diamond Grant"
2011-2013	Scholarship of the Ministry of Science and Higher Education
2010-2013	Scholarship of the Rector of the University of Silesia
2010	Scholarship of the Association of Entrepreneurs of city Jaworzno
2008-2009	Scholarship of the Prime Minister of Poland
2008	Scholarship of the Association of Entrepreneurs of city Jaworzno

Skills

- Languages: Polish (native), English (fluent, certificated)
- Programming languages: bash, AWK, Fortran, C, CUDA C, Python, LaTeX
- Operating systems: Linux, Windows
- Miscellaneous: computer simulations, data visualization and scientific computing; parallel programming; distributed systems; high performance computing

Research interests

Statistical Physics: Random Phenomena and Stochastic Processes

Towarowa 79/16 – PL-43600 Jaworzno – Poland
+48 608 423 674 • j.spiechowicz@gmail.com

Grants

2015-2017 National Science Centre "Anomalous transport phenomena in driven periodic systems" (leader)

2013-2017 Ministry of Science and Higher Education DI2012 018542 "Classical and quantum methods for control of transport on the nanoscale" (leader)

2011-2014 European Science Foundation "Exploring the Physics of Small Devices" (researcher)

2011-2014 National Science Centre N202 052940 "Dynamics and thermodynamics of nanosystems: processes of transport, energy and information conversion" (researcher)

List of publications

[1] J. Spiechowicz, P. Hänggi and J. Łuczka, *Brownian motor efficiency enhanced by nonequlibrium noise*, in press in IEEE Xplore (2015)

[2] J. Spiechowicz and J. Łuczka, *Diffusion anomalies in ac-driven Brownian ratchets*, Physical Review E 91, 062104 (2015)

[3] J. Spiechowicz and J. Łuczka, *Josephson phase diffusion in the SQUID ratchet*, Chaos 25, 053110 (2015)

[4] J. Spiechowicz, M. Kostur and Ł. Machura, *GPU accelerated Monte Carlo simulation of Brownian motors dynamics with CUDA*, Computer Physics Communications 191, 140 (2015)

[5] J. Spiechowicz and J. Łuczka, *Poissonian noise assisted transport in periodic systems*, in press in Physica Scripta (2015)

[6] J. Spiechowicz and J. Łuczka, *Efficiency of the SQUID ratchet driven by external current*, New Journal of Physics 17, 023054 (2015)

[7] J. Spiechowicz, P. Hänggi and J. Łuczka, *Brownian motors in the microscale domain: Enhancement of efficiency by noise*, Physical Review E 90, 032104 (2014)

[8] J. Spiechowicz, P. Hänggi and J. Łuczka, *Josephson junction ratchet: The impact of finite capacitances*, Physical Review B 90, 054520 (2014)

[9] J. Spiechowicz, P. Hänggi and J. Łuczka, *Absolute negative mobility of inertial Brownian particles induced by noise*, IEEE Xplore, 06578913 (2013)

[10] J. Spiechowicz, J. Łuczka and P. Hänggi, *Absolute negative mobility induced by white Poissonian noise*, Journal of Statistical Mechanics: Theory and Experiment, P02044 (2013)

[11] Ł. Machura, J. Spiechowicz and J. Łuczka, *Directed transport in coupled noisy Josephson junctions controlled via ac signals*, Physica Scripta 151, 014021 (2012)

[12] Ł. Machura, J. Spiechowicz, M. Kostur and J. Łuczka, *Two coupled Josephson junctions: dc voltage controlled by biharmonic current*, Journal of Physics: Condensed Matter 24, 085702 (2012)

[13] J. Spiechowicz, Ł. Machura, M. Kostur, J. Łuczka, *Control of transport characteristics in two coupled Josephson junctions*, Acta Physica Polonica B 43, 1203 (2012)

Talks & posters

2015 Frontiers of Quantum and Mesoscopic Thermodynamics, Prague, Czech Republic

2015 7th International Conference on Unsolved Problems of Noise, Barcelona, Casa Convalescència, Spain

2014 XXXVIII International Conference of Theoretical Physics: Correlations & Coherence at Different Scales, Ustroń, Poland

2014 27th Marian Smoluchowski Symposium on Statistical Physics: Fundamentals, Soft Matter and Biocomplexity, Zakopane, Poland

2014 9th International Summer Conference Let's Face Chaos Through Nonlinear Dynamics, Maribor, Slovenia

2013 5th Warsaw School of Statistical Physics, Kazimierz Dolny, Poland

2012 25th Marian Smoluchowski Symposium on Statistical Physics: Fluctuation Relations in Nonequilibrium Regime, Kraków, Poland

2011 24th Marian Smoluchowski Symposium on Statistical Physics: Insights into Stochastic Nonequilibrium, Zakopane, Poland

Scientific papers

Journal of Statistical Mechanics: Theory and Experiment
An IOP and SISSA journal

Absolute negative mobility induced by white Poissonian noise

J Spiechowicz[1], **J Łuczka**[1] **and P Hänggi**[2]

[1] Institute of Physics, University of Silesia, 40-007 Katowice, Poland
[2] Institute of Physics, University of Augsburg, D-86135 Augsburg, Germany
E-mail: j.spiechowicz@gmail.com, Jerzy.Luczka@us.edu.pl
and hanggi@physik.uni-augsburg.de

Received 27 November 2012
Accepted 28 January 2013
Published 27 February 2013

Online at stacks.iop.org/JSTAT/2013/P02044
doi:10.1088/1742-5468/2013/02/P02044

Abstract. We study the transport properties of inertial Brownian particles which move in a *symmetric* periodic potential and are subjected to both a *symmetric*, unbiased time-periodic external force and a biased Poissonian white shot noise (of non-zero average F) which is composed of a random sequence of δ-shaped pulses with random amplitudes. Upon varying the parameters of the white shot noise, one can conveniently manipulate the transport direction and the overall nonlinear response behavior. We find that within tailored parameter regimes the response is *opposite* to the applied average bias F of such white shot noise. This particular transport characteristic thus mimics that of a nonlinear absolute negative mobility (ANM) regime. Moreover, such white shot noise driven ANM is robust with respect to the statistics of the shot noise spikes. Our findings can be checked and corroborated experimentally by the use of a setup that consists of a single resistively and capacitively shunted Josephson junction device.

Keywords: stochastic particle dynamics (theory), stochastic processes (theory), transport properties (theory)

ArXiv ePrint: 1211.5971

 1742-5468/13/P02044+14$33.00

Contents

1. Introduction

In accordance with the Le Chatelier–Braun principle, when an external deterministic force F acts on a particle with all other forces set to zero on average, the long time, stationary average particle velocity $\langle v \rangle$ is expected to become an increasing function of the load F, at least for small bias values F. For an electrical (electronic) device, the current–voltage characteristics exhibits a similar property: if the voltage V increases, the current I increases as well. The Ohmic characteristic $I = (1/R)\,V$ presents an example. This behavior is usually characterized as 'normal transport' behavior. In contrast, the anomalous transport features are (i) a negative differential mobility or conductivity (meaning that the velocity or current decreases with increasing force or voltage) and (ii) an absolute negative mobility (ANM) or conductivity, i.e. the velocity or current exhibits an opposite sign to the applied force which is starting out at zero force or voltage; i.e. the system response is opposite to the applied force.

Such absolute negative mobility has been experimentally detected in a variety of systems, both classical and quantum. Typical situations and cases where ANM has been detected are p-modulation-doped GaAs quantum wells [1], sequential resonant tunneling semiconductor superlattices that are driven by intense terahertz electric fields [2], relaxing Xe plasma ionized by a hard x-ray pulse [3], sliding charge-density waves at sufficiently low temperatures [4], in microfluidic systems with colloidal beads in an aqueous buffer solution [5], in a three-terminal configuration in a two-dimensional electron gas [6], and the transport of vortices in superconductors with inhomogeneous pinning under a driving force [7] and in Josephson junctions [8]. Rather recently, a coherent absolute negative mobility regime has been observed and described for ac and dc driven ultracold atoms in an optical lattice [9].

J. Stat. Mech. (2013) P02044

Yet further examples of ANM have been described theoretically for the nonlinear response in ac–dc driven tunneling transport [10], the dynamics of cooperative Brownian motors [11], Brownian transport containing a complex topology [12, 13] and some multi-state models with state-dependent noise [14]. The effect of an absolute negative mobility can occur also in driven systems such as those of nonlinear inertial Brownian dynamics [15]–[18], overdamped nonlinear Brownian motion in the presence of time-delayed feedback [19], transport of asymmetric particles in a periodically segmented 2D channel [20] and for a system of two coupled resistively shunted Josephson junctions [21].

The key ingredient for the occurrence of ANM in all those listed cases is that the system (i) is driven far away from thermal equilibrium into a time-dependent nonequilibrium state and the resulting dynamics is such that (ii) it is exhibiting a vanishing, unbiased average nonequilibrium response. In the presence of a finite bias F, the ANM response in a symmetric periodic potential is such that an average, anti-symmetric transport velocity $\langle v(F)\rangle$, obeying $\langle v(F)\rangle = -\langle v(-F)\rangle$, occurs around the zero bias force $F = 0$. This situation must be contrasted with the nonequilibrium transport generated by the ratchet mechanism [22]: there, a non-vanishing transport velocity occurs even for vanishing bias $F = 0$, and thus no anti-symmetric mobility behavior occurs around the zero-bias regime. The reader is thus advised to carefully distinguish between anomalous mobility regimes that are characterized as a negative differential mobility regime, or as an absolute negative mobility regime or as a nonlinear negative-valued mobility away from the zero-bias regime [16].

With this work, we substitute the deterministic static force F by a random force $\eta(t)$ of non-zero average. To allow for the comparison with the case of a deterministic load $F \neq 0$, we require that the mean value of the random force $\eta(t)$ equals the value F. As a model for such a random force we use a random sequence of exponentially distributed δ-shaped pulses with random amplitudes. This constitutes a generalized white Poissonian shot noise process; e.g. see [23] for its detailed statistical properties. We demonstrate that this shot noise can induce ANM and in the regime of ANM, it behaves on average statistically similarly to a deterministic constant bias F. Moreover, the ANM phenomenon is robust with respect to the distribution of the random amplitudes of the δ-pulses.

The layout of the present work is as follows. In section 2 we detail the model of a driven inertial Brownian particle. In section 3 we detail more closely the stochastic force acting on the particle and elucidate the resulting transport properties. The findings are contrasted with those for an equivalent setup consisting of a deterministic bias. section 4 provides our summary and some conclusions.

2. The model

In what follows we consider an ensemble of classical, statistically independent Brownian particles undergoing transport in an effectively one-dimensional geometry. For such a one-dimensional system, the *minimal* model of the classical Brownian particle exhibiting the ANM is formulated in terms of the equation of motion for a particle of mass M (i) moving in a symmetric spatially periodic potential $V(x) = V(x + L)$ of period L, (ii) being driven by an unbiased time-periodic force $A\cos(\Omega t)$ with angular frequency Ω and amplitude strength A, and (iii) exposed to a static force F. All three components are essential in order to take the system away from a thermal equilibrium state into a time-dependent

driven nonequilibrium state such that the limiting Le Chatelier–Braun principle no longer applies. The corresponding Langevin equation reads [15]

$$M\ddot{x} + \Gamma\dot{x} = -V'(x) + A\cos(\Omega t) + F + \sqrt{2\Gamma k_{\mathrm{B}}T}\,\xi(t). \tag{1}$$

Here, the dot and the prime denote differentiation with respect to time t and the Brownian particle's coordinate x, respectively. The parameter Γ is the friction coefficient, k_{B} is the Boltzmann constant and T is the temperature. Thermal equilibrium fluctuations are modeled by δ-correlated Gaussian white noise $\xi(t)$ of zero mean and unit intensity, i.e.

$$\langle\xi(t)\rangle = 0, \quad \langle\xi(t)\xi(s)\rangle = \delta(t-s). \tag{2}$$

We are interested in the asymptotic long time regime, where the averaged velocity assumes the periodicity of the driving [24], i.e.,

$$\langle v\rangle = \lim_{t\to\infty}\frac{\Omega}{2\pi}\int_t^{t+2\pi/\Omega} \prec v(s) \succ \,\mathrm{d}s, \tag{3}$$

where $\prec v(s) \succ$ indicates the average over noise realizations (ensemble average). In the deterministic case ($T = 0$), an additional averaging over initial conditions must be performed.

From the symmetry of the Langevin equation it follows that the transformation $F \to -F$ implies $\langle v\rangle \to -\langle v\rangle$. In other words, the average velocity $\langle v\rangle(F)$ as a function of the load F fulfills the relation $\langle v\rangle(-F) = -\langle v\rangle(F)$. In particular, it follows that the transport vanishes identically, $\langle v\rangle \equiv 0$, for $F = 0$. This is in clear contrast to the case for a ratchet mechanism which exhibits finite transport at vanishing static bias [22]. Generally, the averaged velocity $\langle v\rangle$ is a nonlinear function of the bias F. However, for small values of F one can expect a linear response regime to be present and $\langle v\rangle$ assumes the form of a linear function of small bias; i.e.,

$$\langle v\rangle = \mu F. \tag{4}$$

In the normal transport regime, the mobility coefficient μ is positive, $\mu > 0$; in distinct contrast, $\mu < 0$ for ANM. In [15], it has been shown that the above system exhibits ANM and there are two fundamentally different mechanisms for ANM: (a) induced by thermal fluctuations and (b) generated by deterministic dynamics.

We now substitute the deterministic static force F by a stochastic force $\eta(t)$. Such a case is important because it could help to explain and clarify the understanding of unusual transport properties not only in physical but also in biological systems, e.g., the bi-directionality of the net cargo transport inside living cells, where there is no systematic deterministic load but rather random collisions in the form of kicks and impulses. Thus, in place of equation (1) we shall consider the setup

$$M\ddot{x} + \Gamma\dot{x} = -V'(x) + A\cos(\Omega t) + \eta(t) + \sqrt{2\Gamma k_{\mathrm{B}}T}\,\xi(t). \tag{5}$$

The potential $V(x)$ is assumed to be in the simplest *symmetric* form

$$V(x) = \Delta V\sin(2\pi x/L). \tag{6}$$

In order to make the comparison with the case of the deterministic load $F \neq 0$, we set the mean value of the random force $\eta(t)$ equal to F; i.e. $\langle\eta(t)\rangle = F$. As a model for such a stochastic biased forcing we propose a random sequence of δ-shaped pulses with random

amplitudes defined in terms of generalized white Poissonian shot noise [23, 25]:

$$\eta(t) = \sum_{i=1}^{n(t)} z_i \delta(t - t_i), \tag{7}$$

where the t_i are the arrival times of a Poissonian counting process $n(t)$ with parameter λ. Put differently, the probability for occurrence of k impulses in the time interval $[0, t]$ is governed by the Poisson distribution; i.e.,

$$\Pr\{n(t) = k\} = \frac{(\lambda t)^k}{k!} \mathrm{e}^{-\lambda t}. \tag{8}$$

Likewise, the interval s between successive Poisson arrival times $s = t_i - t_{i-1}$ is exponentially distributed with the probability density $\lambda \exp(-\lambda s)$. The parameter λ determines the mean number of δ-pulses per unit time or equivalently the mean spiking rate of the δ-pulses. The amplitudes $\{z_i\}$ of the δ-pulses denote independent random variables. These amplitudes are statistically distributed according to a common probability density $\rho(z)$. The process $\eta(t)$ presents white noise of finite mean and a covariance given by

$$\langle \eta(t) \rangle = \lambda \langle z_i \rangle, \quad \langle \eta(t)\eta(s) \rangle - \langle \eta(t) \rangle \langle \eta(s) \rangle = 2D_{\mathrm{P}} \delta(t - s), \tag{9}$$

where $\langle z_i \rangle$ is an average over the amplitude distribution $\rho(z)$. Poissonian white noise is statistically symmetric if the density $\rho(z)$ is symmetric, i.e. when $\rho(z) = \rho(-z)$. Consequently, $\langle \eta(t) \rangle = 0$. However, we shall not consider unbiased driving but instead consider biased white Poissonian noise for which $\langle \eta(t) \rangle \neq 0$. The white Poissonian noise intensity D_{P} reads

$$D_{\mathrm{P}} = \frac{\lambda \langle z_i^2 \rangle}{2}. \tag{10}$$

We further assume that thermal equilibrium noise $\xi(t)$ is uncorrelated with nonequilibrium noise $\eta(t)$, so $\langle \xi(t)\eta(s) \rangle = \langle \xi(t) \rangle \langle \eta(s) \rangle = 0$.

Next we use a dimensionless form of equation (5). This can be achieved in several ways. Here we propose the use of the period L as a length scale and for time the scale $\tau = L\sqrt{M/\Delta V}$ [26]. Consequently, equation (5) can be rewritten in a dimensionless form as

$$\ddot{\hat{x}} + \gamma \dot{\hat{x}} = -\hat{V}'(\hat{x}) + a \cos(\omega \hat{t}) + \hat{\eta}(\hat{t}) + \sqrt{2\gamma D_{\mathrm{G}}}\, \hat{\xi}(\hat{t}), \tag{11}$$

where $\hat{x} = x/L$ and $\hat{t} = t/\tau$. Other rescaled dimensionless parameters are the friction coefficient $\gamma = \tau\Gamma/M$, the amplitude $a = LA/\Delta V$ and the angular frequency $\omega = \tau\Omega$ of the time-periodic driving. The rescaled potential $\hat{V}(\hat{x}) = V(L\hat{x})/\Delta V = \sin(2\pi\hat{x})$ possesses the unit period: $\hat{V}(\hat{x}) = \hat{V}(\hat{x}+1)$. We introduced the dimensionless thermal noise intensity $D_{\mathrm{G}} = k_{\mathrm{B}}T/\Delta V$, so the Gaussian white noise of vanishing mean $\hat{\xi}(\hat{t})$ possesses the autocorrelation function $\langle \hat{\xi}(\hat{t})\hat{\xi}(\hat{s}) \rangle = \delta(\hat{t}-\hat{s})$. Similarly, the rescaled Poissonian white shot noise is δ-correlated as well; i.e., $\langle \hat{\eta}(\hat{t})\hat{\eta}(\hat{s}) \rangle - \langle \hat{\eta}(\hat{t}) \rangle \langle \hat{\eta}(\hat{s}) \rangle = 2\hat{D}_{\mathrm{P}} \delta(\hat{t} - \hat{s})$, with $\hat{D}_p = \hat{\lambda} \langle \hat{z}_i^2 \rangle / 2$, where $\hat{\lambda} = \tau\lambda$ and $\hat{z}_i = z_i/\sqrt{M\Delta V}$. Hereafter, we will use only dimensionless variables and shall omit the 'hat' notation in all quantities appearing in equation (11).

The deterministic dynamics corresponding to equation (11) exhibits an extremely rich and complex behavior. Depending on the parameter values, periodic, quasiperiodic and

J. Stat. Mech. (2013) P02044

chaotic motion can be observed [27]. In some regimes, ergodicity is broken and the direction of the spontaneous transport depends on the choice for the initial conditions. Different initial conditions of position and velocity may lead to radically different asymptotic behavior; i.e. various attractors may coexist. The asymptotic regime can be classified as either being a locked or a running state. The regime of the running state is the crucial ingredient for the occurrence of non-vanishing transport in the deterministic regime, allowing the system to explore all of space. At non-zero temperature, the system will be typically ergodic with thermal fluctuations enabling diffusive transport with stochastic escape events connecting coexisting deterministic disjoint attractors [28]. In particular, transitions between neighboring locked states give rise to diffusive directed transport.

There exist a wealth of physical systems that can be described by using equations of the form in equation (11). An important case that comes to mind is that of the semi-classical dynamics of a phase difference across a resistively and capacitively shunted Josephson junction which is driven by both a time-periodic and a random force [29]. For this setup the space coordinate of the Brownian particle x and the driving force correspond to the phase difference and the current applied to the Josephson junction, respectively. Other specific systems are rotating dipoles in external fields [30], superionic conductors [31] and charge-density waves [32], to name but a few.

3. Transport properties of a Brownian particle driven by white Gaussian and white Poissonian shot noise

The Fokker–Planck–Kolmogorov–Feller master equation corresponding to the Langevin equation (11) (cf. [25]) cannot be studied using closed analytical forms. Consequently, we have to resort to comprehensive numerical simulations of the white Gaussian and white shot noise driven Langevin dynamics. Details of the numerical scheme employed can be found in [33, 34]. We have chosen the time step to be $0.002 \times 2\pi/\omega$ and used initial conditions $\{x(0), \dot{x}(0)\}$ that are equally distributed over the interval $[0, 1]$ and $[-2, 2]$, respectively (remember that the rescaled potential possesses the unit period). Noise averaging has been performed over 10^3–10^6 different stochastic realizations and, additionally, over one period of the external driving period $2\pi/\omega$. All numerical calculations have been done by use of a CUDA environment implemented on a modern desktop GPU. This scheme allowed for a speed-up of a factor of the order $\sim$100 times as compared to a common present-day CPU method [35].

To gain insight into the role of the white Poissonian shot noise we first examine the influence of the noise parameters λ and D_{P} on the characteristics of the stochastic realizations. To be definite, we assume that the amplitudes $\{z_i\}$ of the δ-kicks are exponentially distributed with the probability density

$$\rho_1(z) = \zeta^{-1}\theta(z)\mathrm{e}^{-z/\zeta}, \tag{12}$$

where $\theta(z)$ denotes the Heaviside step function; i.e. the noise amplitudes take on only positive values, $z_i > 0$. According to equation (12), the statistical moments of these amplitudes $\{z_i\}$ are given by

$$\langle z_i^k \rangle = k!\zeta^k, \qquad k = 1, 2, 3, \ldots. \tag{13}$$

J. Stat. Mech. (2013) P02044

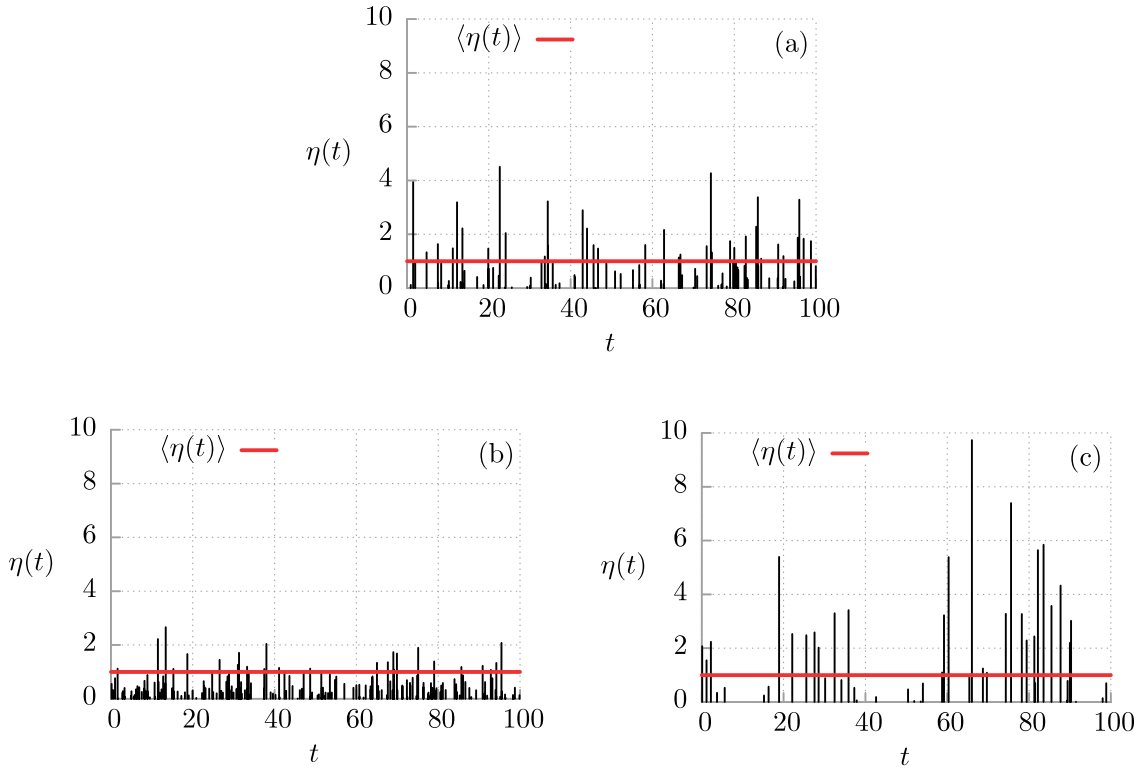

Figure 1. Three illustrative realizations of Poissonian white shot noise $\eta(t)$. The amplitudes $\{z_i\}$ of the δ-spikes are distributed according to the exponential probability density (12). In all three cases, the mean value is held fixed, i.e., $\langle\eta(t)\rangle = \zeta\lambda = \sqrt{\lambda D_{\rm P}} = 1$. The spike rate λ and the noise intensity $D_{\rm P}$ are varied as follows: in (a): $\lambda = 1$, $D_{\rm P} = 1$; in (b): $\lambda = 2$, $D_{\rm P} = 0.5$; in (c): $\lambda = 0.5$, $D_{\rm P} = 2$.

From equations (9) and (10) it follows that the mean value $\langle\eta(t)\rangle$ and the intensity $D_{\rm P}$ of the white shot noise read

$$\langle\eta(t)\rangle = \lambda\zeta, \qquad D_{\rm P} = \lambda\zeta^2. \tag{14}$$

We next use λ and $D_{\rm P}$ as the quantifiers for transport; this yields $\langle\eta(t)\rangle = \sqrt{\lambda D_{\rm P}}$ and $\zeta = \sqrt{D_{\rm P}/\lambda}$. Three typical realizations of white Poissonian noises are depicted in figure 1. In figure 1(a), the mean spiking rate of pulses λ and the noise intensity $D_{\rm P}$ are fixed at 1. In order to ensure that the condition $\langle\eta(t)\rangle = 1$ holds, we may proceed in two different ways. In the first approach we increase the spiking rate λ while correspondingly reducing the noise intensity $D_{\rm P}$. Then the particle is *frequently* kicked by *weak* δ-pulses. This case is depicted in figure 1(b). In the second approach we decrease the spiking rate λ and increase the noise intensity $D_{\rm P}$. Then the particle is *rarely* kicked by *large* amplitudes of the δ-spikes; cf. figure 1(c). It is worth mentioning that in the limit of vanishing amplitudes z_i, when $\zeta \to 0$, and for a divergent spiking rate $\lambda \to \infty$, with $\lambda\zeta^2 = D_{\rm P}$ held fixed, the zero-mean process $\eta(t) - \langle\eta(t)\rangle$ approaches Gaussian white noise of intensity $D_{\rm P}$.

doi:10.1088/1742-5468/2013/02/P02044

J. Stat. Mech. (2013) P02044

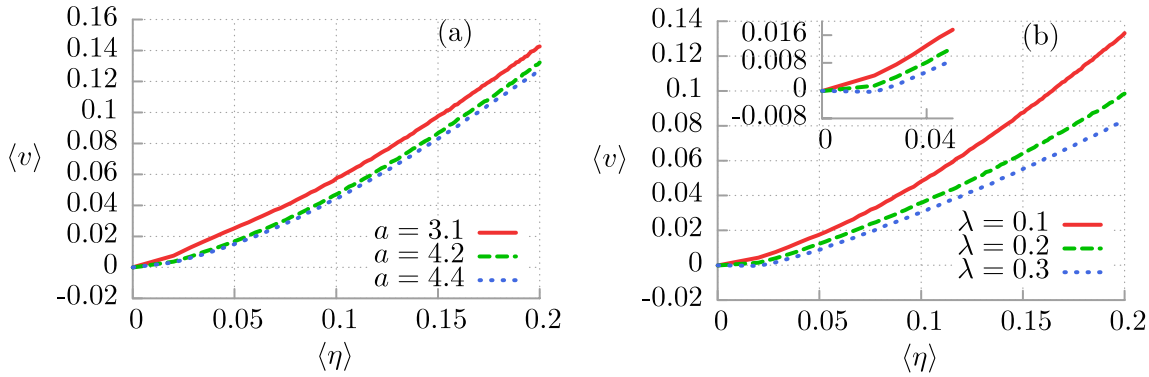

Figure 2. Ohmic-like dependence of the asymptotic, time-averaged asymptotic velocity $\langle v \rangle$ on the mean value of the shot noise $\langle \eta(t) \rangle$. Panel (a): the influence of the amplitude strength a of the time-periodic driving is illustrated for fixed spiking rate $\lambda = 0.1$ of the δ-spikes. Panel (b): the role of the spiking rate is depicted for the ac driving amplitude $a = 4.2$. The spike amplitudes $\{z_i\}$ of the δ-kicks are distributed according to the exponential probability density $\rho_1(z)$ in equation (12). The remaining parameters are fixed as follows: the friction coefficient is $\gamma = 0.9$, the thermal fluctuation intensity is $D_G = 0.001$ and the angular driving frequency is $\omega = 4.9$.

3.1. The Ohmic-like transport regime

Let us comment first on the long time behavior of the driven system considered in equation (11). If the Poissonian white shot noise is absent in equation (11), then the average velocity $\langle v \rangle$ vanishes identically. This feature follows from the presence of reflection symmetry of the potential $V(x)$ and the time reversal symmetry of harmonic driving. Put differently, a directed ratchet transport [22] is absent.

In the presence of white Poissonian shot noise driving, however, a statistical bias emerges [36], which is due to the non-vanishing average. This causes a non-zero mean velocity, which typically assumes the sign of the average of the white shot noise. We recall that there are only *positive* δ-kicks and therefore we expect the average velocity to be positive as well. An opposite behavior would be counterintuitive. Because the dynamics as determined by equation (11) is strongly nonlinear and the stochastic phase space of the system is multidimensional, it should not come as a surprise that the dependence of the average velocity on $\langle \eta(t) \rangle$ is nonlinear as well and may even behave in the non-monotonic manner of the system parameters. The normal expected behavior for the ensemble-averaged and time-averaged velocity is that of an increasing function for $\langle \eta(t) \rangle$. Such a normal regime is depicted in figure 2. We used therein the following parameter values: the friction coefficient has been chosen as $\gamma = 0.9$, the thermal fluctuation intensity is $D_G = 0.001$, and the angular driving frequency is $\omega = 4.9$. In panel (a), the influence of the driving amplitude a is shown. Panel (b) depicts the role of the spiking rate λ of the δ-pulses. The corresponding shot noise characteristics corresponds to rare but large δ-spikes. As a consequence, the average velocity varies almost linearly with the mean value of the shot noise $\langle \eta(t) \rangle$, resulting in an Ohmic-like transport behavior.

J. Stat. Mech. (2013) P02044

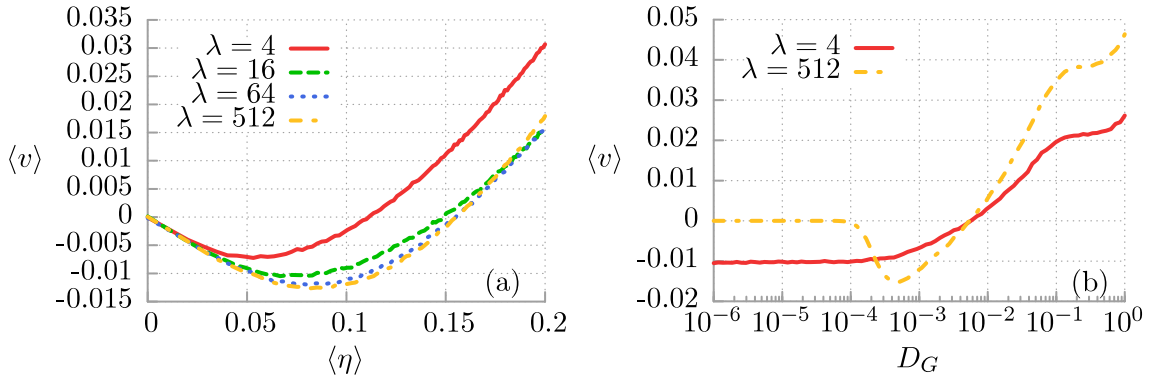

Figure 3. Absolute negative mobility (ANM). Panel (a): the asymptotic time-averaged velocity $\langle v\rangle$ as a function of the mean value of the white shot noise $\langle \eta(t)\rangle$ for various spiking frequencies λ and fixed thermal fluctuation intensity $D_{\mathrm{G}} = 0.001$. In panel (b) the role of the thermal fluctuations is shown for two spiking frequencies $\lambda = 4$ (solid line, $D_{\mathrm{P}} = 6 \times 10^{-4}$) and $\lambda = 512$ (dotted line, $D_{\mathrm{P}} = 2 \times 10^{-5}$). Note that for the value $\lambda = 512$, ANM is induced by thermal fluctuations. There occurs an optimal temperature D_{G} at which ANM is most pronounced. In both panels: the amplitudes $\{z_i\}$ of the δ-spikes are exponentially distributed; the friction coefficient is $\gamma = 0.9$, and the ac driving amplitude is $a = 4.2$ with an angular driving frequency $\omega = 4.9$.

3.2. The regime of absolute negative mobility

We have randomly searched the parameter space and found that the normal, Ohmic-like transport regime dominates in the parameter space. Keeping in mind that there are only positive δ-kicks of white shot noise acting on the Brownian particle, we inquire whether we can identify parameter regimes for which the stationary mean velocity of the particle assumes negative values, i.e. the particle moves on average oppositely to the applied δ-spikes. In figure 3(a) we exemplify this situation. The characteristic feature is the emergence of extended regimes, $\langle \eta(t)\rangle > 0$, where the average velocity $\langle v\rangle$, starting out from zero, assumes a *negative* response; i.e. ANM occurs. Moreover, there exists an optimal strength for $\langle \eta(t)\rangle$ at which the average velocity assumes its minimal value. We detect that if the spiking rate λ increases, then the minimum of the resulting average transport velocity is lowered. Notably, we have found that there exists a limiting minimal value for the transport velocity which is assumed for $\lambda \to \infty$. For $\lambda > 512$ (see the dotted line) the velocity characteristics becomes numerically indistinguishable.

The role of thermal fluctuations is depicted in panel (b). Two distinct mechanisms for the ANM-like effect can be observed. For $\lambda = 4$, the negative velocity is caused by deterministic chaotic dynamics because even at zero temperature, $D_{\mathrm{G}} = 0$, the velocity is negative. In this regime, temperature plays a destructive role for ANM: increase of temperature monotonically diminishes the negative average velocity. For $\lambda = 512$, the negative velocity is solely induced by thermal fluctuations. For low temperatures (small D_{G}) ANM does not occur. If thermal fluctuations grow (D_{G} increases) the ANM effect emerges and intensifies up to the optimal temperature where ANM is most pronounced. Subsequent increase of the temperature reduces ANM and finally temperature destroys it

J. Stat. Mech. (2013) P02044

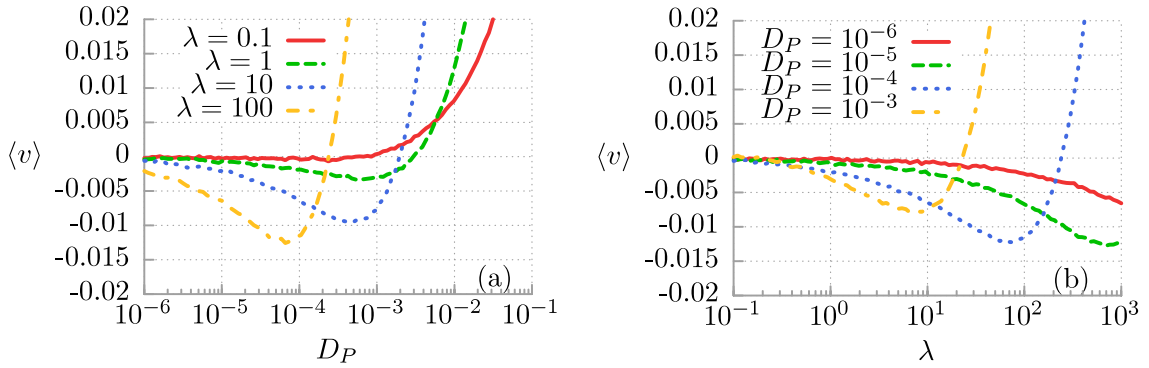

Figure 4. Panel (a): the time-averaged asymptotic velocity $\langle v\rangle$ as a function of the white shot noise intensity D_{P} for selected values of the spiking frequencies λ. Panel (b): average velocity as a function of the spiking rate λ for several values of the white shot noise intensity D_{P}. The amplitudes $\{z_i\}$ of the δ-kicks are generated according to the distribution $\rho_1(z)$ and the thermal fluctuation intensity $D_{\mathrm{G}} = 0.001$. Other parameters are the same as those detailed in figure 3.

completely. For 'high' temperature, transport is normal. The reader may find a detailed explanation of the origin of anomalous transport in such systems in [15].

3.3. Controlling transport

The transport properties of the Brownian particle can be controlled by varying the parameters of the white Poissonian noise; i.e., the values for λ or D_{P}. The dependence of the asymptotic average velocity $\langle v\rangle$ on these white shot noise parameters is presented in figures 4(a) and (b). In figure 4(a) we study the role of an increasing white shot noise intensity D_{P}. As an example, consider the case with $\lambda = 10$ in figure 4(a). For weak shot noise intensity D_{P} the velocity exhibits ANM and its minimal value decreases with increasing D_{P}. For strong white shot noise, however, when the intensity D_{P} is sufficiently large, the average transport velocity turns around towards a normal regime, undergoing a current reversal at some finite noise strength D_{P}.

The spiking rate λ of the white shot noise also serves as a control parameter for ANM. The numerical findings are depicted in figure 4(b) for a set of selected values of the white shot noise intensity D_{P}. As before we find that the ANM can be controlled upon varying the spiking rate λ. Again we detect a current reversal at finite spiking rate λ; this reversal value shifts to much larger spiking frequencies with decreasing white shot noise intensity D_{P}. In summary, one can conveniently manipulate the direction of the particle transport and tune the ANM regime upon varying the two shot noise parameters.

3.4. The robustness of ANM to amplitude statistics

We also address the dependence of ANM transport for different statistics of the amplitude $\{z_i\}$ entering the generalized white shot noise. In doing so we choose two additional amplitude statistics that derive from special cases of the Gamma distribution. In

J. Stat. Mech. (2013) P02044

particular, we study

$$\rho_2(z) = \zeta^{-2}\theta(z)z\mathrm{e}^{-z/\zeta} \tag{15}$$

and

$$\rho_3(z) = \tfrac{1}{2}\zeta^{-3}\theta(z)z^2\mathrm{e}^{-z/\zeta}, \tag{16}$$

where $\theta(z)$ is the Heaviside function. For the density $\rho_2(z)$, the first two moments read

$$\langle z_i\rangle = 2\zeta, \qquad \langle z_i^2\rangle = 6\zeta^2. \tag{17}$$

As a result, upon inspecting equations (9) and (10), we see that the mean value is $\langle\eta(t)\rangle = 2\sqrt{D_\mathrm{P}\lambda/3}$ and the white shot intensity reads $D_\mathrm{P} = 3\lambda\zeta^2$. Likewise, for the density $\rho_3(z)$, we obtain

$$\langle z_i\rangle = 3\zeta, \qquad \langle z_i^2\rangle = 12\zeta^2. \tag{18}$$

In this case we find that $\langle\eta(t)\rangle = \sqrt{3D_\mathrm{P}\lambda/2}$ and $D_\mathrm{P} = 6\lambda\zeta^2$. The main difference between the exponential probability density $\rho_1(z)$ in equation (12) and these two integrable densities is a non-monotonic, bell-shaped form; see figure 5(a). As a consequence, with $\rho_1(z)$, very small noise amplitudes are the most likely. In the case of $\rho_2(z)$, the maximum of the density occurs for the amplitudes $z_i = \zeta$, while for $\rho_3(z)$, the amplitudes $z_i = 2\zeta$ are most probable. All three probability densities are depicted in figure 5(a). Panel (b) of this figure depicts the dependence of the averaged velocity $\langle v\rangle$ on the three statistical densities for shot noise amplitudes $\{z_i\}$ at a fixed spiking rate $\lambda = 10$.

We observe that in the regime of ANM, white Poissonian noise with amplitude density $\rho_3(z)$ is slightly more effective. In figure 5(c) we show the behavior for the various amplitude statistics when the spiking rate λ is varied. Overall we find (for the chosen set of three examples) a weak dependence of the ANM regime on the statistics for the noise amplitudes. We therefore may assume that the statistics of the amplitudes only weakly impacts the overall ANM regime, apart from possibly for some cases with abnormal, stylized density features.

3.5. The comparison with deterministic bias

As a final point of analysis, we compare ANM generated by Poissonian shot noise and the external force F which is constant in space and time. So, we have to consider the dimensionless form of the Langevin equation corresponding to (1), namely,

$$\ddot{x} + \gamma\dot{x} = -V'(x) + a\cos(\omega t) + f + \sqrt{2\gamma D_\mathrm{G}}\,\xi(t), \tag{19}$$

where the dimensionless deterministic constant force $f = (L/\Delta V)\,F$. In order to compare the scenario of the deterministic force f with the system driven by Poissonian white shot noise, we need to impose the additional condition

$$\langle\eta(t)\rangle = f. \tag{20}$$

We consider the following parameter regime: the friction coefficient is $\gamma = 0.9$, the ac driving amplitude is $a = 4.2$, the angular driving frequency is $\omega = 4.9$ and the thermal fluctuation intensity is $D_\mathrm{G} = 0.001$. We stress that it is the same parameter regime as in figure 2(b), where the Ohmic-like transport is observed for the case of a low spiking rate $\lambda \leq 0.3$. In figure 6, we show the dependence of the asymptotic average velocity $\langle v\rangle$ on the

J. Stat. Mech. (2013) P02044

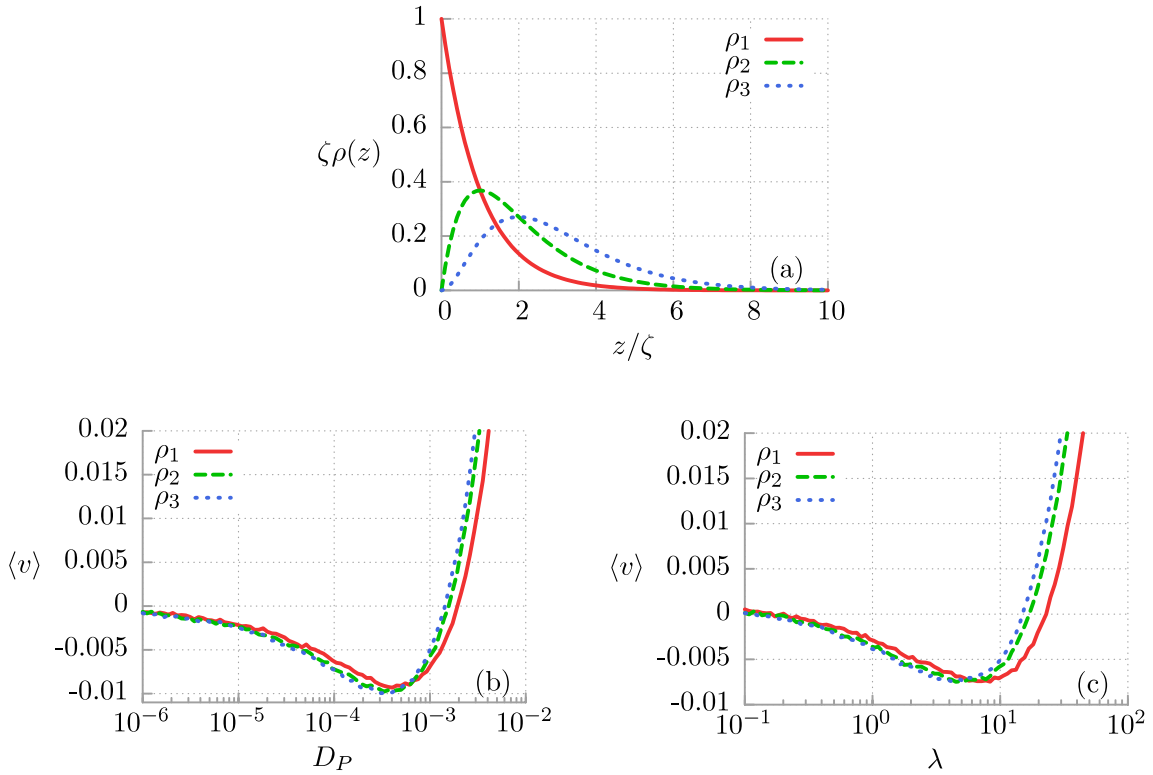

Figure 5. Panel (a): plots of three probability densities of the amplitudes $\{z_i\}$. Panel (b): the dependence of the time-averaged, asymptotic velocity $\langle v\rangle$ on the intensity $D_{\rm P}$ of the shot noise $\eta(t)$ for three statistical distributions of the amplitudes $\{z_i\}$ of the δ-pulses and for $\lambda = 10$. Panel (c): asymptotic time-averaged transport velocity versus the spiking rate λ for three amplitude densities as depicted in panel (a) and for an overall white shot noise intensity $D_{\rm P} = 10^{-3}$. The remaining parameters are as those given in figure 3 and the thermal fluctuation intensity $D_{\rm G} = 0.001$.

constant deterministic bias and the mean value of the shot noise $\langle\eta(t)\rangle$ for the case of (i) a moderate spiking rate $\lambda = 4$ and (ii) a large spiking rate $\lambda = 512$. For the low firing rate, one can observe normal transport; for moderate values of the spiking rate λ, we detect small windows of occurrence of ANM. Seemingly, the case with the deterministic bias is most effective for ANM, yielding a wide regime of bias values f. For a large spiking rate of the white shot noise, we do indeed detect convergence towards the deterministic constant bias case; cf. panel (b) in figure 6.

4. Conclusions

With this work we presented a detailed study of the transport properties of an inertial Brownian particle which moves in a periodic, symmetric potential and which in addition is exposed to periodic harmonic ac driving and (generalized) Poissonian white shot noise of finite bias F. We have demonstrated the possibility of manipulating the *direction*

J. Stat. Mech. (2013) P02044

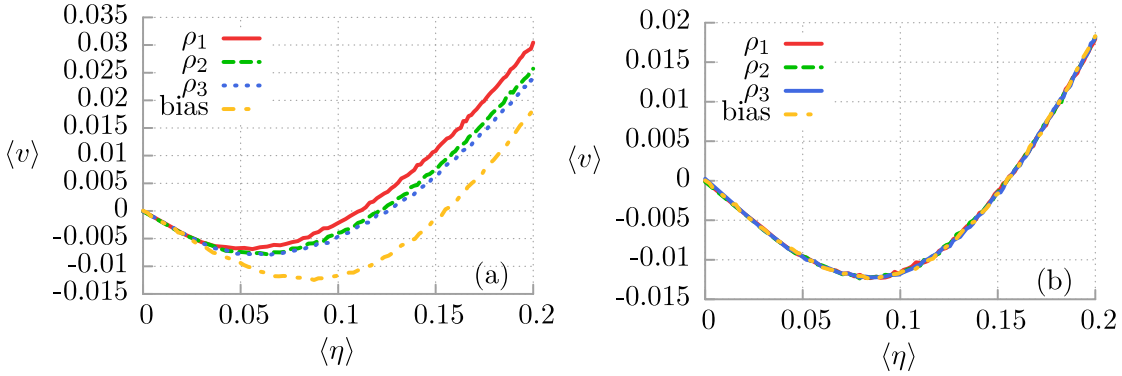

Figure 6. The dependence of the asymptotic time-averaged velocity $\langle v \rangle$ on the constant bias f versus the asymptotic time-averaged mean value of the shot noise $\langle \eta(t) \rangle$ for $\lambda = 4$ in panel (a) and $\lambda = 512$ in panel (b). The thermal fluctuation intensity is $D_{\mathrm{G}} = 0.001$. The remaining parameters are the same as in panel (b) of figure 2. Perfect equivalence (i.e. indistinguishable line plots) of the deterministic and random forcing is observed for a high spiking rate of δ-pulses of Poissonian noise .

of transport just by adjusting the parameters of the white shot noise. Moreover, in such systems, Poissonian white shot noise can induce anomalous transport effects. In particular, such dynamics is able to exhibit an absolute negative mobility regime. This ANM phenomenon has its roots in a purely stochastic dynamics of the system and is robust with respect to the distribution of the random amplitudes of the δ-pulses. In some regions of parameter space, one can find an impact of Poissonian shot noise similar to that of the deterministic bias. In general, the exact equivalence of the two sources of bias does not hold true. However, in the ANM regime the equivalence is observed in the limiting case of a spiking rate $\lambda \to \infty$ of the δ-pulses. For moderate to large λ, the ANM induced by shot noise is suppressed as compared with the case for a deterministic bias. Notably, for a small spiking rate λ, the ANM response is no longer present and instead a normal, Ohmic-like behavior occurs.

Our results can readily be experimentally tested with an accessible setup consisting of a single resistively and capacitively shunted Josephson junction device operating in its classical regime.

Acknowledgments

This work was supported in part by the grant N202 052940 (JS and JL) and the ESF Program 'Exploring the Physics of Small Devices' (PH and JL).

References

[1] Höpfel R A, Shah J, Wolff P A and Gossard A C, 1986 *Phys. Rev. Lett.* **56** 2736
[2] Keay B J, Zeuner S, Allen S J, Maranowski K D, Gossard A C, Bhattacharya U and Rodwell M J W, 1995 *Phys. Rev. Lett.* **75** 4102
Zeuner S *et al,* 1996 *Phys. Rev.* B **53** R1717

J. Stat. Mech. (2013) P02044

Cannon E H, Kusmartsev F V, Alekseev K N and Campbell D K, 2000 *Phys. Rev. Lett.* **85** 1302
[3] Warman J M, Sowada U and De Haas M P, 1985 *Phys. Rev.* A **31** 1974
Suvakov M, Ristivojevic Z, Petrovic Z Lj, Dujko S, Raspopovic Z M, Dyatko N A and Napartovich A P, 2005 *IEEE Trans. Plasma Sci.* **33** 532
[4] van der Zant H S J, Slot E, Zaitsev-Zotov S V and Artemenko S N, 2001 *Phys. Rev. Lett.* **87** 126401
[5] Ros A, Eichhorn R, Regtmeier J, Duong T T, Reimann P and Anselmetti D, 2005 *Nature* **436** 928
Eichhorn R, Regtmeier J, Anselmetti D and Reimann P, 2010 *Soft Matter.* **6** 1858
[6] Kaya I I and Eberl K, 2007 *Phys Rev. Lett.* **98** 186801
[7] Xu X B *et al,* 2007 *Phys. Rev.* B **75** 224507
[8] Nagel J, Speer D, Gaber T, Sterck A, Eichhorn R, Reimann P, Ilin K, Siegel M, Koelle D and Kleiner R, 2008 *Phys. Rev. Lett.* **100** 217001
[9] Salger T, Kling S, Denisov S, Ponomarev A V, H änggi P and Weitz M, 2012 arXiv:1202.5174
[10] Hartmann L, Grifoni M and Hänggi P, 1997 *Europhys. Lett.* **38** 497
[11] Reimann P, Kawai R, Van den Broeck C and Hänggi P, 1999 *Europhys. Lett.* **45** 545
Van den Broeck C, Bena I, Reimann P and Lehmann J, 2000 *Ann. Phys.* **9** 713
[12] Eichhorn R, Reimann P and Hänggi P, 2002 *Phys. Rev. Lett.* **88** 190601
[13] Eichhorn R, Reimann P and Hänggi P, 2002 *Phys. Rev.* E. **66** 066132
[14] Cleuren B and Van den Broeck C, 2002 *Phys. Rev.* E **65** 030101(R)
Haljas A, Mankin R, Sauga A and Reiter E, 2004 *Phys. Rev.* E **70** 041107
[15] Machura L, Kostur M, Talkner P, Łuczka J and Hänggi P, 2007 *Phys. Rev. Lett.* **98** 040601
[16] Machura L, Kostur M, Talkner P, Hänggi P and Łuczka J, 2008 *Phys. Rev.* B **77** 104509
Machura L, Kostur M, Talkner P, Hänggi P and Łuczka J, 2010 *Physica* E **42** 590
[17] Machura L, Kostur M, Łuczka J, Talkner P and Hänggi P, 2008 *Acta Phys. Pol.* B **39** 1115
[18] Speer D, Eichhorn R and Reimann P, 2007 *Phys. Rev.* E **76** 051110
[19] Hennig D, 2009 *Phys. Rev.* E **79** 041114
Du L-C and Mei D-C, 2011 *J. Stat. Mech.* P11016
[20] Hänggi P, Marchesoni F, Savel'ev S and Schmid G, 2010 *Phys. Rev.* E **82** 041121
[21] Januszewski M and Łuczka J, 2011 *Phys. Rev.* E **83** 051117
[22] Hänggi P and Marchesoni F, 2009 *Rev. Mod. Phys.* **81** 387
Astumian R D and Hänggi P, 2002 *Phys. Today* **55** 33
[23] Hänggi P, 1978 *Z. Phys.* B **30** 85
[24] Jung P and Hänggi P, 1990 *Phys. Rev.* A **41** 2977
Jung P and Hänggi P, 1991 *Phys. Rev.* A **44** 8032
Gammaitoni L, Hänggi P, Jung P and Marchesoni F, 1998 *Rev. Mod. Phys.* **70** 223
[25] Hänggi P, 1980 *Z. Phys.* B **36** 271
Hänggi P, 1981 *Z. Phys.* B **43** 269
[26] Łuczka J, 1999 *Physica* A **274** 200
Machura L, Kostur M and Łuczka J, 2008 *BioSystems* **94** 253
[27] Jung P, Kissner J G and Hänggi P, 1996 *Phys. Rev. Lett.* **76** 3436
Mateos J L, 2000 *Phys. Rev. Lett.* **84** 258
[28] Hänggi P, Talkner P and Borkovec M, 1990 *Rev. Mod. Phys.* **62** 251
[29] Kautz R L, 1996 *Rep. Prog. Phys.* **59** 935
[30] Coffey W T, Kalmykov Yu P and Waldron J T, 2004 *The Langevin Equation* (Singapore: World Scientific)
[31] Fulde P, Pietronero L, Schneider W R and Strässler S, 1975 *Phys. Rev. Lett.* **35** 1776
Dieterich W, Peschel I and Schneider W R, 1977 *Z. Phys.* B **27** 177
Geisel T, 1979 *Solid State Commun.* **32** 739
[32] Grüner G, Zawadowski A and Chaikin P M, 1981 *Phys. Rev. Lett.* **46** 511
[33] Kim C, Lee E, Hänggi P and Talkner P, 2007 *Phys. Rev.* E **76** 011109
[34] Grigoriu M, 2009 *Phys. Rev.* E **80** 026704
[35] Januszewski M and Kostur M, 2010 *Comput. Phys. Commun.* **181** 183
[36] Hänggi P, Bartussek R, Talkner P and Łuczka J, 1996 *Europhys. Lett.* **35** 315
Łuczka J, Bartussek R and Hänggi P, 1995 *Europhys. Lett.* **31** 431

J. Stat. Mech. (2013) P02044

Brownian motors in the microscale domain: Enhancement of efficiency by noise

J. Spiechowicz,[1] P. Hänggi,[2,3] and J. Łuczka[1,4]
[1]*Institute of Physics, University of Silesia, 40-007 Katowice, Poland*
[2]*Institute of Physics, University of Augsburg, 86135 Augsburg, Germany*
[3]*Nanosystems Initiative Munich, Schellingstrasse, 4, D-80799 München, Germany*
[4]*Silesian Center for Education and Interdisciplinary Research, University of Silesia, 41-500 Chorzów, Poland*
(Received 20 May 2014; published 2 September 2014)

We study a noisy drive mechanism for efficiency enhancement of Brownian motors operating on the microscale domain. It was proven [J. Spiechowicz *et al.*, J. Stat. Mech. (2013) P02044] that biased noise $\eta(t)$ can induce normal and anomalous transport processes similar to those generated by a static force F acting on inertial Brownian particles in a *reflection-symmetric* periodic structure in the presence of *symmetric* unbiased time-periodic driving. Here, we show that within selected parameter regimes, noise $\eta(t)$ of the mean value $\langle\eta(t)\rangle = F$ can be significantly more effective than the deterministic force F: the motor can move much faster, its velocity fluctuations are much smaller, and the motor efficiency increases several times. These features hold true in both normal and absolute negative mobility regimes. We demonstrate this with detailed simulations by resource to generalized white Poissonian noise. Our theoretical results can be tested and corroborated experimentally by use of a setup that consists of a resistively and capacitively shunted Josephson junction. The suggested strategy to replace F by $\eta(t)$ may provide a new operating principle in which micro- and nanomotors could be powered by biased noise.

DOI: 10.1103/PhysRevE.90.032104 PACS number(s): 05.40.−a, 05.60.−k, 05.10.Gg, 85.25.Cp

I. INTRODUCTION

Transport occurring in the microscale domain is strongly influenced by fluctuations and random perturbations. In certain regimes they can play a dominant role. The typical situation is then that randomness hampers directed transport with respect to quantifiers such as the average transport velocity with particle motions being erratic and thus uncontrollable. However, a constructive role of both equilibrium and nonequilibrium fluctuations has since been demonstrated for many situations with the occurrence of several intriguing, noise-assisted phenomena such as Brownian ratchets [1], stochastic resonance [2], molecular motors and machines [3,4], genetic and biochemical regulatory systems [5], intracellular transport [6], energy transport [7], to mention a few. Fluctuations and noise may enhance the average velocity, reverse the natural transport direction, or induce anomalous transport processes. The conventional way to transport particles into a desired direction is to apply a constant force F pointing in this direction. Here we consider transport in spatially periodic systems and study a class of systems where both normal and anomalous transport regimes exist. We show that a stochastic force $\eta(t)$ of equal mean value as the deterministic force F proves to be more effective than the deterministic counterpart. Our idea and main message is: replace the deterministic forces by suitable noise, which in some regimes can appear to be much more effective. The proposal is in some sense universal and can be realized both in classical and quantum systems; in condensed matter physics and soft matter physics; in physical and biological systems. Examples where this idea could be realized are: motors which are cold atoms in optical lattices [8], carbon nanotube motors based upon the torque generated by a flux of electrons passing through a chiral nanotube [9], motors based on the chaotic quantum dots [10].

The paper is organized as follows. In Sec. II we describe a mathematical model of the inertial Brownian motor, which is driven by a time-periodic force and a constant force F or biased noise $\eta(t)$. The model has been previously studied in various aspects and is proved to exhibit a rich diversity of anomalous transport characteristics [11–14]. Section III contains a detailed analysis of three quantifiers characterizing transport processes, namely a long-time average velocity, its fluctuations and efficiency. Section IV provides summary and some conclusions.

II. MODEL OF BROWNIAN MOTOR

Modeling systems and understanding their generic properties discloses which components of the setup are crucial and which elements may be subrelevant. Here we demonstrate this with an archetype class of Brownian motors, which is composed of a minimal number of elements but nevertheless is able to exhibit a wide class of anomalous transport features, such as absolute negative mobility (ANM) in a linear response regime, negative mobility in a nonlinear response regime, and negative differential mobility [11]. The modeling uses a classical Brownian particle moving in a one-dimensional periodic potential landscape. Using dimensionless variables, the model consists of the following parts [12,13]: (i) a particle of mass $M = 1$, (ii) moving in a *symmetric*, spatially periodic potential $V(x) = V(x + 1) = \sin(2\pi x)$ of period $L = 1$, (iii) being driven by an unbiased time-periodic force $a\cos\omega t$ with amplitude a and angular frequency ω, and (iv) subjected to a constant force F. We also consider the counterpart by replacement of the force F with biased noise $\eta(t)$. In order to make a comparison with the case of the deterministic force F, we set the mean value of the random force $\eta(t)$ equal to F, namely $\langle\eta(t)\rangle = F$ (Fig. 1). The corresponding dimensionless Langevin equations therefore read

$$\ddot{x} + \gamma\dot{x} = -V'(x) + a\cos(\omega t) + \sqrt{2\gamma D_T}\,\xi(t) + F, \qquad (1)$$

$$\ddot{x} + \gamma\dot{x} = -V'(x) + a\cos(\omega t) + \sqrt{2\gamma D_T}\,\xi(t) + \eta(t). \qquad (2)$$

Here, the dot and the prime denote a differentiation with respect to time t and the Brownian particle's space coordinate x, respectively. The parameter γ characterizes the friction

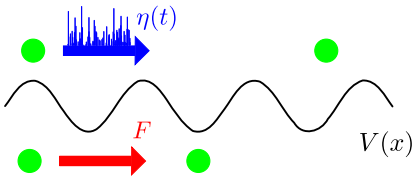

FIG. 1. (Color online) Brownian motors moving in symmetric periodic structures in the presence of an unbiased harmonic force $a\cos\omega t$ and driven by a static, biasing force F can be transported much faster and in a more effective way when F is replaced by noise $\eta(t)$ of equal average bias $\langle\eta(t)\rangle = F$.

coefficient. Thermal noise due to the coupling of the particle with thermostat is modeled by symmetric and unbiased δ-correlated Gaussian white noise $\xi(t)$ with $\langle\xi(t)\rangle = 0$ and $\langle\xi(t)\xi(s)\rangle = \delta(t-s)$. Its intensity $D_T \propto k_B T$ is proportional to the thermal energy, where T is the bath temperature with k_B the Boltzmann constant. The dimensional version of Eq. (1) and corresponding scalings of length and time, etc., is detailed in Ref. [12] for an interested reader. From the symmetry property it follows that $F \to -F$ implies $\dot{x}(t) \to -\dot{x}(t)$ and in the following we assume a positive valued force $F > 0$. As a model of biased noise $\eta(t) > 0$ we choose a random sequence of δ pulses with random amplitudes defined in terms of *generalized white Poissonian noise* [15],

$$\eta(t) = \sum_{i=1}^{n(t)} z_i \delta(t - t_i), \tag{3}$$

where t_i are the arrival times of Poissonian counting process $n(t)$ with Poisson parameter λ; i.e., the probability that k pulses occur in the interval $(0,t)$ is given by the Poisson distribution $\Pr\{n(t) = k\} = (\lambda t)^k \exp(-\lambda t)/k!$, with λ being the mean number of δ pulses per unit time. The amplitudes $\{z_i\}$ of the pulses are mutually independent random variables of a common density $\rho(z)$ and are independent of the counting process $n(t)$. They are assumed to be exponentially distributed; i.e., $\rho(z) = \zeta^{-1}\theta(z)\exp(-z/\zeta)$, where $\theta(z)$ is the Heaviside step function. In consequence, all amplitudes $\{z_i\}$ are *positive* and realizations of the process $\eta(t)$ are *nonnegative*; i.e., $\eta(t) \geqslant 0$. This biased nonequilibrium noise thus has a finite mean $\langle\eta(t)\rangle = \lambda\langle z_i\rangle = \sqrt{\lambda D_P}$ with covariance, $(\langle\eta(t)\eta(s)\rangle - \langle\eta(t)\rangle\langle\eta(s)\rangle) = 2D_P\delta(t-s)$. We introduced the Poissonian noise intensity $D_P = \lambda\langle z_i^2\rangle/2 = \lambda\zeta^2$, where $\langle z_i^k\rangle = k!\zeta^k$ are the statistical moments of the amplitudes $\{z_i\}$. We also assume that the thermal equilibrium fluctuations $\xi(t)$ are uncorrelated with nonequilibrium noise $\eta(t)$; i.e., $\langle\xi(t)\eta(s)\rangle = \langle\xi(t)\rangle\langle\eta(s)\rangle = 0$. The influence of the Poissonian noise parameters λ and D_P on stochastic realizations of $\eta(t)$ is presented in Ref. [14]. Here, we only mention two extreme regimes. The first limiting case is when both λ and D_P are large, then the particle is frequently kicked by large δ pulses. On the contrary, when both λ and D_P are small, then the particle it is rarely kicked by δ pulses of small amplitudes.

III. EFFICIENCY OF MOTOR

The most important quantity characterizing a Brownian motor is its directed average velocity. In the asymptotic long-time regime it is determined by the relation [2,16,17]

$$\langle v\rangle = \lim_{t\to\infty} \frac{\omega}{2\pi} \int_t^{t+2\pi/\omega} \mathbb{E}[v(s)]\, ds, \tag{4}$$

where $\mathbb{E}[v(t)]$ denotes the average of the actual velocity $v(t) = \dot{x}(t)$ over the noise realizations and initial conditions. Although this average velocity is a main quantifier for the transport, it is, however, not necessarily of decisive character in attaining an optimal efficiency for the working operation. For example, a large transport velocity is of little use if the fluctuations are too erratic around the average velocity, thus spoiling effectiveness. We next study the size of the velocity fluctuations. In the long-time regime these are given by

$$\sigma_v^2 = \langle v^2\rangle - \langle v\rangle^2. \tag{5}$$

Typically the velocity mainly assumes values within the interval $v(t) \in (\langle v\rangle - \sigma_v, \langle v\rangle + \sigma_v)$. If these fluctuations are very large, i.e., if $\sigma_v > \langle v\rangle$, it implies that the Brownian motor can move for some time in the direction opposite to its average velocity $\langle v\rangle$. As a measure of its effectiveness we consider a common measure, namely its Stokes *efficiency* ε_S [18,19]: it is evaluated as the ratio of the dissipated power $F_v\langle v\rangle$, associated with the directional movement against the mean viscous force $F_v = \gamma\langle v\rangle$, to the input power $P_{\rm in}$ [20,21]; i.e.,

$$\varepsilon_S = \frac{F_v\langle v\rangle}{P_{\rm in}} = \frac{\gamma\langle v\rangle^2}{P_{\rm in}} = \frac{\langle v\rangle^2}{\langle v^2\rangle - D_T}\,. \tag{6}$$

Here, $P_{\rm in}$ is supplied to the system by all external forces, i.e., by both the ac-driving $a\cos(\omega t)$ and the static force F or the random force $\eta(t)$. From an energy balance of the underlying equations of motion, Eqs. (1) or (2), it follows that $P_{\rm in} = \gamma(\langle v\rangle^2 + \sigma_v^2 - D_T) = \gamma(\langle v^2\rangle - D_T)$,which is always positive valued [20–22]. We note that this nonequilibrium efficiency Eq. (6) does not coincide with the thermodynamic efficiency; e.g., see the discussion on p. 218 of Ref. [3]. Physical intuition tells us that a decrease of the variance σ_v^2 generates a smaller input power and hence to an increase of the overall efficiency. Put differently, transport is optimized in regimes that *maximize* the directed velocity and *minimize* its fluctuations.

The deterministic system dynamics, i.e., if $D_T = D_P = 0$ in Eq. (1), is extremely rich in complexity [23,24]. Particularly, main features of the asymptotic behavior are locked states in which the motion of the Brownian particle is bounded to one or several spatial periods, chaotic and running states in which movement is unbounded in space. The latter modes of transport are crucial for the occurrence of the deterministic directed transport. Adding the Poissonian noise $\eta(t)$ or thermal fluctuations $\xi(t)$ activates a stochastic dynamics for which transitions between neighboring states are induced and therefore can result in diffusive or even directed transport. Since the Fokker-Planck-Kolmogorov-Feller master equation [15] corresponding to the white noise driven Langevin Eqs. (1) or (2) surely cannot be solved analytically, we performed extensive numerical simulations. The specific details of the employed numerical code can be found in Ref. [14]. Here, we only mention that all numerical simulations were done by use of a CUDA environment, which is implemented on a modern desktop GPU. This scheme allowed for a speedup of a factor

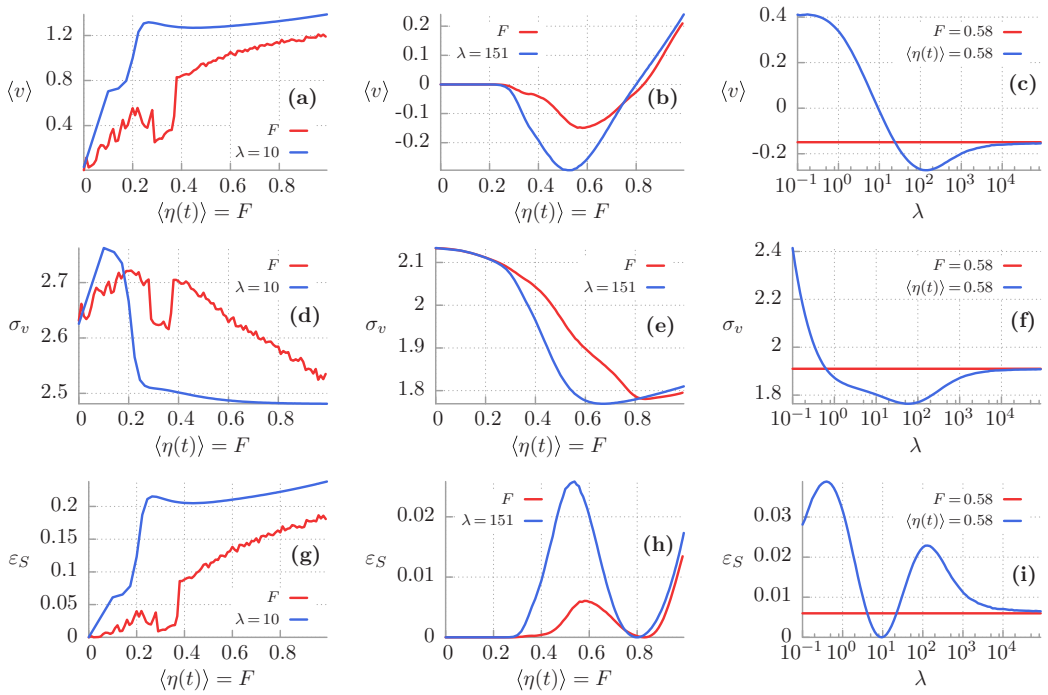

FIG. 2. (Color online) Normal (left panels) and anomalous (middle panels) transport regimes. Upper horizontal panels: the asymptotic averaged velocity $\langle v \rangle$. Middle horizontal panels: the velocity fluctuations σ_v. Bottom horizontal panels: the Stokes efficiency ε_S. All as a function of the deterministic constant bias F and the random force $\eta(t)$ modeled here by white Poissonian noise of the mean value $\langle \eta(t) \rangle = F$. In right panels, the dependence on the spiking rate λ is shown for fixed mean value of noise $\langle \eta \rangle = 0.58$. Parameters in the left panels: $a = 27.5$, $\omega = 8.5$, $\gamma = 1.194$, $D_T = 10^{-6}$, $\lambda = 10$. In the middle and right panels they are as follows: $a = 8.95$, $\omega = 3.77$, $\gamma = 1.546$, $D_T = 0.001$, $\lambda = 151$.

of the order 10^3 as compared to a present-day CPU method [25]. Our so obtained main results are presented next.

A. Normal and ANM regimes

The vast majority of stable running states point into the positive direction for $F > 0$. However, there are also running stable states that on average move in the opposite direction to $F > 0$ and the phenomenon of ANM occurs [12]. It can been shown [14] that similar anomalous transport processes occur for the system Eq. (2). The negative mobility is generated by various mechanisms. In some regimes it is caused by thermal equilibrium fluctuations [12] and ANM is absent for vanishing fluctuations. In other regimes, ANM can occur in the deterministic system while noise either destroys the effect or diminishes its strength [11,13]. Nevertheless, the origin of ANM is in the noise-free structure of stable and unstable orbits; see a detailed discussion in Ref. [26].

Not surprisingly, it is practically sheer impossible to probe numerically the full parameter space $\{\gamma, a, \omega, D_T, F, \lambda, D_P\}$. We have chosen our simulations in regimes that exhibit a most important and intriguing transport behavior. We start with the asymptotic average velocity. This transport velocity is reduced when the deterministic force F acting on the Brownian motor is replaced by the biased noisy drive $\eta(t)$, as one naively would also expect. However, there are regimes in the parameters space where the use of a random force is more effective. In Fig. 2, we illustrate two specific cases. The average velocity is depicted as a function of the mean random force, i.e., the static bias, $\langle \eta(t) \rangle = F$. Figure 2(a) corresponds to a normal transport regime with average velocity pointing into the direction of the bias. For this specific set of parameters, the average velocity as a function of the bias F is jagged and not smooth. The reason is that the chosen temperature is very small and both amplitude and frequency of the ac-driving are relatively high. On the other hand, the noisy force $\eta(t)$ causes a smoothing of $\langle v \rangle$ and in parallel it enhances its magnitude. In particular, for a bias $\langle \eta(t) \rangle \approx 0.3$, the random force increases the average velocity by a factor of four in comparison to the application of a deterministic force F.

In Fig. 2(b), the regime of ANM is depicted. The characteristic feature is the emergence of an interval where for sufficiently large $\langle \eta(t) \rangle > 0$ the random force can induce negative average velocity $\langle v \rangle < 0$. Moreover, there exists an optimal value for the bias $\langle \eta(t) \rangle \approx 0.58$ at which the average velocity takes its minimal value. Most interesting is the fact that in the case of the stochastic force the minimal value of $\langle v \rangle$ is nearly two times lower than in the corresponding deterministic case. The origin of this effect is illustrated in Fig. 2(c), where we depict the average velocity $\langle v \rangle$ as a function of the spiking rate λ for fixed mean value $\langle \eta(t) \rangle = \sqrt{\lambda D_P} = 0.58$. We see that depending on the frequency λ of δ pulses we are dealing with three qualitatively different regimes. For small λ the Brownian motor is rarely kicked by large δ pulses (because the intensity D_P is large). This situation corresponds to normal, Ohmic-like transport behavior. On the contrary, when λ is sufficiently increased and the particle is very frequently kicked by small δ pulses. In this case the response of the system is anomalous and similar to the scenario when an equivalent

static, deterministic force acts [14]. The most interesting effect takes place for moderate λ. Then the motor operates in the anomalous regime, moves in the negative direction, and its average velocity is enhanced as compared to the case of the static force. There exists an optimal value of λ for which this effect is most pronounced, namely $\lambda = 151$. Moreover, the spiking rate λ also serves as a control parameter for the direction of motor movement.

B. Velocity fluctuations

Let us next discuss the relation between the average velocity and its fluctuations. This study is of relevance for the optimization of efficiency. In Figs. 2(d) and 2(e), the velocity variance σ_v is depicted as a function of the mean value of the white Poissonian noise $\langle \eta(t) \rangle$ and the corresponding static force F. Upon closer inspection one observes that the velocity fluctuations undergo rapid changes, yielding a large variance for small bias. This statement holds true regardless of the choice of the symmetry-breaking mechanism. Further increase of the random or deterministic bias leads to a decrease of the velocity fluctuations for both analyzed scenarios. However, when the motor is driven by the random force these fluctuations become reduced faster. This is clearly noticeable in the normal transport regime; see Fig. 2(d). The result seems to be counterintuitive as one would expect that the random force should enhance fluctuations. Furthermore, as is shown in Fig. 2(e), there exists an optimal value for bias $\langle \eta(t) \rangle$ at which the velocity fluctuations assume a minimal value. One should notice that this minimum nearly coincides with value of $\langle \eta(t) \rangle$ for which the negative average velocity in the anomalous regime take their minimal values; cf. Fig. 2(b). This bring us to the conclusion that the replacement of the deterministic force with the white generalized Poissonian noise not only decreases the negative-valued average velocity but simultaneously also minimizes its fluctuation behavior.

Figure 2(f) illustrates the impact of the spiking frequency λ on the velocity fluctuations for fixed mean $\langle \eta(t) \rangle = 0.58$ in the anomalous regime. When λ is very small the Brownian particle is rarely kicked with large δ pulses and its velocity undergoes rapid changes yielding a large variance. The opposite situation takes place in the case of a very large spiking frequency λ. For small to moderate λ the velocity fluctuations are smaller as compared to the case with the static force. Moreover, there exists an optimal value for the spiking frequency λ at which the velocity fluctuations are minimal.

C. Stokes efficiency

Of main interest is the overall efficiency of the Brownian motor operation. In Figs. 2(g) and 2(h) we depict the Stokes efficiency ε_S versus the mean $\langle \eta(t) \rangle$ and F. From its definition, the Stokes efficiency approaches zero for small statistical or deterministic bias values F. In both the normal and the anomalous transport regimes there occurs an optimal Stokes efficiency. By use of the biased random force, ε_S, this efficiency grows by a factor of 4 over the value obtained with a deterministic force. This effect is directly related to the property that the stochastic force enhances the absolute value of velocity and also minimize its fluctuations. Further increase of the bias leads to a decrease of the efficiency of the occurring transport process. For very large $\langle \eta(t) \rangle$ it approaches the value 1.

Figure 2(i) depicts the dependence of ε_S on the spiking rate λ for fixed $\langle \eta(t) \rangle$. The reader can observe two peaks. The first one corresponds to the regime of small λ which represents normal, Ohmic-like transport. This maximum is associated with the fact that in that case the Brownian motor moves with large positive average velocity and its fluctuations are moderate. The second peak is located in the ANM-transport regime. It occurs for medium spiking rates λ. When λ is large, then the transport process induced by this nonequilibrium noise approaches the behavior of the deterministic drive. This result corroborates with the previous statement concerning the qualitative equivalence between the white Poissonian noise and the deterministic force for very large spiking rates.

IV. SUMMARY

We have investigated two models of the inertial Brownian motors: one driven by the deterministic force F and the other propelled by biased nonequilibrium noise $\eta(t)$. We find domains in the parameters space such that when F is replaced by $\eta(t)$ of equal average bias, the motor velocity is several times greater, the velocity fluctuations are reduced several times, and its efficiency becomes several times enhanced within tailored parameter regimes, both in its normal and its absolute negative mobility regime. Specific results are detailed for generalized white Poissonian noise. The main conclusion remains valid, however, as well for other models of random perturbations (not depicted). Thus, the idea that random biased forces can be beneficial over deterministic biasing carries potential for practical realization in physics of Brownian motors. For example, it can be validated by use of a setup consisting of the resistively and capacitively shunted Josephson junction device operating in corresponding experimentally accessible regimes. An exemplary set of physical parameters in the ANM regime can be similar as in the experiment [27]. In order to evaluate this set, we follow the method described in Ref. [11]. For operational temperature $T = 4\text{K}$ and the set of parameters presented in the middle panels of Fig. 2, the critical Josephson current $I_c \approx 170\,\mu\text{A}$. For a realistic capacitance $C = 20\,\text{pF}$, the plasma frequency $\omega_p \approx 160\,\text{GHz}$. The amplitude of the ac current is $I_a \approx 240\,\mu\text{A}$, the ac-angular frequency is $\Omega \approx 96\,\text{GHz}$, and the dc current or the mean value of the Poisson noise is $I_d \approx 15.5\,\mu\text{A}$. Under these conditions, the negative-valued ANM voltage is $V \approx -15.7\,\mu\text{V}$ for the Poissonian noise case and $V \approx -7.9\,\mu\text{V}$ for the deterministic force.

The proposed mechanism of a "reduction of noise by noise" may explain exotic transport phenomena not only in physical but also in biological settings and, additionally, can be implemented in enhancing the working efficiency of synthetic molecular motors, all of which *in situ* operate in strongly fluctuating environments.

ACKNOWLEDGMENTS

This work was supported by the MNiSW program Diamond Grant (J.S.) and NCN Grant No. DEC-2013/09/B/ST3/01659 (J.Ł.).

[1] P. Hänggi and F. Marchesoni, Rev. Mod. Phys. **81**, 387 (2009).
[2] L. Gammaitoni, P. Hänggi, P. Jung, and F. Marchesoni, Rev. Mod. Phys. **70**, 223 (1998).
[3] M. Schliwa (ed.), *Molecular Motors* (Viley-VCH, Weinheim, 2003).
[4] E. R. Kay, Angew. Chem. Int. Ed. **46**, 72 (2007).
[5] R. Steuer, C. Zhou, and J. Kürths, Biosystems **72**, 241 (2003).
[6] P. C. Bressloff and J. M. Newby, Rev. Mod. Phys. **85**, 135 (2013).
[7] R. de J. León-Montiel and J. P. Torres, Phys. Rev. Lett. **110**, 218101 (2013).
[8] R. Gommers, S. Denisov, and F. Renzoni, Phys. Rev. Lett. **96**, 240604 (2006).
[9] R. Bustos-Marún, G. Refael, and F. von Oppen, Phys. Rev. Lett. **111**, 060802 (2013).
[10] S. W. D. Bailey, I. Amanatidis, and C. J. Lambert, Phys. Rev. Lett. **100**, 256802 (2008).
[11] M. Kostur, Ł. Machura, P. Talkner, P. Hänggi, and J. Łuczka, Phys. Rev. B **77**, 104509 (2008).
[12] L. Machura, M. Kostur, P. Talkner, J. Łuczka, and P. Hänggi, Phys. Rev. Lett. **98**, 040601 (2007).
[13] D. Speer, R. Eichhorn, and P. Reimann, Europhys. Lett. **79**, 10005 (2007).
[14] J. Spiechowicz, J. Łuczka, and P. Hänggi, J. Stat. Mech. (2013) P02044.
[15] P. Hänggi, Z. Phys. B **30**, 85 (1978); **36**, 271 (1980); **43**, 269 (1981).
[16] P. Jung and P. Hänggi, Phys. Rev. A **41**, 2977 (1990).
[17] P. Jung, Phys. Rep. **234**, 175 (1993).
[18] H. Wang and G. Oster, Europhys. Lett. **57**, 134 (2002).
[19] H. Wang, Appl. Math. Lett. **22**, 79 (2009).
[20] Ł. Machura, M. Kostur, P. Talkner, J. Łuczka, F. Marchesoni, and P. Hänggi, Phys. Rev. E **70**, 061105 (2004).
[21] Ł. Machura, M. Kostur, P. Talkner, P. Hänggi and J. Łuczka, Physica E **42**, 590 (2010), and references therein.
[22] P. Jung and F. Marchesoni, Chaos **21**, 047516 (2011).
[23] P. Jung, J. G. Kissner, and P. Hänggi, Phys. Rev. Lett. **76**, 3436 (1996).
[24] J. L. Mateos, Phys. Rev. Lett. **84**, 258 (2000).
[25] M. Januszewski and M. Kostur, Comp. Phys. Commun. **181**, 183 (2009).
[26] M. Kostur, Ł. Machura, J. Łuczka, P. Talkner, and P. Hänggi, Acta Phys. Polon. B **39**, 1115 (2008).
[27] J. Nagel, D. Speer, T. Gaber, A. Sterck, R. Eichhorn, P. Reimann, K. Ilin, M. Siegel, D. Koelle, and R. Kleiner, Phys. Rev. Lett. **100**, 217001 (2008).

APP Template V1.70 Article id: pstop510436 Typesetter: MPS Date received by MPS: 17/03/2015 PE: MAC003220 CE: LE:

IOP Publishing | Royal Swedish Academy of Sciences Physica Scripta

Phys. Scr. **00** (2015) 000000 (6pp)

Poissonian noise assisted transport in periodic systems

J Spiechowicz and J Łuczka

Institute of Physics, University of Silesia, Katowice, Poland

E-mail: jerzy.luczka@us.edu.pl

Received 2 April 2014
Accepted for publication 21 November 2014
Published DD MM 2015

Abstract

We revisit the problem of transport of a harmonically driven inertial particle moving in a *symmetric* periodic potential, subjected to *unbiased* non-equilibrium generalized white Poissonian noise and coupled to a thermal bath. Statistical asymmetry of Poissonian noise is sufficient to induce transport and under the presence of external harmonic driving this system exhibits a phenomenon of multiple velocity reversals. Consequently, one can manipulate the direction of transport by simply adjusting the parameters of externally applied forces.

SQ1 (Some figures may appear in colour only in the online journal)

1. Introduction

Transport of Brownian particles in periodic substrates can be controlled by a deterministic, external biased force [1]. Less trivial is the situation when control is performed by unbiased, zero-mean force [2, 3]. If additionally the unbiased force is random the method of transport control by such random perturbations is non-trivial. In this paper we revisit this problem and study an inertial particle moving in a symmetric, spatially periodic potential. The particle is driven by a simple harmonic force and subjected to both thermal equilibrium fluctuations and asymmetric Poissonian shot noise [4]. All forces acting on the particles are of zero mean and directed motion of the particle is induced by asymmetry of the Poissonian noise. We demonstrate that velocity reversal can be detected in the system and show how to conveniently manipulate the direction of the Brownian particle velocity.

The paper is organized as follows. In section 2 we recall details of the model under study. Section 3 is devoted to analysis of the transport characteristics of the Brownian particle. Last but not least, section 4 provides a summary and some conclusions.

2. Model

In what follows we concentrate on transport of a classical Brownian particle of mass M moving in one-dimensional geometry. Our model consists of the following elements: (i) the particle moves in a *symmetric* spatially periodic potential $V(x) = V(x + L) = \Delta V \sin(2\pi x/L)$ of period L, (ii) it is driven by an unbiased *symmetric* time-periodic force $A\cos\Omega t$ with amplitude A and angular frequency Ω, and (iii) it is coupled to a thermostat of temperature T. All three elements (i)–(iii) are symmetrical. Therefore the averaged velocity $\langle v\rangle$ of the particle is zero in the stationary regime. In order to obtain directed transport with $\langle v\rangle \neq 0$, symmetry has to be broken. We introduce the last element which breaks the symmetry, namely (iv) the zero-mean Poissonian shot noise $\eta(t)$. Now, the dynamics of the Brownian particle is determined by the Langevin equation in the form [4]

$$M\ddot{x} + \Gamma\dot{x} = -V'(x) + A\cos(\Omega t) + \eta(t) + \sqrt{2\Gamma k_B T}\,\xi(t), \tag{1}$$

where a dot and prime denote differentiation with respect to time t and the Brownian particle's coordinate x, respectively. *Symmetrical* thermal fluctuations due to the coupling of the particle with the thermostat are modelled by unbiased δ-correlated Gaussian white noise $\xi(t)$ of zero mean and unit intensity, so $\langle\xi(t)\rangle = 0$ and $\langle\xi(t)\xi(s)\rangle = \delta(t - s)$. The parameter Γ is the friction coefficient and k_B is the Boltzmann constant. The noise intensity factor $2\Gamma k_B T$ follows from the fluctuation–dissipation theorem [5–7] and ensures the canonical Gibbs state when $A = 0$ and $\eta(t) = 0$. All four forces in the rhs of equation (1) are of zero mean: the mean conservative force $\langle F(x)\rangle = -\langle V'(x)\rangle = 0$ over the space period L and the mean external driving $\langle f(t)\rangle = \langle A\cos(\Omega t)\rangle = 0$ over the time period $T = 2\pi/\Omega$.

The zero-mean non-equilibrium force $\eta(t)$ is chosen in the form of a random sequence of Dirac δ-shaped pulses with random amplitudes z_i defined in terms of generalized white *Poissonian shot noise*

$$\eta(t) = \sum_{i=1}^{n(t)} z_i \delta(t - t_i) - \lambda \langle z_i \rangle. \tag{2}$$

The random times t_i form a Poisson sequence, i.e., the probability that a sequence of k impulses occurs in the interval $(0, t)$ is given by the Poisson distribution

$$\Pr\{n(t) = k\} = \frac{(\lambda t)^k}{k!} e^{-\lambda t}. \tag{3}$$

The parameter λ is the mean number of δ-pulses per unit time. The amplitudes $\{z_i\}$ of the δ-pulses are independent random variables distributed according to a common probability density $\rho(z)$. As an example, we consider the density $\rho(z)$ in the exponential form

$$\rho(z) = \zeta^{-1}\theta(z)\exp(-z/\zeta), \tag{4}$$

where $\theta(z)$ denotes the Heaviside step function. Hence, the amplitudes take only positive values, $z_i > 0$. Their moments, according to (4), are given by the relation

$$\langle z_i^k \rangle = k!\zeta^k, \quad k = 1, 2, 3. \tag{5}$$

In particular, the mean value $\langle z \rangle = \zeta$ and it provides an interpretation of the parameter ζ. The process $\eta(t)$ is white noise of zero mean and the Dirac delta autocorrelation function, namely,

$$\langle \eta(t) \rangle = 0, \quad \langle \eta(t)\eta(s) \rangle = 2\lambda\zeta^2\delta(t - s). \tag{6}$$

The last equation defines the Poissonian noise intensity

$$D_P = \lambda\zeta^2. \tag{7}$$

Moreover, we assume that thermal equilibrium noise $\xi(t)$ is uncorrelated with non-equilibrium noise $\eta(t)$, so

$$\langle \xi(t)\eta(s) \rangle = \langle \xi(t) \rangle \langle \eta(s) \rangle = 0. \tag{8}$$

Such white Poissonian noise commonly occurs in various micro-structures [8] and is characterized by a *temporal asymmetry*, i.e. sharp δ-pulses of zero duration are followed by a constant negative bias which lasts over an exponentially distributed waiting time. In [9], it has been demonstrated that the white noise nature of such *additive*, *temporally asymmetric* fluctuations is sufficient to induce directed transport in periodic structures, in the presence and in the absence of an internal asymmetry. This should be contrasted with the case of *temporally symmetric* white Poissonian noise (i.e. with equally probable positive and negative amplitudes $\rho(z) = \rho(-z)$) which is able to generate a net macroscopic velocity only if the reflection symmetry of the periodic structure is broken, hence only for the so-called ratchet systems [3]. A directed transport emerges non-trivially if backward as well as forward transitions drive the particle and if no balancing between them takes place. The white Poissonian noise characterizes non-equilibrium fluctuations and therefore detailed balance does not hold. However, this alone does not guarantee a non-zero averaged particle velocity. The necessary condition is a source of *statistical asymmetry*. In the case of white Poissonian noise this asymmetry has its roots in the non-vanishing odd higher order cumulants, namely [10]

$$\begin{aligned} C_{2n+1}(t_1, ..., t_{2n+1}) &= \langle \eta(t_1) ... \eta(t_{2n+1}) \rangle \\ &= \lambda(2n + 1)!\zeta^{2n+1}\delta(t_1 - t_2) ... \delta(t_{2n} - t_{2n+1}), \end{aligned} \tag{9}$$

where $n = 1, 2, ...$ The reader should always remember that the statistics of the process $\eta(t)$ is given by all cumulants and according to the above equation it is clearly not symmetric. As a result, the backward and forward transitions are not equal and the directed transport can emerge.

Let us now introduce the dimensionless form of (1). This can be done in several different ways. Here we propose to use the period L as a length scale and for time the scale $\tau = L\sqrt{M/\Delta V}$ [4]. Then (1) can be rewritten in the form

$$\ddot{\hat{x}} + \gamma\dot{\hat{x}} = -\hat{V}'(\hat{x}) + a\cos(\omega\hat{t}) + \hat{\eta}(\hat{t}) + \sqrt{2\gamma D_G}\,\hat{\xi}(\hat{t}), \tag{10}$$

where $\hat{x} = x/L$ and $\hat{t} = t/\tau$. Other re-scaled dimensionless parameters are the friction coefficient $\gamma = \tau\Gamma/M$, the amplitude $a = LA/\Delta V$ and the angular frequency $\omega = \tau\Omega$ of the time-periodic driving. The rescaled potential $\hat{V}(\hat{x}) = V(L\hat{x})/\Delta V = \sin(2\pi\hat{x})$ possesses the unit period: $\hat{V}(\hat{x}) = \hat{V}(\hat{x} + 1)$. The rescaled zero-mean thermal noise has intensity $D_G = k_B T/\Delta V$ and the auto-correlation function $\langle \hat{\xi}(\hat{t})\hat{\xi}(\hat{s}) \rangle = \delta(\hat{t} - \hat{s})$. Similarly, the re-scaled zero-mean Poissonian white shot noise is δ-correlated: $\langle \hat{\eta}(\hat{t})\hat{\eta}(\hat{s}) \rangle = 2\hat{D}_P\delta(\hat{t} - \hat{s})$ with intensity $\hat{D}_p = \hat{\lambda}\langle \hat{z}_i^2 \rangle/2$, where $\hat{\lambda} = \tau\lambda$ and $\hat{z}_i = z_i/\sqrt{M\Delta V}$. Hereafter, we will use only dimensionless variables and shall omit the notation 'hat' in all quantities appearing in equation (10).

The most prominent transport quantity for the system (10) is the average dimensionless velocity $\langle \dot{x}(t) \rangle$ of the Brownian particle. In the long time limit, it can be presented in the form of a series of all possible harmonics, namely,

$$\lim_{t\to\infty} \langle \dot{x}(t) \rangle = \langle v \rangle + v_\omega(t) + v_{2\omega}(t) + ..., \tag{11}$$

where $\langle v \rangle$ is a dc (time-independent) component and $v_{n\omega}(t)$ are time-periodic functions which time-averaged over a basic period ω are zero . In this case the dc component $\langle v \rangle$ is obtained after averaging over the temporal period of the driving and the corresponding ensemble-average [11], namely, Q1

$$\langle v \rangle = \lim_{t\to\infty} \frac{\omega}{2\pi} \int_t^{t+2\pi/\omega} \prec \dot{x}(s) \succ ds, \tag{12}$$

where $\prec \cdot \succ$ denotes the average over noise realizations. In the deterministic case ($D_G = D_P = 0$), an additional averaging over initial conditions must be performed.

3. Transport properties

In order to obtain the relevant transport characteristics we have performed comprehensive numerical simulations of driven Langevin dynamics determined by equation (10). Details of the employed numerical scheme can be found in [12, 13]. We have set the time step to be $0.0005 \cdot 2\pi/\omega$ and for the initial conditions $\{x(0), \dot{x}(0)\}$ we used a uniform distribution over the interval [0, 1] and [−2, 2], respectively. Quantity of interest was ensemble-averaged over 10^3–10^4 different trajectories which evolved over 10^3–10^4 periods of the external AC driving. All numerical calculations were carried out using a CUDA environment implemented on a modern desktop GPU. This scheme allowed for a speed-up of a factor on the order of 10^3 times compared to a common present-day CPU method [14].

Let us start our analysis of transport properties of inertial Brownian particles described by (10) with a brief comment on the impact of the Poissonian noise parameters λ and D_P on its stochastic realizations. The reader can find detailed discussion on this topic in [4]. Here, we only mention two limiting cases. The first extreme regime is when both λ and D_P are large. Then the Brownian particle is very frequently kicked by large δ-pulses. Since the distance between two successive Poissonian arrival times is very short there are only a few moments when merely the negative valued bias of the process acts on the system. On the contrary, when both λ and D_P are small, the particle is very rarely kicked by weak δ-pulses. This also means that there are long periods of time in which the system is exposed only to the action of the negative bias of the non-equilibrium noise.

The equation given by (10) has a multidimensional parameter space, namely $\{\gamma, a, \omega, \lambda, D_P, D_G\}$. To eliminate one of them we first look at the dynamics in the case when $D_G = 0$. We limit our considerations to positive driving amplitudes a noting that the system (10) is invariant under changes of sign of a. It is sufficient to investigate low and moderate driving frequencies ω because under very fast positive and negative oscillations of driving the average velocity $\langle v \rangle$ cannot be induced. This procedure leaves us with five-dimensional parameter space, the detailed exploration of which is still hopeless numerically even for the powerful personal GPU supercomputers currently available. Therefore we present selected transport regimes which exhibit interesting behaviour. Figure 1 depicts the influence of variation of the Poissonian noise intensity D_P and the frequency λ of the Dirac δ-pulses on the velocity $\langle v \rangle$. Transport is negligibly small for both small and large values of the Poissonian noise intensity D_P regardless of the magnitude of the spiking rate λ. There are only two clear distinguished islands corresponding to the negative and positive velocity, respectively. Moreover, one can observe that for particular, fixed non-equilibrium noise intensities D_P the direction of transport is constant irrespective of the variation of the spiking frequency of the δ-kicks. Probably the most interesting is the existence of a wide window of the rates λ for which one can conveniently manipulate the direction of transport process by simply adjusting the noise intensity D_P. These findings are confirmed

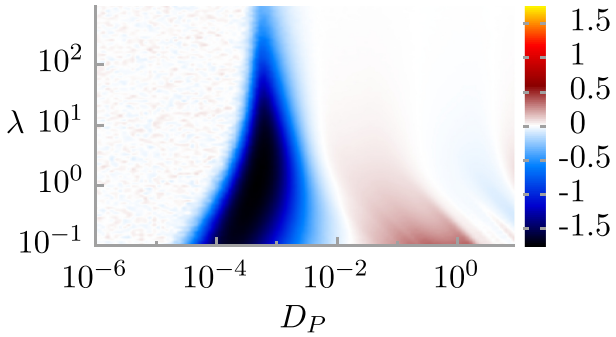

Figure 1. Regions of positive (red) and negative (blue) averaged velocity $\langle v \rangle$ in the parameter plane $\{D_P, \lambda\}$ of the white Poissonian noise intensity D_P and the spiking rate λ. Other parameters are: $a = 10.8$, $\omega = 3.77$, $\gamma = 1.04$ and $D_G = 0$.

in figure 2 where sample cuts of the previous panel are presented. In particular, panel (a) illustrates the dependence of the average velocity $\langle v \rangle$ on the Poissonian noise intensity D_P for several selected values of the spiking rate λ. According to the previous statement one can observe there the phenomenon of multiple velocity reversals [15–18] (see the case $\lambda = 1$). Moreover, it is seen that an increase of the frequency λ has a destructive impact on the modulus of the directed velocity $\langle v \rangle$. The non-equilibrium noise of very small and very large intensity cannot induce noticeable velocity. In panel (b) the same transport characteristic is depicted but versus the spiking rate λ for two Poissonian noise intensities D_P corresponding to the minimum and maximum of the curve presented in figure 2(a). It is worth noting that for both fixed noise intensities there is an optimal frequency λ to generate a non-zero velocity. However, its direction is constant regardless of the value of the spiking rate λ.

The next three panels are devoted to the role of the harmonic force in the transport process. In particular, the first depicts the same characteristic as in figure 2(a) but in the absence of the driving, i.e. when $a = 0$. One should note that, in line with earlier remarks for sufficiently large D_P, the white Poissonian noise is able to solely induce finite asymptotic long time average velocity $\langle v \rangle$. There is an optimal region of D_P in which the stationary velocity is maximal. However, for the case $a = 0$ there is no phenomenon of velocity reversal. Consequently, in this regime the harmonic driving force plays a crucial role and allows for steering of the direction of transport. Its significance is further analysed in the remaining two plots of figure 3. Panels (b) and (c) illustrate the average velocity $\langle v \rangle$ versus the amplitude a and the frequency ω of the harmonic driving, respectively. One can see there that the amplitude a can serve as a convenient parameter to manipulate the direction of transport. The same conclusion also holds true in the case of the frequency ω of the harmonic driving force (cf figure 3(c)). Furthermore, the dependence of the average velocity of the Brownian particle on the parameters of the driving $a\cos(\omega t)$ often depicts the resonance-like behaviour: small variation of their magnitude can lead to rapid changes of the sign and value of the velocity. For small non-equilibrium noise intensities $D_P \to 0$ the velocity $\langle v \rangle$ is

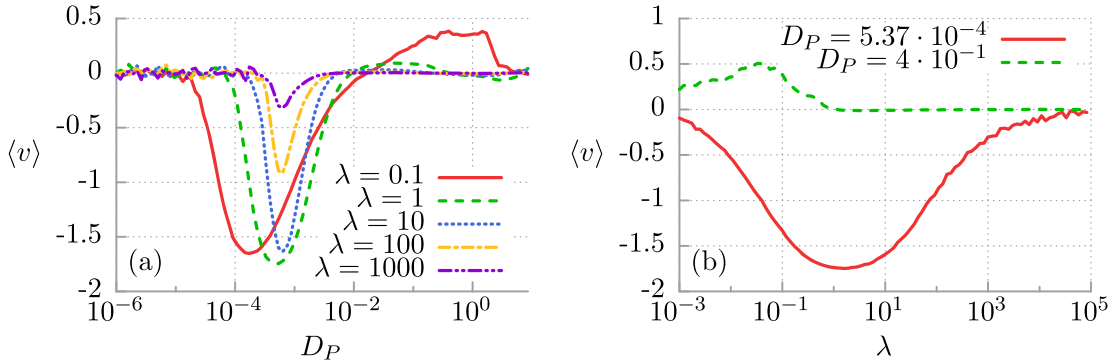

Figure 2. Averaged velocity of the Brownian particles $\langle v \rangle$ is presented as a function of the white Poissonian noise intensity D_P and the spiking frequency λ in the panel (a) and (b), respectively. Other parameters are the same as in figure 1.

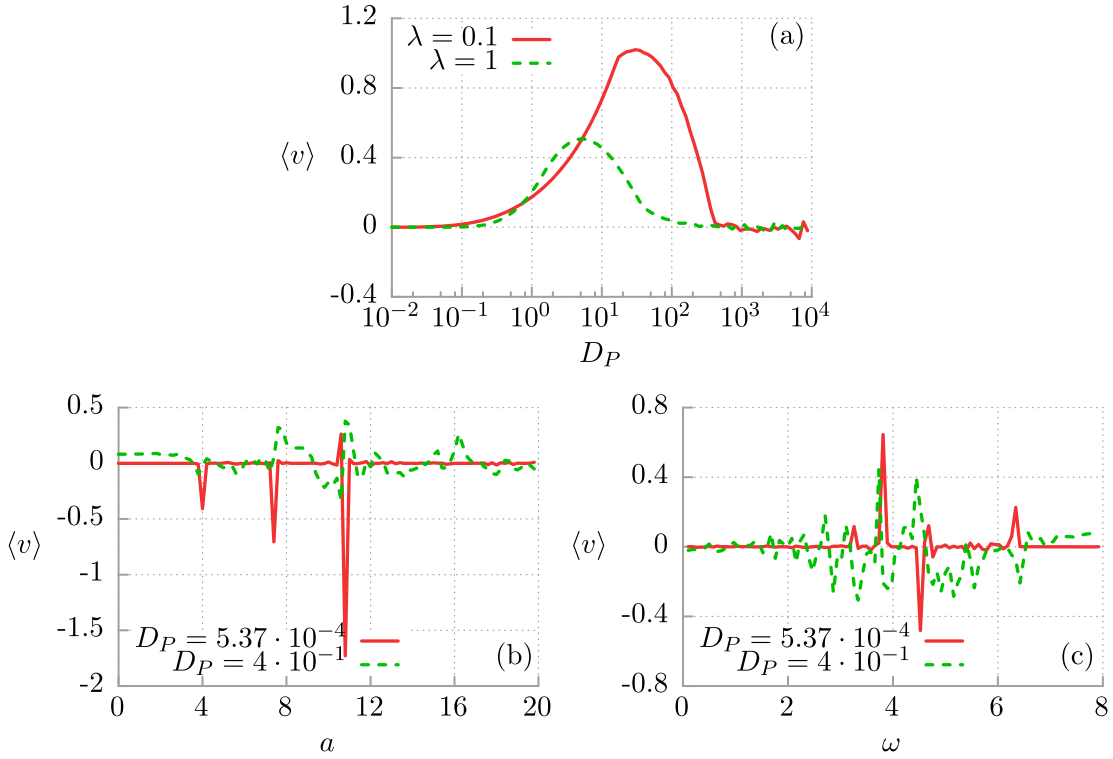

Figure 3. The role of the harmonic driving in the transport process. (a) The asymptotic long time average velocity $\langle v \rangle$ as a function of the white Poissonian noise intensity D_P in the absence of the harmonic driving force $a = 0$. (b) The dependence of the particle velocity on the amplitude a of the driving. (c) The influence of the variation of the frequency ω of the harmonic force on the average directed velocity $\langle v \rangle$. Other parameters are the same as in figure 1.

negligibly small in both of the limiting cases of $\omega \to 0$ and $\omega \to \infty$.

We now analyse the impact on the transport process of coupling the particle to a thermostat, see figure 4, where the average velocity $\langle v \rangle$ is plotted for different values of thermal noise intensity $D_G \propto T$. Temperature T has a smoothing effect on the plots, erasing the finer details of the structures visible in previous figures. This is to be expected, because the introduction of thermal noise causes additional random transitions between coexisting basins of attraction. The common opinion on thermal noise says that it has a negative impact on the transport processes. This case is also realized here. A careful inspection of figure 4(c) reveals that indeed an increase of thermal noise intensity leads to a decrease of the observed particle velocity. It is an example of the destructive influence of thermal noise on the transport process. However, both presented regimes are quite temperature resistant as the average velocity $\langle v \rangle$ starts to drop significantly only for high intensities of thermal fluctuations. The non-zero velocity is caused by stochastic, complex chaotic dynamics and even at zero temperature $D_G = 0$, the average velocity is non-zero.

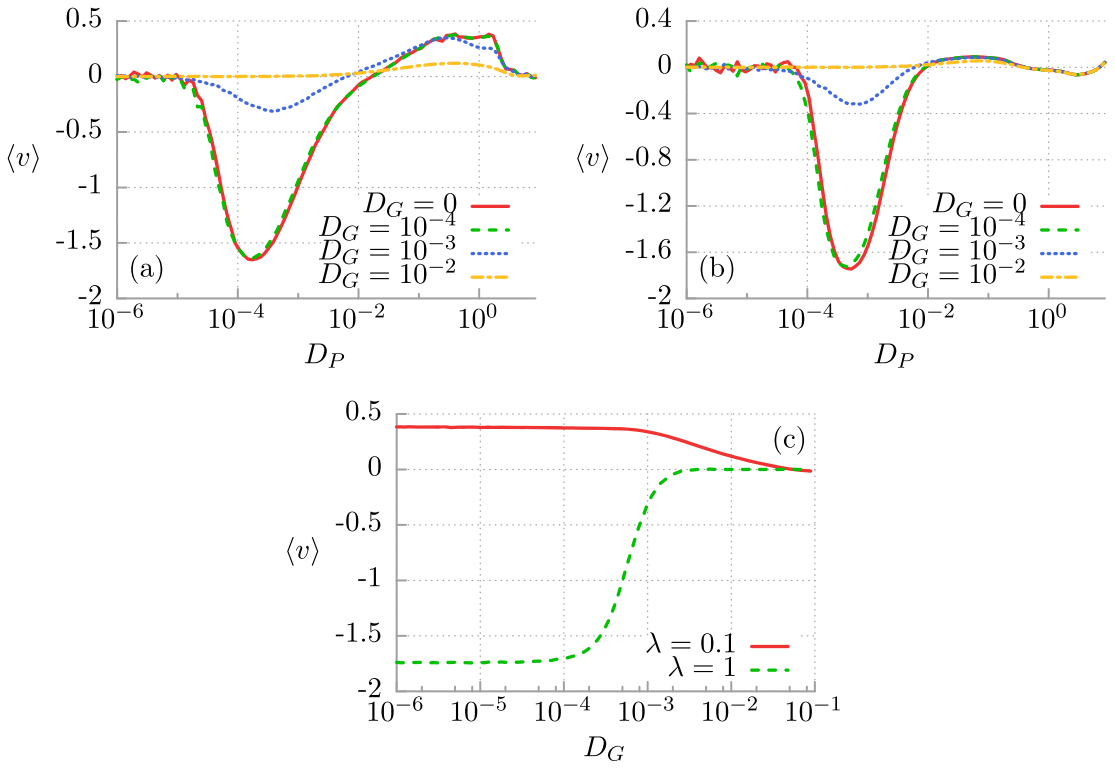

Figure 4. The role of the coupling of the particle to the heat bath in the observed transport process. (a), (b) The asymptotic long time average velocity $\langle v \rangle$ as a function of the white Poissonian noise intensity D_P for several different thermal noise intensities D_G and two spiking rates $\lambda = 0.1$ and $\lambda = 1$, respectively. (c) The dependence of the particle velocity on the thermal fluctuation intensity D_G for $\lambda = 0.1$, $D_P = 4 \cdot 10^{-1}$ (red, solid line) and $\lambda = 1$, $D_P = 5.37 \cdot 10^{-4}$ (green, dashed line). Other parameters are the same as in figure 1.

4. Summary

In this paper, we analysed the transport properties of inertial Brownian particles which move in a *symmetric* periodic potential and are subjected to both a *symmetric*, unbiased time-periodic external force and a *temporally asymmetric* generalized white Poissonian noise. First we demonstrated that the white noise nature of such temporally asymmetric fluctuations is sufficient to generate the directed transport of the under-damped system in the spatially periodic structure. Secondly, under the presence of the external harmonic driving it is possible to observe the phenomenon of multiple velocity reversals. One can conveniently manipulate the direction of the particle velocity by tuning of the parameters of unbiased time-periodic external force and the white Poissonian noise intensity. We have also elucidated that this transport phenomenon emerges as a result of statistical asymmetry of the non-equilibrium noise and is quite robust with respect to the variation of temperature.

Finally, let us recall that the Langevin equation (1) has a similar form as an equation of motion for the phase difference $\Psi = \Psi(t)$ between the macroscopic wave functions of the Cooper pairs on both sides of the Josephson junction. The quasi-classical dynamics of the resistively and capacitively shunted Josephson junction is well known in the literature as the Stewart–McCumber model [19–22]. Therefore our results can readily be experimentally tested with an accessible setup consisting of a single Josephson junction device operating in its quasi-classical regime.

Acknowledgments

JS is supported by the FORSZT project co-financed by the EU from the European Social Fund and JŁ is supported by the NCN grant DEC-2013/09/B/ST3/01659.

References

Q2

[1] Machura Ł, Kostur M, Talkner P, Łuczka J and Hänggi P 2007 *Phys. Rev. Lett.* **98** 40601
[2] Łuczka J 1999 *Physica* A **274** 200
[3] Hänggi P and Marchesoni F 2009 *Rev. Mod. Phys.* **81** 387
[4] Spiechowicz J, Łuczka J and Hänggi P 2013 *J. Stat. Mech.* P **02044**
[5] Kubo R 1966 *Rep. Prog. Phys.* **29** 255
[6] Zwanzig R 1973 *J. Stat. Phys.* **9** 215
[7] Łuczka J 2005 *Chaos* **15** 026107
[8] Czernik T, Kula J, Łuczka J and Hänggi P 1997 *Phys. Rev.* E **55** 4057
[9] Ram J, Bartussek R and Hänggi P 1995 *Europhys. Lett.* **31** 431
[10] Hänggi P, Bartussek R, Talkner P and Łuczka J 1996 *Europhys. Lett.* **35** 315
[11] Jung P 1993 *Phys. Rep.* **234** 175

[12] Kim C, Lee E, Hänggi P and Talkner P 2007 *Phys. Rev.* E **76** 011109
[13] Grigoriu M 2009 *Phys. Rev.* E 80 026704 181 183
[14] Januszewski M and Kostur M 2009 *Comp. Phys. Commun* **181** 183
[15] Jung P, Kissner J G and Hänggi P 1996 *Phys. Rev. Lett.* **76** 3436
[16] Mateos J L 2000 *Phys. Rev. Lett.* **84** 258
[17] Mateos J L 2003 *Physica* A **325** 92
[18] Kostur M and Łuczka J 2000 *Phys. Rev.* E **63** 021101
[19] Stewart W C 1968 *Appl. Phys. Lett.* **12** 277
[20] McCumber D E 1968 *J. Appl. Phys.* **39** 3113
[21] Barone A and Paternò G 1982 *Physics and Application of the Josephson Effect* (New York: Wiley)
[22] Kautz R L 1996 *Rep. Prog. Phys.* **59** 935

Josephson junction ratchet: The impact of finite capacitances

Jakub Spiechowicz,[1] Peter Hänggi,[2,3] and Jerzy Łuczka[1,4]
[1]*Institute of Physics, University of Silesia, 40-007 Katowice, Poland*
[2]*Institute of Physics, University of Augsburg, D-86135 Augsburg, Germany*
[3]*Nanosystems Initiative Munich, Schellingstrasse 4, D-80799 München, Germany*
[4]*Silesian Center for Education and Interdisciplinary Research, University of Silesia, 41-500 Chorzów, Poland*
(Received 1 July 2014; revised manuscript received 11 August 2014; published 27 August 2014)

We study transport in an asymmetric superconducting quantum interference device (SQUID) which is composed of a loop with three capacitively and resistively shunted Josephson junctions: two in series in one arm and the remaining one in the other arm. The loop is threaded by an external magnetic flux and the system is subjected to both a time-periodic and a constant current. We formulate the deterministic and, as well, the stochastic dynamics of the SQUID in terms of the Stewart-McCumber model and derive an equation for the phase difference across one arm, in which an effective periodic potential is of the ratchet type, i.e., its reflection symmetry is broken. In doing so, we extend and generalize an earlier study by Zapata *et al.* [Phys. Rev. Lett. **77**, 2292 (1996)] and analyze directed transport in wide parameter regimes: covering the overdamped to the moderate damping regime up to its fully underdamped regime. As a result we detect the intriguing features of a negative (differential) conductance, repeated voltage reversals, noise-induced voltage reversals, and solely thermal noise-induced ratchet currents. We identify a set of parameters for which the ratchet effect is most pronounced and show how the direction of transport can be controlled by tailoring the external magnetic flux.

DOI: 10.1103/PhysRevB.90.054520 PACS number(s): 74.25.F−, 85.25.Dq, 05.40.−a, 05.60.−k

I. INTRODUCTION

Josephson junctions are physical devices of prominent, widespread scientific and practical use. Moreover, these can be used in testing the fundamentals of quantum mechanics and in studies for the many faces of chaotic complexity in classical physics. Scientists exploit them for a multitude of diverse theoretical and experimental studies. Applications in physics, electronics, and other branches of engineering are well established: magnetometers, superconducting quantum interference devices (SQUIDs), superconducting qubits, rapid single-flux-quantum circuitry—all use a Josephson junction as a primary building block. Here, we engineer a SQUID device which is composed of three Josephson junctions and behaves as a physical ratchet system, i.e., a periodic structure which exhibits reflection-symmetry breaking [1–4].

A similar system was analyzed in Ref. [5] for the overdamped case of resistively shunted Josephson junctions. Here, we extend the study to include inertial effects by accounting for a finite capacitance (mass). This therefore leads to a modeling of the capacitively and resistively shunted cases. In terms of classical mechanics, the former corresponds to the overdamped Brownian motion dynamics while the latter includes both finite dissipation and observable inertial effects. This extension is nontrivial because in the latter case the system allows for classical chaos. When the SQUID is driven by both a time-periodic and a constant current, it exhibits anomalous transport behavior including an absolute negative conductance in the linear response regime and negative static resistance in the nonlinear response regime.

This paper is organized as follows. In Sec. II we describe the circuit with three Josephson junctions and derive an equation which governs the dynamics of the studied system. Section III contains a detailed analysis of the deterministic transport processes occurring in our working model. In Sec. IV we study the role of thermal noise on the dynamics of the system. In Sec. V we seek the regime for which the ratchet effect arising in the device is most pronounced. In Sec. VI we propose the method of controlling the voltage direction by an external magnetic flux. Last but not least, Sec. VII provides a summary and conclusions. In the Appendix we derive an expression for the voltage across the SQUID.

II. MODEL

We study transport properties of an experimental realization of the rocking ratchet mechanism in an asymmetric superconducting quantum interference device [5–11]. We analyze the current-voltage characteristics in the framework of the Stewart-McCumber theory [12,13]. The Stewart-McCumber model describes the semiclassical regime of a small Josephson junction for which a spatial dependence of characteristics can be neglected. Let us recall that in this theory the current $I(t)$ flowing through the junction is split into three components: the displacement current associated with its capacitance C, the normal Ohmic current due the finite resistance R of the junction, and the supercurrent of Cooper pairs characterized by the critical current J. Its explicit form reads

$$I(t) = C\dot{V}(t) + \frac{V(t)}{R} + J\sin\varphi(t), \tag{1}$$

where $\varphi(t)$ is the phase difference between the macroscopic wave functions of the Cooper electrons in both sides of the junction, an overdot denotes differentiation with respect to time t, and $V(t)$ is the voltage across the device which obeys the Josephson relation [14]

$$V(t) = \frac{\hbar}{2e}\dot{\varphi}(t). \tag{2}$$

If we insert (2) into (1) and include according to the fluctuation-dissipation relation [15] the effect of a nonzero temperature $T > 0$ by adding Johnson-Nyquist noise, the above

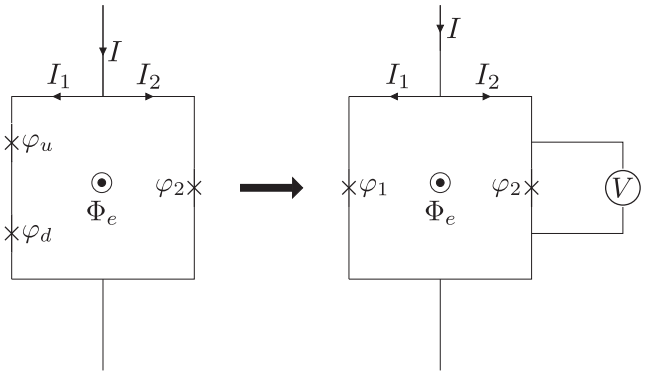

FIG. 1. The asymmetric SQUID composed of three Josephson junctions and the equivalent circuit composed of two junctions, where the Josephson phase difference is $\varphi_1 = \varphi_u + \varphi_d$. The physical quantity of interest is the long-time average voltage V across the SQUID which is expressed by the relation $V = \hbar\langle\dot{\varphi}_1\rangle/2e = \hbar\langle\dot{\varphi}_2\rangle/2e$; see Eq. (A1) in the Appendix.

Stewart-McCumber equation takes the form

$$I(t) = \frac{\hbar}{2e}C\ddot{\varphi} + \frac{\hbar}{2e}\frac{1}{R}\dot{\varphi} + J\sin\varphi + \sqrt{\frac{2k_BT}{R}}\,\xi(t), \qquad (3)$$

where $\varphi \equiv \varphi(t)$, k_B is the Boltzmann constant and thermal fluctuations are modeled by δ-correlated Gaussian white noise $\xi(t)$ of zero mean and unit intensity,

$$\langle\xi(t)\rangle = 0, \quad \langle\xi(t)\xi(s)\rangle = \delta(t-s). \qquad (4)$$

Following the proposal in Refs. [5,9] we consider a SQUID ratchet which is composed of three Josephson junctions as sketched in Fig. 1. The loop contains two Josephson junctions in series in the left arm and one junction in the other arm. All elements are shunted with resistances (R_u, R_d, R_2) and corresponding capacitances (C_u, C_d, C_2). We safely can ignore the individual subgap resistances of the unshunted junctions, those being much larger than the shunt resistances. Moreover, the loop is pierced by an external magnetic flux Φ_e. For each element in the left arm, exposed to the Kirchhoff left-arm current $I_1(t)$, we can write the Stewart-McCumber relation

$$I_1(t) = \frac{\hbar}{2e}C_u\ddot{\varphi}_u + \frac{\hbar}{2e}\frac{1}{R_u}\dot{\varphi}_u + J_u\sin\varphi_u + \sqrt{\frac{2k_BT}{R_u}}\,\xi_u(t), \qquad (5a)$$

$$I_1(t) = \frac{\hbar}{2e}C_d\ddot{\varphi}_d + \frac{\hbar}{2e}\frac{1}{R_d}\dot{\varphi}_d + J_d\sin\varphi_d + \sqrt{\frac{2k_BT}{R_d}}\,\xi_d(t), \qquad (5b)$$

where $\xi_u(t)$ and $\xi_d(t)$ are independent Gaussian white noises of the same statistics as in (4). The processes $\xi_u(t)$ and $\xi_d(t)$ have to be independent to ensure the physically correct equilibrium Gibbs state.

Next, we consider the case when the two junctions in the left arm are identical, i.e., $J_u = J_d \equiv J_1, R_u = R_d \equiv R_1/2, C_u = C_d \equiv 2C_1$. Using these equal parameters we make us of the fact that ideally the supercurrent in the *left arm* is conserved. Therefore, we find that the realizations of the two phase solutions are synchronous in the absence of the two noise terms for the same initial conditions and temperature $T = 0$. This singles out the unique and equal phases $\varphi_u = \varphi_d$. It implies that a solution of (5a) also obeys (5b) with the same imposed left-arm current $I_1(t)$ [5,9]. The Kirchhoff law remains valid also in the presence of current noise with the identical (now random) left-arm current $I_1(t)$. Because of the additional inhomogeneous Nyquist current noise term in each junction, however, the two solutions generally no longer stay perfectly synchronized. Assuming small noise intensities for the two thermal independent Gaussian noise sources of equal strength, we approximate the phases as being synchronized nevertheless, i.e., $\varphi_u = \varphi_d = \varphi_1/2$, with $\varphi_1 \equiv \varphi_u + \varphi_d$. Taking half of each relation in (5a) and (5b) and adding gives for the stochastic current $I_1(t)$ the result

$$\begin{aligned} I_1(t) = {} & \frac{\hbar}{2e}C_1\frac{d^2}{dt^2}(\varphi_u + \varphi_d) + \frac{\hbar}{2e}\frac{1}{R_1}\frac{d}{dt}(\varphi_u + \varphi_d) \\ & + J_1\sin\left(\frac{\varphi_u + \varphi_d}{2}\right)\cos\left(\frac{\varphi_u - \varphi_d}{2}\right) \\ & + \sqrt{\frac{k_BT}{R_1}}\,\xi_u(t) + \sqrt{\frac{k_BT}{R_1}}\,\xi_d(t). \end{aligned} \qquad (6)$$

With equal solutions $\varphi_u = \varphi_d$ this expression yields the Langevin equation

$$I_1(t) = \frac{\hbar}{2e}C_1\ddot{\varphi}_1 + \frac{\hbar}{2e}\frac{1}{R_1}\dot{\varphi}_1 + J_1\sin\left(\frac{\varphi_1}{2}\right) + \sqrt{\frac{2k_BT}{R_1}}\,\xi_1(t). \qquad (7)$$

Here, we used the fact that the linear combination of two independent Gaussian white noises of intensities $D_u = k_BT/2R_u$ and $D_d = k_BT/2R_d$ gives again Gaussian white noise with the total intensity described by $D_1 = D_u + D_d = 2k_BT/R_1$. Note that the stochastic process in (7) amounts to a Johnson-Nyquist thermal noise for an overall shunt resistance $R_1 \equiv 2R_u = 2R_d$.

From the above analysis it follows that two identical junctions in series can be considered as one for which the supercurrent-phase relation assumes the form $J_1\sin(\varphi_1/2)$ [5,16,17]. This result was obtained in Ref. [16] in the framework of the Ginzburg-Landau theory; cf. Eq. (23) therein.

Let us discuss the above assumed synchronized phase approximation in the presence of small current noise in more detail. In the overdamped limit ($C_1 = 0$) this result agrees for identical junctions in the left arm with that used for the three-junction SQUID rocking ratchet experiment investigated by Sterck *et al.* [9]; see Eqs. (4)–(7) therein. In reality, however, slightly different junction parameters will physically lead to asynchronous phase variations in the two junctions in the left arm. Likewise, finite temperatures will, as indicated above, also destroy the perfect synchronous motion of the noisy solutions $\varphi_u = \varphi_d$, as assumed above at all times. However, the actual temperatures are experimentally very *small* [7,9]. As it turns out, the physical ratchet effect for the average voltage emerging from this approximation itself remains *robust*. The latter has been verified before with simulations in the overdamped limit and also has been tested from experimental evidence in the corresponding low-temperature

limit. It was validated explicitly (i) numerically in [5,9] and also (ii) experimentally for the three-junction SQUID ratchet setup realized in the works [9,11]. Put differently, because we focus here on the Josephson voltage across the device, i.e., the *average behavior* of the rate of change of the phase φ_1 but not on explicit stochastic values, the substitution of the $\cos[(\varphi_u - \varphi_d)/2]$ term by unity is justified in practice, as the corrections due to higher moments of the asynchronous phase difference can be safely neglected. In addition it must be kept in mind that the use of the Stewart-McCumber model is itself an approximation. Therefore, our theoretical predictions following from (7) must be used as a guide towards "physical reality" for the experimenter rather than taken as granted without "error" [5,9,17].

For the junction in the right arm, the Stewart-McCumber equation reads

$$I_2(t) = \frac{\hbar}{2e} C_2 \ddot{\varphi}_2 + \frac{\hbar}{2e}\frac{1}{R_2}\dot{\varphi}_2 + J_2 \sin\varphi_2 + \sqrt{\frac{2k_BT}{R_2}}\,\xi_2(t). \tag{8}$$

We next add the constraint for the phases in the loop threaded by the magnetic flux [18]

$$\varphi_2 - \varphi_1 = 2\pi\frac{\Phi}{\Phi_0}, \tag{9}$$

where $\Phi_0 = h/2e$ is the flux quantum and the actual flux Φ is a sum of the external flux Φ_e and the flux due to the flow of currents,

$$\Phi = \Phi_e + Li(t), \tag{10}$$

where L is the loop inductance and $i(t)$ is the *circulating* current which tends to screen the magnetic flux. If the current is fed to the loop symmetrically then $i(t) = I_1(t) - I_2(t)$. An asymmetric case is presented in the Appendix. We consider the scenario when the second contribution is small, namely,

$$|Li(t)| \ll \Phi_0. \tag{11}$$

In this regime the internal flux increases monotonically with the external one and this operating mode is often called "dispersive" [18]. Then, from Eqs. (9)–(11) we find

$$\varphi_2 = \varphi_1 + \tilde{\Phi}_e, \quad \tilde{\Phi}_e = 2\pi\frac{\Phi_e}{\Phi_0}. \tag{12}$$

The total current $I(t)$ flowing through the SQUID is

$$I(t) = I_1(t) + I_2(t). \tag{13}$$

We insert $I_1(t)$ and $I_2(t)$ from (7) and (8) and use (12) to eliminate φ_2. The result is

$$\frac{\hbar}{2e}C\ddot{\varphi}_1 + \frac{\hbar}{2e}\frac{1}{R}\dot{\varphi}_1 = -J_1\sin\left(\frac{\varphi_1}{2}\right) - J_2\sin(\varphi_1 + \tilde{\Phi}_e) + I(t) - \sqrt{\frac{2k_BT}{R}}\,\xi(t), \tag{14}$$

where $C = C_1 + C_2$ and $R^{-1} = R_1^{-1} + R_2^{-1}$. The Gaussian white noise $\xi(t)$ is a linear combinations of $\xi_1(t)$ and $\xi_2(t)$ and has the same statistics as in (4); cf. the similar transformation from (6) to (7).

Let the device be driven by an additional external current $I(t)$ which is composed of the static dc bias I_0 and the ac driving of amplitude A and angular frequency Ω, i.e.,

$$I(t) = I_0 + A\cos(\Omega t). \tag{15}$$

The mean value over the period $2\pi/\Omega$ is constant, $\langle I(t)\rangle = I_0$. As a consequence we obtain that

$$\frac{d\langle I(t)\rangle}{dt} = \frac{d\langle I_1(t)\rangle}{dt} + \frac{d\langle I_2(t)\rangle}{dt} = 0. \tag{16}$$

In the Appendix, we show that in this case the voltage V across the SQUID, averaged over the period of the ac current, is given by the relation

$$V = \frac{\hbar}{2e}\langle\dot{\varphi}_1\rangle, \tag{17}$$

where φ_1 is a solution of (14) and $\langle\cdot\rangle$ denotes a temporal average over one period of the ac current.

Going to a dimensionless formulation

We next transform (14) into its dimensionless form. This can be achieved in several ways. It is known [19] that for such a system there are four characteristic frequencies: the plasma frequency $\omega_p^2 = 2eJ_1/\hbar C$, the characteristic frequency of the junction $\omega_c = 2eRJ_1/\hbar$, the frequency $\omega_r = 1/RC$ related to the relaxation time, and the frequency Ω of the ac current. There are three independent characteristic time scales related to these frequencies (note that $\omega_p^2 = \omega_c\omega_r$). Here, we follow [5] and define the new phase x and the dimensionless time $\hat{t}$ as

$$x = \frac{\varphi + \pi}{2}, \quad \hat{t} = \frac{t}{\tau_c}, \quad \tau_c = \frac{\hbar}{eRJ_1}. \tag{18}$$

The corresponding dimensionless form of (14) reads

$$\tilde{C}\ddot{x}(\hat{t}) + \dot{x}(\hat{t}) = -U'(x(\hat{t})) + F + a\cos(\omega\hat{t}) + \sqrt{2D}\,\hat{\xi}(\hat{t}), \tag{19}$$

where the overdot and prime denote differentiation over the dimensionless time $\hat{t}$ and the phase x, respectively. We introduced a spatially periodic potential $U(x)$ of period 2π of the following form [5]:

$$U(x) = -\sin(x) - \frac{j}{2}\sin(2x + \tilde{\Phi}_e - \pi/2). \tag{20}$$

This potential is reflection symmetric if there exists x_0 such that $U(x_0 + x) = U(x_0 - x)$ for any x. If $j \neq 0$, it is generally asymmetric and its reflection symmetry is broken. We classify this characteristic as a ratchet potential. However, even for $j \neq 0$ there are certain values of the external flux $\tilde{\Phi}_e$ for which it is is still symmetric. The dimensionless capacitance $\tilde{C}$ is the ratio between two characteristic time scales $\tilde{C} = \tau_r/\tau_c$, where the relaxation time is $\tau_r = RC$. Other rescaled parameters are $j = J_2/J_1$, $F = I_0/J_1$, $a = A/J_1$, and $\omega = \Omega\tau_c$. It is worth noting that the noise intensity $D = ek_BT/\hbar J_1$ is the quotient of the thermal energy and the Josephson coupling energy. The rescaled Gaussian white noise is of vanishing mean and the autocorrelation function $\langle\hat{\xi}(\hat{t})\hat{\xi}(\hat{s})\rangle = \delta(\hat{t} - \hat{s})$. Hereafter, we shall use only dimensionless variables and shall omit the caret notation in all quantities appearing in (19). In Fig. 2, the ratchet potential $U(x)$ is shown for $j = 1/2$ and two values of

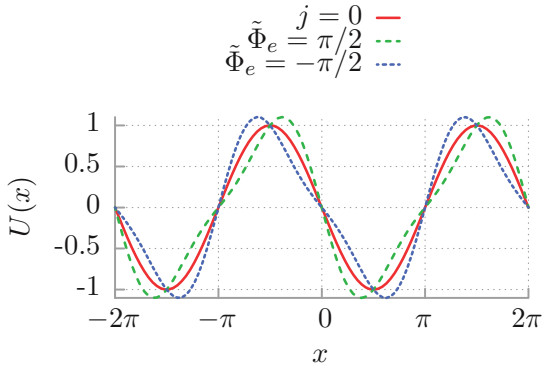

FIG. 2. (Color online) The symmetric potential $U(x) = -\sin(x)$ for $j = 0$ (solid red line) is depicted in comparison with the ratchet potential given by (20) for $j = 1/2$ and two values of the external magnetic flux $\tilde{\Phi}_e = \pi/2$ (dashed green line) and $\tilde{\Phi}_e = -\pi/2$ (dotted blue line).

the external magnetic flux $\tilde{\Phi}_e = \pi/2$ (positive "polarity") and $\tilde{\Phi}_e = -\pi/2$ (negative "polarity"). The symmetric potential for $j = 0$ is also depicted. We would like to add that (19) has a mechanical interpretation: it is identical to the Langevin equation of a classical Brownian particle of mass $m = \tilde{C}$ (i) moving in a spatially periodic ratchet potential $U(x)$, (ii) being rocked by an unbiased harmonic force $a\cos(\omega t)$, and (iii) exposed to a static force F. In this mechanical framework the phase x and the voltage V translate to the space coordinate and the velocity of the Brownian particle, respectively.

The most important characteristic of the transport behavior of the SQUID is the current-voltage curve in the stationary regime. The voltage (17) or its dimensionless counterpart $\langle v\rangle = \langle \dot{x}\rangle$ is determined by (19). In the long-time limit, it takes the form of a Fourier series over all harmonics [20], namely,

$$\lim_{t\to\infty}\langle \dot{x}(t)\rangle = \langle v\rangle + v_\omega(t) + v_{2\omega}(t) + \cdots, \tag{21}$$

where $\langle v\rangle$ is a dc (time-independent) component and $v_{n\omega}(t)$ are time-periodic functions of zero average over a basic period $2\pi/\omega$. In this case the dc component $\langle v\rangle$ is obtained after averaging over both the temporal period of the driving and the corresponding ensemble [20],

$$\langle v\rangle = \lim_{t\to\infty}\frac{\omega}{2\pi}\int_t^{t+2\pi/\omega}\mathbb{E}[\dot{x}(s)]\,ds, \tag{22}$$

where $\mathbb{E}[\dot{x}(s)]$ denotes an average over initial conditions and all realizations of the thermal noise. The actual stationary voltage is then given as

$$V = RJ_1\langle v\rangle. \tag{23}$$

Because the SQUID is driven by the external current (15), the system is far away from thermal equilibrium and a time-dependent nonequilibrium state is reached in the long-time limit. The key ingredient for the occurrence of directed transport $\langle v\rangle \neq 0$ is the symmetry breaking. This is the case when the dc current $F \neq 0$ or the reflection symmetry of the potential $U(x)$ is broken.

III. DETERMINISTIC DYNAMICS

First, let us consider the corresponding deterministic version of the Langevin equation (19), i.e., we formally set $D = 0$. This is not the manifest realistic physical situation as thermal noise is present as well. However, it can help to understand general properties of the system. When $D = 0$, (19) is equivalent to a system of three autonomous differential equations of the first order and the phase space is three dimensional. It is a minimal dimension for chaotic behavior to occur. Indeed, periodic, quasiperiodic, and chaotic trajectories can be detected. A rough classification can be made into locked states in which the motion of x is bounded to a few spatial periods and running states in which it is unlimited in the space of x. The latter are crucial for the occurrence of deterministic transport. For some regimes, ergodicity is broken and a systematic nonzero voltage emerges with its sign depending on the choice of selected initial conditions. However, in the presence of small noise the system typically becomes ergodic and transitions between possibly coexisting deterministic disjoint attractors are probable. In particular, this give rise to diffusive directed transport.

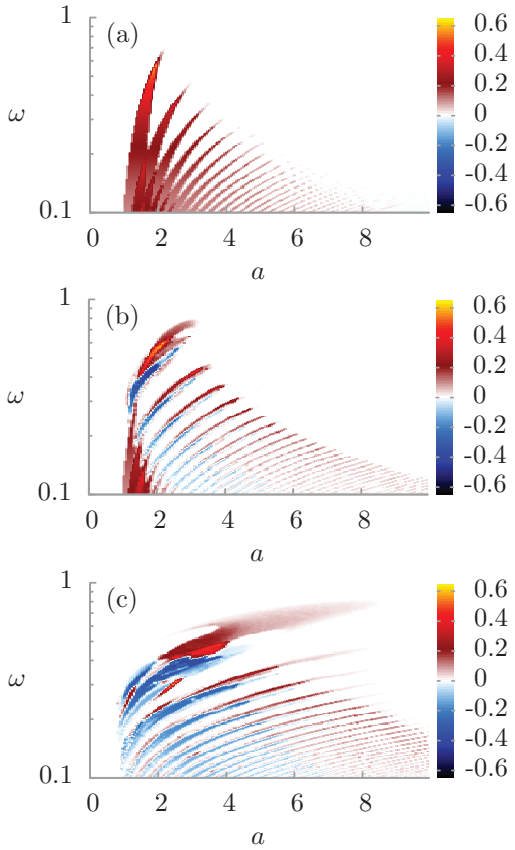

FIG. 3. (Color online) The deterministic transport behavior as a function of ac driving strength a and its angular frequency ω of the dynamics in (19) within three distinct regimes: (a) overdamped regime ($\tilde{C} = 0.2$), (b) moderate damping regime ($\tilde{C} = 2$), and (c) underdamped regime ($\tilde{C} = 7$). The average voltage $\langle v\rangle$ is presented for vanishing bias $F = 0$ and thermal noise $D = 0$. The periodic potential $U(x)$ has a positive polarity: $j = 1/2$ and $\tilde{\Phi}_e = \pi/2$.

In order to obtain the relevant transport characteristics we have to resort to comprehensive numerical simulations of driven Langevin dynamics. We integrated (19) by employing a weak version of the stochastic second-order predictor-corrector algorithm [21] with a time step typically set to about $10^{-3}\times 2\pi/\omega$. Since (19) is a second-order differential equation, we have to specify two initial conditions, $x(0)$ and $\dot{x}(0)$. Moreover, because for some regimes the system may be nonergodic in order to avoid the dependence of the presented results on the specific selection of initial conditions, we have chosen phases $x(0)$ and dimensionless voltages $\dot{x}(0)$ equally distributed over the intervals $[0,2\pi]$ and $[-2,2]$, respectively. All quantities of interest were ensemble averaged over 10^3–10^4 different trajectories which evolved over 10^3–10^4 periods of the external ac driving. Numerical calculations were done by use of a CUDA environment implemented on a modern desktop GPU. This scheme allowed for a speed-up of a factor of the order of 10^3 times as compared to a common present-day CPU method [22].

A. General behavior

The system described by (19) possesses a five-dimensional parameter space $\{\tilde{C},a,\omega,F,D\}$. In this section we consider the deterministic case $D=0$. Let us study the nontrivial ratchet effect by putting $F=0$. Then, all forces on the right-hand side of (19) are zero on average: the mean potential force $-\langle U'(x)\rangle = 0$ on the interval $[x,x+2\pi]$ and the average ac driving $\langle a\cos(\omega t)\rangle = 0$ on the time interval $[t,t+2\pi/\omega]$. If $\langle v\rangle \neq 0$, we detect the ratchet effect. Now, the parameter space $\{\tilde{C},a,\omega\}$ is three dimensional and its exploration is tractable numerically with the currently available personal GPU computers. Depending on the value of the dimensionless capacitance $\tilde{C}$ the device can operate in three distinct regimes: overdamped ($\tilde{C}\ll 1$), moderate ($\tilde{C}\sim 1$), and underdamped ($\tilde{C}\gg 1$). The first regime has been extensively studied in Refs. [5,6,9–11]. In particular, it is known that in the deterministic case the average voltage $\langle v\rangle$ is almost quantized, displaying Shapiro-like steps in the current-voltage characteristic for adiabatic and nonadiabatic ac driving frequencies ω. As long as the potential $U(x)$ is asymmetric, generally $\langle v\rangle \neq 0$ with $F=0$ [23,24]. Since very fast positive and negative changes of the driving current cannot induce a nonzero average voltage, it is sufficient to limit our considerations to low and moderate ac driving frequencies ω. We have performed scans of the parameter space: $\tilde{C}\times a\times\omega \in [0.1;10]\times[0;10]\times[0.1;1]$ at a resolution of 200 points per interval to determine the general behavior of the system. The results are depicted in Fig. 3 for the positive polarity of the potential $U(x)$, i.e., for the external magnetic flux $\tilde{\Phi}_e = \pi/2$; cf. Fig. 2.

On all (a,ω) cuts, there occurs no ratchet effect for $a<1$ and high driving frequencies ω. The domains of nonzero average voltage $\langle v\rangle$ have a striped structure. Although there is no obvious direct connection to chaotic properties of the system, we have found that for regimes where the ratchet effect is present a chaotic behavior is typically observed. For a fixed amplitude a, the ratchet behavior generally tends to disappear as the frequency ω grows. On the other hand, for a fixed frequency ω, there is an optimal amplitude a that maximizes the ratchet effect. The increase of the capacitance $\tilde{C}$ causes the appearance of regions for which the average voltage $\langle v\rangle$ reverses its sign. This should be contrasted with

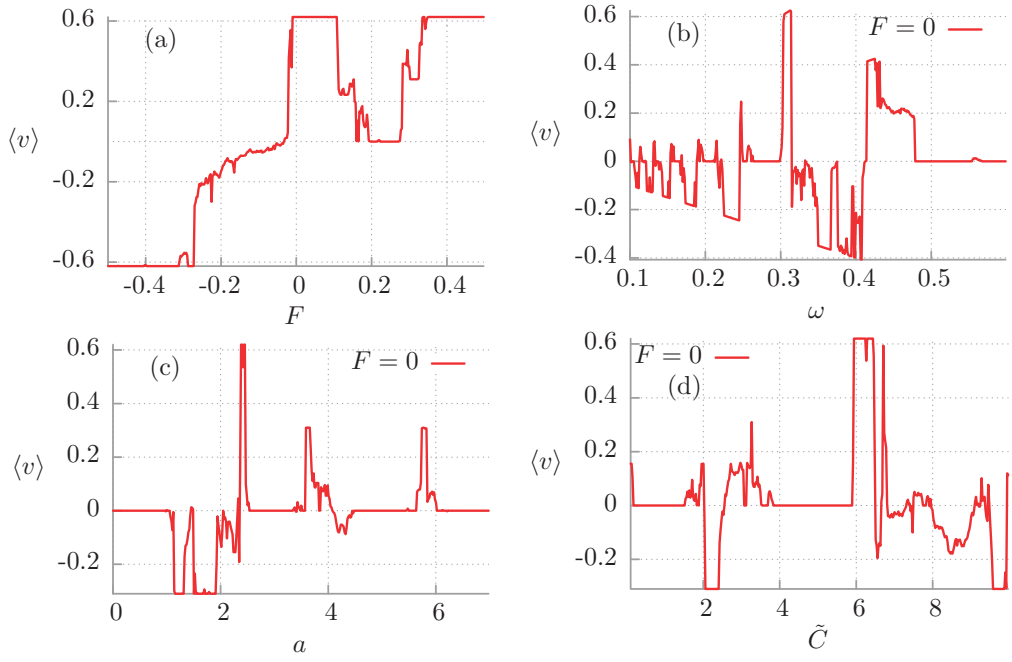

FIG. 4. (Color online) Representative transport characteristics of the rocked SQUID in the deterministic regime ($D=0$) and for the potential $U(x)$ with a positive polarity: $j=1/2$ and $\tilde{\Phi}_e=\pi/2$. (a) Current-voltage curve for driving strength $a=2.4$, driving angular frequency $\omega=0.31$, and capacitance $\tilde{C}=6.31$. (b) Dependence of the average voltage $\langle v\rangle$ on the ac driving frequency ω. (c) Influence of the ac driving amplitude a on the dc voltage. (d) Dependence of the average voltage $\langle v\rangle$ on the SQUID capacitance $\tilde{C}$. Remaining parameters in (b)–(d) are the same as in (a).

the overdamped regime in which the average voltage drop across the device is never negative for a potential with positive polarity. Consequently, the capacitance $\tilde{C}$ of the device together with the amplitude a and frequency ω of the ac driving can serve as convenient parameters to manipulate the direction of transport processes occurring in the system (19).

B. Voltage vs dc current: Negative conductance

Because the dynamics determined by (19) is nonlinear and the system is multidimensional, it should not come as surprise that the current-voltage curve is also nonlinear and often depicts a nonmonotonic function of the system parameters. Typically, the average voltage $\langle v\rangle$ is an increasing function of the dc current F. This is true especially for large F. Such regimes correspond in the parameter space to normal, Ohmic-like transport behavior. However, there are also regimes of anomalous transport exhibiting negative conductance [25]: If the average voltage $\langle v\rangle$ is a decreasing function of the static bias F, the differential conductance

$$\mu(F) = \left[\frac{dv(F)}{dF}\right]^{-1} \tag{24}$$

can take negative values within some interval of F. Such a situation is depicted in Fig. 4(a). Clearly, there are several windows of the static current F for which this effect is observed. It is worth noting that this phenomenon is missing in the overdamped regime ($\tilde{C} \to 0$) or in the absence of ac driving [26,27]. Moreover, in Fig. 4(a) we show the ratchet effect: for $F = 0$ the voltage is nonzero and for small negative dc current, $F < 0$, the voltage is positive, $\langle v\rangle > 0$. The latter phenomenon is named absolute negative conductance [28].

C. Multiple voltage reversals

According to the previous statement, on the basis of general scans in the parameter space, the typical transport characteristics depicted in Fig. 4 exhibit multiple reversals of the voltage $\langle v\rangle$ for the zero dc current, $F = 0$. However, it should be stressed that this effect is not present in the overdamped regime ($\tilde{C} \to 0$) when for a fixed potential polarity the voltage has a fixed sign. The phenomenon of multiple voltage reversal [29–32] is most pronounced for moderate values of the amplitude a and the frequency ω of the time-oscillating harmonic driving. In Figs. 4(b)–4(d) we observe several local extrema and one global maximum of the voltage. For the increasing capacitance $\tilde{C}$ there are more regions in the parameter space for which this effect occurs. One can conveniently manipulate the direction of transport processes occurring in the system just by variation of its capacitance $\tilde{C}$, amplitude a, or frequency ω.

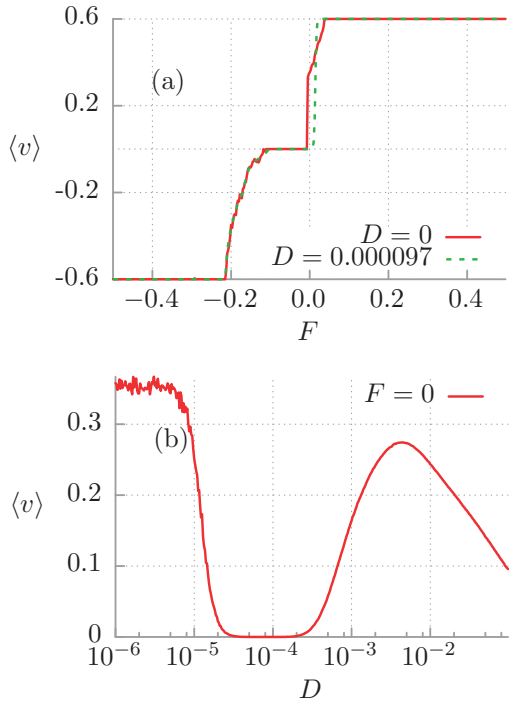

FIG. 5. (Color online) Destructive influence of thermal noise on the ratchet effect. (a) The current-voltage characteristic is presented in the deterministic limit ($D = 0$, solid red line) and for the thermal-noise-driven case ($D = 9.7\times10^{-5}$, dashed green line) case. (b) The dependence of the average voltage $\langle v\rangle$ on the thermal noise intensity D for vanishing bias $F = 0$. The remaining parameters are $a = 1.9$, $\omega = 0.6$, and $\tilde{C} = 0.645$. The potential $U(x)$ has the positive polarity: $j = 1/2$ and $\tilde{\Phi}_e = \pi/2$.

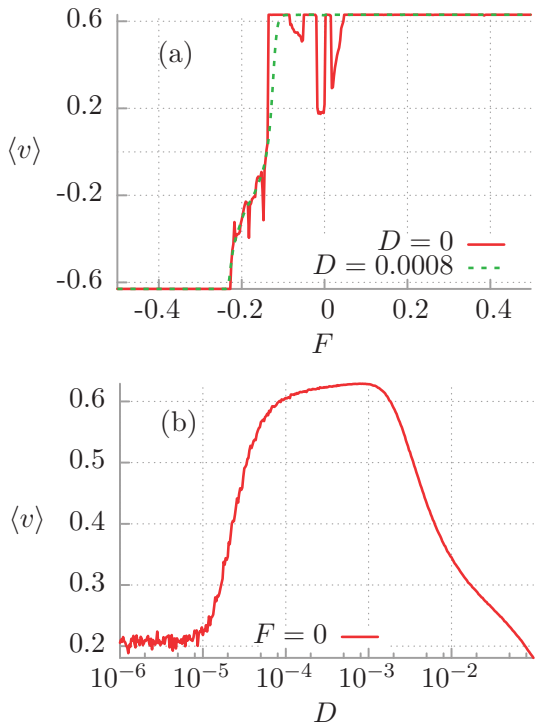

FIG. 6. (Color online) Constructive influence of thermal noise on the ratchet effect. (a) The current-voltage characteristics is presented in the deterministic limit ($D = 0$, solid red line) and the noise-driven case ($D = 0.0008$, dashed green line) case. (b) The dependence of the average voltage $\langle v\rangle$ on the thermal noise intensity D. The remaining parameters are $a = 2.3, \omega = 0.63, \tilde{C} = 1.98, j = 1/2$, and $\tilde{\Phi}_e = \pi/2$.

IV. ROLE OF THERMAL NOISE

We can expect that thermal noise perturbs deterministic dynamics and can thus reduce or even destroy some deterministic effects. However, more interesting are the regimes for which it can enhance or induce new features for the system dynamics. We analyze the role of thermal fluctuations and discuss the influence of temperature on the stationary voltage. The regimes presented below are optimal in the sense that the effects are most pronounced for the illustrated parameter domains.

A. Destructive role of thermal fluctuations

An example of a regime where thermal fluctuations play a destructive role is illustrated with Fig. 5. Figure 5(b) shows the dependence of the stationary average voltage $\langle v\rangle$ on the thermal noise intensity or temperature, $D \propto T$. A careful inspection of that figure reveals that indeed there is a window of temperature for which the dc voltage is practically zero. One should also note that a small increase of temperature causes a sharp reduction of the voltage $\langle v\rangle$ and therefore this phenomenon can be useful to trap the phase x in one of the potential wells [33–35]. In Fig. 5(a) we depict the current-voltage curves for the deterministic $D = 0$ and noisy $D = 9.7\times10^{-5}$ cases. Essentially, temperature plays a destructive role: there is no ratchet effect for the noise intensity D corresponding to the minimum of the curve in Fig. 5(b).

B. Constructive role of thermal fluctuations

The opposite scenario occurs when thermal noise has a positive effect on relevant transport characteristics. It means that the voltage exhibits a maximum as a function of the thermal noise intensity D. In the mechanical framework it is equivalent to the situation when the mean first passage time for the particle to escape over the potential barrier is shortened by the increase of the thermal noise intensity D. This effect is exemplified in Fig. 6. Figure 6(b) shows the dependence of the average voltage $\langle v\rangle$ on temperature. Evidently, its increase causes an increase in the voltage. There is an optimal temperature, corresponding to $D \approx 0.0008$, for which the voltage $\langle v\rangle$ assumes a maximal value. This finding is confirmed in the current-voltage curve presented in Fig. 6(a). Temperature plays a constructive role; the ratchet effect is strengthened by noise.

C. Noise-induced voltage reversals

We have found a regime where thermal fluctuations are able to reverse the dc voltage from positive to negative values and vice versa. Such regimes are illustrated in Fig. 7. In Fig. 7(b) the first situation is presented: the average voltage $\langle v\rangle$ is negative in the deterministic limit and increases with increasing temperature. There is a critical value of the thermal noise intensity D for which the dc voltage changes its sign and becomes positive for higher temperature. Figure 7(a) shows the current-voltage curves corresponding to this regime. At this point it is worth noting that for this set of parameters the phenomenon of negative differential conductance is also detected. In particular, we can observe that this effect is robust with respect to small changes of the thermal noise intensity D. Figures 7(c) and 7(d) depict the opposite scenario: starting

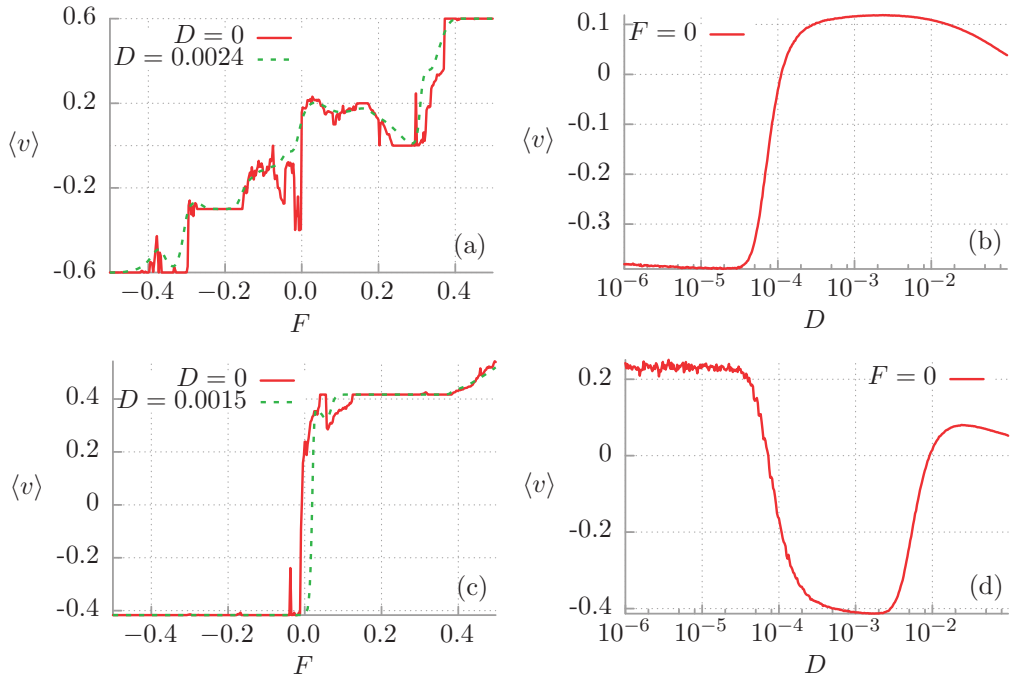

FIG. 7. (Color online) Destructive influence of thermal noise on the ratchet effect. In (a) and (b) thermal noise may reverse the sign of the dc voltage from negative to positive in comparison to the deterministic case. (c) and (d) depict an opposite situation when the sign is shifted from positive to negative. Parameters for (a) and (b) read $a = 1.7$, $\omega = 0.2$, and $\tilde{C} = 7.97$. For (c) and (d) they are as follows: $a = 3.2$, $\omega = 0.417$, $\tilde{C} = 7$. The parameters of the potential $U(x)$ are $j = 1/2$ and $\tilde{\Phi}_e = \pi/2$.

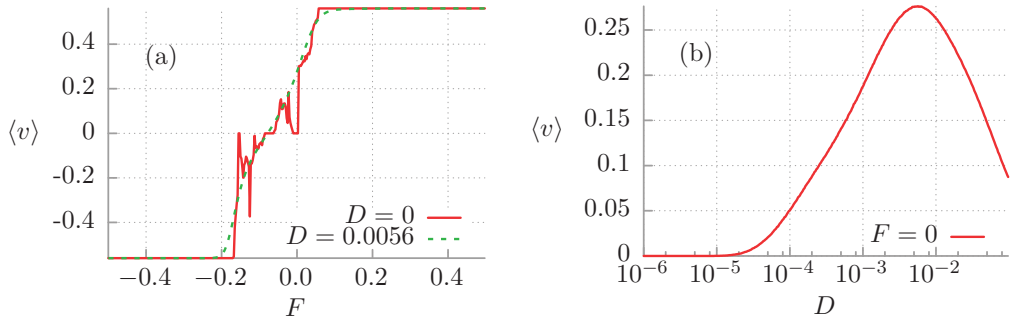

FIG. 8. (Color online) Noise-induced ratchet effect. (a) shows the current-voltage characteristic in this regime. (b) depicts the dependence of the average voltage $\langle v\rangle$ on the thermal noise intensity D in the absence of a bias $F = 0$. Other parameters are $a = 1.8$, $\omega = 0.56$, $\tilde{C} = 1$, $j = 1/2$, and $\tilde{\Phi}_e = \pi/2$.

from low temperature the increase of D changes the voltage from positive to negative values.

D. Noise-induced ratchet effect

The next interesting phenomenon, which is activated by thermal fluctuations, is the noise-induced ratchet effect. It corresponds to the situation when there is no directed transport in the deterministic regime $D = 0$ for vanishing static dc bias $F = 0$ but it is observed when the thermal noise intensity is nonzero, $D \neq 0$. Such a scenario is depicted in Fig. 8: The average voltage $\langle v\rangle$ vanishes for low thermal noise intensity D and starts to increase with increasing temperature. There emerges also an optimal value of the thermal noise intensity $D \approx 0.0056$ for which the ratchet effect becomes most pronounced. This regime can be considered as a special case of a constructive influence of thermal noise on the ratchet phenomenon. Our finding is confirmed in the current-voltage curve which is presented in Fig. 8(a).

V. TAILORING THE RATCHET CURRENT

Modern personal GPU computers have given us the opportunity to scan the parameter space of the system with high resolution in a reasonable time and therefore we were able to find a regime for which the ratchet effect is *globally* maximal; see Fig. 9. All transport characteristics corresponding to this set of parameters are presented below. It turns out that the ratchet effect is optimal in the moderate capacitance regime $\tilde{C} \approx 1.65$, for the moderate amplitude $a \approx 2.25$, and the frequency $\omega \approx 0.638$ of the time-oscillating current. Moreover, there are several clearly indicated peaks in the dependence of the dc voltage on the system parameters. The effect of thermal noise on the ratchet effect is destructive for this set of parameters. However, it is worth noting that this regime is temperature

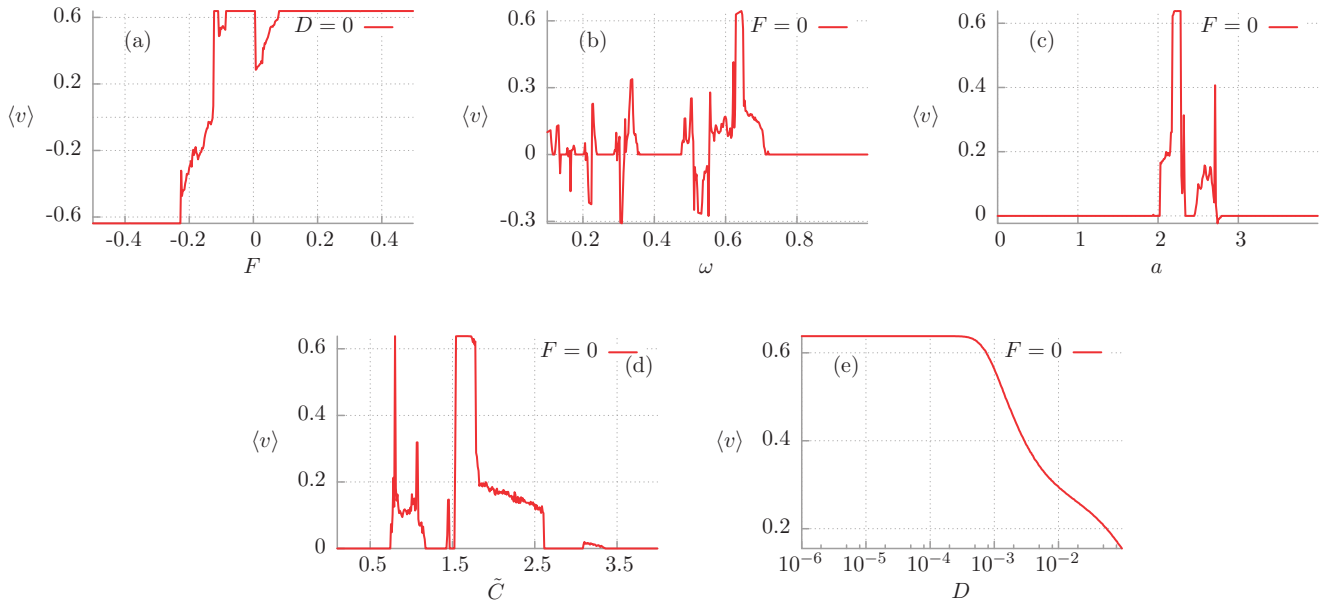

FIG. 9. (Color online) Optimal regime for the occurrence of the ratchet transport. The dependence of the average voltage $\langle v\rangle$ on the static dc bias F, the angular frequency ω, amplitude a, capacitance $\tilde{C}$, and thermal noise intensity D is presented in (a)–(e). The chosen parameters are $D = 0$, $F = 0$, $a = 2.25$, $\omega = 0.638$, $\tilde{C} = 1.65$, $j = 1/2$, and $\tilde{\Phi}_e = \pi/2$.

robust because the average voltage $\langle v \rangle$ starts to decrease significantly only for thermal noise intensities higher than $D \approx 5\times10^{-4}$; cf. Fig. 9(e).

VI. CONTROL OF TRANSPORT BY EXTERNAL MAGNETIC FLUX

Transport measured as the stationary dc voltage can be controlled in several ways. It seems that from the experimental point of view the simplest way is to vary the dc current F or an external constant magnetic flux $\tilde{\Phi}_e$. We first consider the unbiased domain with $F = 0$. In Fig. 10 we depict how the dc voltage behaves in the parameter plane $\{\tilde{\Phi}_e, \tilde{C}\}$ for two cases: $D = 0$ [Fig. 10(a)] and $D = 10^{-3}$ [Fig. 10(b)]. The most important feature of these plots is the symmetry with respect to the magnetic flux $\tilde{\Phi}_e$. For an arbitrary integer number n, the transformation $\tilde{\Phi}_e \to 2\pi n - \tilde{\Phi}_e$ reverses the polarity of the potential (20) and as a consequence reverses also the voltage sign. The geometric structure of the domains in the depicted regime of the $\{\tilde{\Phi}_e, \tilde{C}\}$ variation is complex. There are islands of positive and negative voltage.

For the deterministic case ($D = 0$) we reveal the refined structure. Some of these regions survive when the temperature is increased while others disappear. We detect a few robust regimes for which "islands" of nonzero voltage persist. It is seen that if the capacitance is fixed at the proper value the direction of transport can be changed by the magnetic field. In some regions, several voltage reversals can be obtained by use of this method. If the dc current is applied, the above symmetry is destroyed. This case is shown in Fig. 11. However, there are still regimes where the magnetic field is a relevant control parameter for the direction of transport.

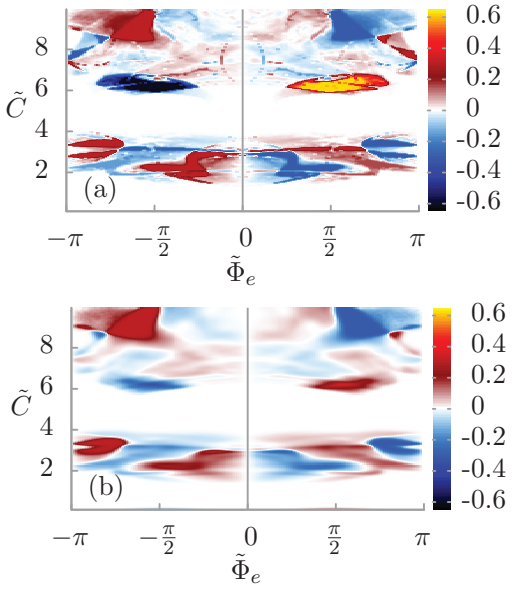

FIG. 10. (Color online) Voltage across the the rocked SQUID in the parameter plane $\{\tilde{\Phi}_e, \tilde{C}\}$. Upper panel: The deterministic case $D = 0$. Lower panel: The role of temperature $D = 10^{-3}$. The dc current is absent, i.e., $F = 0$. The remaining parameters are $a = 2.4$, $\omega = 0.31, j = 1/2$.

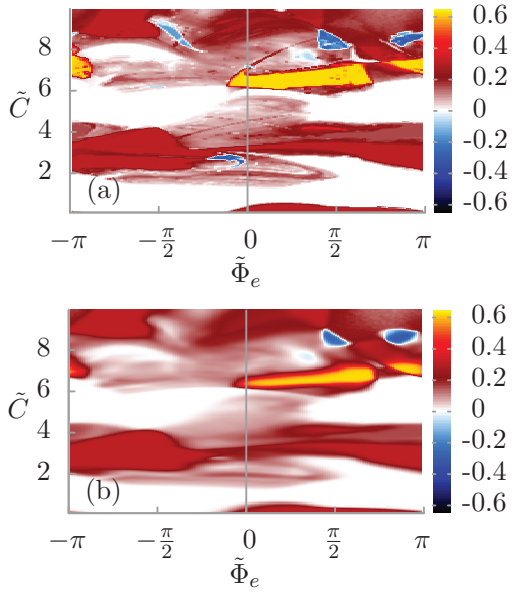

FIG. 11. (Color online) Voltage across the the rocked SQUID in the parameter plane $\{\Phi_e, \tilde{C}\}$. Upper panel: the deterministic case $D = 0$. Lower panel: influence of temperature $D = 10^{-3}$. The dc current $F = 0.1$. The remaining parameters are $a = 2.4$, $\omega = 0.31, j = 1/2$.

VII. SUMMARY

We analyzed the characteristics of the voltage across an asymmetric SQUID device composed of three capacitively and resistively shunted Josephson junctions which are threaded by a magnetic flux. We derived the evolution equation which governs the dynamics of the phase across the SQUID. The effective potential experienced by the phase displays a symmetry breaking in the form of a ratchet potential. Under the influence of an oscillating current source, the current-voltage characteristic yields the possibility to obtain a finite dc voltage in the presence of a vanishing dc current, i.e., a ratchet effect is obtained. Within a tailored range of parameters, the same sign of the dc voltage can be obtained regardless of the sign of the external dc current.

With this comprehensive study we have taken into consideration the role of a finite capacitance of the SQUID. As a consequence, the resulting ratchet dynamics becomes rather rich, giving rise to features which are absent in the overdamped limit. With the help of the computational power of modern GPU computers we have identified a whole range of interesting phenomena inherent in the ratchet current. These are a negative (differential) conductance, repeated dc voltage reversals, noise-induced dc voltage reversals, and particular forms of solely noise-induced ratchet features. For given tailored sets of parameters the ratchet voltage assumes optimal values. Last but not least, we have been able to detect the set of parameters for which the ratchet effect is globally maximal and demonstrated how the direction of transport can be manipulated by tailoring the threading external magnetic flux.

The main goal of this work was the exploration and identification of parameter regimes for directed ratchet transport in realistic SQUID devices possessing *finite* capacitances. Such

a study is of relevance for applications which make use of generation and control of the induced ratchet voltages, their direction (sign), magnitude, and intrinsic sensitive dependence on system parameters.

Other transport quantifiers concerning the overall quality of the inertia-induced transport, such as the nature of the ratchet-voltage fluctuations (yielding in turn a diffusion dynamics of the phase across the SQUID), or the efficiency of the device [36–39] have not been addressed here. Given the underlying complexity of the inertial ratchet dynamics these numerical studies are even more cumbersome than the ones presented.

Finally, an interesting question concerns the robustness of our results with respect to slightly different junction parameters in series; an assumed exact mathematically equality of parameters for two junctions is in practice difficult to achieve. This question has been answered in the positive for the case of the overdamped regime [5], where it was found that the corresponding results remain robust. For the underdamped regime, the complexity of the problem becomes even more highly multidimensional and therefore this task is presently beyond the scope of this work. Nevertheless, those additional aspects are on our agenda when the corresponding cumbersome numerical investigations become technically more feasible.

ACKNOWLEDGMENTS

This work was supported in part by the MNiSW program Diamond Grant (J.S.), NCN Grant No. DEC-2013/09/B/ST3/01659 (J.Ł.), and by a Grant No. HA1517/-2 from the Deutsche Forschungsgemeinschaft (DFG) (P.H.). The authors also wish to thank Peter Talkner for constructive discussions.

APPENDIX: VOLTAGE ACROSS THE ASYMMETRIC SQUID

We demonstrate that in the "dispersive" operating mode of the SQUID, i.e., when the condition (11) holds true, the averaged voltage developed across the SQUID can be expressed in the form

$$V = \frac{\hbar}{2e}\langle\dot{\varphi}_1\rangle = \frac{\hbar}{2e}\langle\dot{\varphi}_2\rangle. \tag{A1}$$

We follow the method presented in Ref. [40] and consider an asymmetric junction configuration for which the total flux is

$$\Phi = \Phi_e + \Phi_1 + \Phi_2 = \Phi_e + \mathcal{L}_1 I_1(t) - \mathcal{L}_2 I_2(t), \tag{A2}$$

where Φ_1 and Φ_2 are the fluxes produced by the currents $I_1(t)$ and $I_2(t)$, respectively. The coefficients $\mathcal{L}_1$ and $\mathcal{L}_2$ are related to the loop inductance via the relation

$$L = \mathcal{L}_1 + \mathcal{L}_2. \tag{A3}$$

The total voltage across the SQUID calculated along the left arm is the sum

$$V = V_1 + L_1\langle\dot{I}_1(t)\rangle + M\langle\dot{I}_2(t)\rangle. \tag{A4}$$

Similarly, along the right side we have

$$V = V_2 + L_2\langle\dot{I}_2(t)\rangle + M\langle\dot{I}_1(t)\rangle, \tag{A5}$$

where L_1 and L_2 are the self-inductances of the left and the right arm, respectively. Generally, they are different from $\mathcal{L}_i$; see Refs. [40,41]. The mutual inductance between the two arms is M and

$$V_i = \frac{\hbar}{2e}\langle\dot{\varphi}_i\rangle, \quad i = 1,2, \tag{A6}$$

are the voltage drops across the left and right junctions, respectively. Now, we use (16) to get

$$V = V_1 + L_1\langle\dot{I}_1(t)\rangle - M\langle\dot{I}_1(t)\rangle, \tag{A7a}$$

$$V = V_2 - L_2\langle\dot{I}_1(t)\rangle + M\langle\dot{I}_1(t)\rangle. \tag{A7b}$$

Adding both sides of these equations and utilizing (A6) yields

$$2V = (\hbar/2e)(\langle\dot{\varphi}_1\rangle + \langle\dot{\varphi}_2\rangle) + (L_1 - L_2)\langle\dot{I}_1(t)\rangle. \tag{A8}$$

By differentiating (12) and making use of (16) we obtain

$$\begin{aligned}\frac{\hbar}{2e}(\langle\dot{\varphi}_1\rangle - \langle\dot{\varphi}_2\rangle) &= \frac{2\pi}{\Phi_0}\dot{\Phi} = \frac{2\pi}{\Phi_0}(\mathcal{L}_2\langle\dot{I}_2(t)\rangle - \mathcal{L}_1\langle\dot{I}_1(t)\rangle) \\ &= -\frac{2\pi}{\Phi_0}(\mathcal{L}_1 + \mathcal{L}_2)\langle\dot{I}_1(t)\rangle. \end{aligned}\tag{A9}$$

From this equation we calculate $\langle\dot{I}_1(t)\rangle$ and insert it into (A8) to obtain

$$2V = \left(\frac{\hbar}{2e} + \epsilon\right)\langle\dot{\varphi}_1\rangle + \left(\frac{\hbar}{2e} - \epsilon\right)\langle\dot{\varphi}_2\rangle, \tag{A10}$$

where

$$\epsilon = \frac{1}{L}(L_1 - L_2). \tag{A11}$$

Up to here we used (16). From (11) and (12) it follows that $\langle\dot{\varphi}_1\rangle = \langle\dot{\varphi}_2\rangle$. In this case the result (A1) follows directly from the result in (A10).

[1] P. Hänggi and F. Marchesoni, Rev. Mod. Phys. **81**, 387 (2009).
[2] R. D. Astumian and P. Hänggi, Phys. Today **55**(11), 33 (2002).
[3] P. Hänggi, F. Marchesoni, and F. Nori, Ann. Phys. (NY) **14**, 51 (2005).
[4] P. Reimann and P. Hänggi, Appl. Phys. A **75**, 169 (2014).
[5] I. Zapata, R. Bartussek, F. Sols, and P. Hänggi, Phys. Rev. Lett. **77**, 2292 (1996).
[6] S. Weiss, D. Koelle, J. Müller, R. Gross, and K. Barthel, Europhys. Lett. **51**, 499 (2000).
[7] A. Sterck, S. Weiss, and D. Koelle, Appl. Phys. A **75**, 253 (2002).
[8] J. Berger, Phys. Rev. B **70**, 024524 (2004).
[9] A. Sterck, R. Kleiner, and D. Koelle, Phys. Rev. Lett. **95**, 177006 (2005).
[10] S. Savel'ev, A. L. Rakhmanov, and F. Nori, Phys. Rev. E **72**, 056136 (2005).

[11] A. Sterck, D. Koelle, and R. Kleiner, Phys. Rev. Lett. **103**, 047001 (2009).
[12] W. C. Stewart, Appl. Phys. Lett. **12**, 277 (1968).
[13] D. E. McCumber, J. Appl. Phys. **39**, 3113 (1968).
[14] B. D. Josephson, Phys. Lett. **1**, 251 (1962).
[15] R. Kubo, Rep. Prog. Phys. **29**, 255 (1966); R. Zwanzig, J. Stat. Phys. **9**, 215 (1973).
[16] I. Zapata and F. Sols, Phys. Rev. B **53**, 6693 (1996); see Eq. (23) therein.
[17] P. Reimann, Phys. Rep. **361**, 57 (2002); see p. 152–154.
[18] A. Barone and G. Paternò, *Physics and Application of the Josephson Effect* (Wiley, New York, 1982).
[19] R. L. Kautz, Rep. Prog. Phys. **59**, 935 (1996).
[20] P. Jung, Phys. Rep. **234**, 175 (1993).
[21] E. Platen and N. Bruti-Liberati, *Numerical Solution of Stochastic Differential Equations with Jumps in Finance* (Springer, Berlin, 2010).
[22] M. Januszewski and M. Kostur, Comput. Phys. Commun. **181**, 183 (2009).
[23] R. Bartussek, P. Hänggi, and J. G. Kissner, Europhys. Lett. **28**, 459 (1994).
[24] M. Borromeo, G. Costantini, and F. Marchesoni, Phys. Rev. E **65**, 041110 (2002).
[25] M. Kostur, L. Machura, P. Hänggi, J. Łuczka, and P. Talkner, Physica A **371**, 20 (2006).
[26] L. Machura, M. Kostur, P. Talkner, J. Łuczka, and P. Hänggi, Phys. Rev. Lett. **98**, 040601 (2007).
[27] D. Speer, R. Eichhorn, and P. Reimann, Europhys. Lett. **79**, 10005 (2007).
[28] M. Kostur, L. Machura, P. Talkner, P. Hänggi, and J. Łuczka, Phys. Rev. B **77**, 104509 (2008).
[29] P. Jung, J. G. Kissner, and P. Hänggi, Phys. Rev. Lett. **76**, 3436 (1996).
[30] J. L. Mateos, Phys. Rev. Lett. **84**, 258 (2000).
[31] J. L. Mateos, Physica A **325**, 92 (2003).
[32] M. Kostur and J. Łuczka, Phys. Rev. E **63**, 021101 (2001).
[33] E. Goldobin, D. Koelle, R. Kleiner, and A. Buzdin, Phys. Rev. B **76**, 224523 (2007).
[34] H. Sickinger, A. Lipman, M. Weides, R. G. Mints, H. Kohlstedt, D. Koelle, R. Kleiner, and E. Goldobin, Phys. Rev. Lett. **109**, 107002 (2012).
[35] E. Goldobin, R. Kleiner, D. Koelle, and R. G. Mints, Phys. Rev. Lett. **111**, 057004 (2013).
[36] L. Machura, M. Kostur, P. Talkner, J. Łuczka, F. Marchesoni, and P. Hänggi, Phys. Rev. E **70**, 061105 (2004).
[37] L. Machura, M. Kostur, F. Marchesoni, P. Talkner, P. Hänggi, and J. Łuczka, J. Phys.: Condens. Matter **17**, S3741 (2005).
[38] L. Machura, M. Kostur, F. Marchesoni, P. Talkner, P. Hänggi, and J. Łuczka, J. Phys.: Condens. Matter **18**, 4111 (2006).
[39] L. Machura, M. Kostur, P. Talkner, P. Hänggi, and J. Łuczka, Physica E **42**, 590 (2010).
[40] C. D. Tesche and J. Clarke, J. Low Temp. Phys. **29**, 301 (1977).
[41] T. A. Fulton, L. N. Dunkleberger, and R. C. Dynes, Phys. Rev. B **6**, 855 (1972).

Efficiency of the SQUID Ratchet Driven by External Current

J. Spiechowicz[1] **and J. Łuczka**[1,2]

[1] Institute of Physics, University of Silesia, 40-007 Katowice, Poland
[2] Silesian Center for Education and Interdisciplinary Research, University of Silesia, 41-500 Chorzów, Poland

Abstract. We study theoretically the efficiency of an asymmetric superconducting quantum interference device (SQUID) which is constructed as a loop with three capacitively and resistively shunted Josephson junctions. Two junctions are placed in series in one arm and the remaining one is located in the other arm. The SQUID is threaded by an external magnetic flux and driven by an external current of both constant (dc) and time periodic (ac) components. This system acts as a nonequilibrium ratchet for the dc voltage across the SQUID with the external current as a source of energy. We analyze the power delivered by the external current and find that it strongly depends on thermal noise and the external magnetic flux. We explore a space of the system parameters to reveal a set for which the SQUID efficiency is *globally maximal*. We detect the intriguing feature of the thermal noise enhanced efficiency and show how the efficiency of the device can be tuned by tailoring the external magnetic flux.

PACS numbers: 74.25.F-, 85.25.Dq, 05.40.-a, 05.60.-k.

1. Introduction

The SQUID is the most sensitive instrument which is capable of detecting and measuring even extremely small magnetic fields. It has been used successfully not only for magnetometry but also for voltage and current measurements. Its applications go far beyond the research laboratories often into commercial apparatus exploited in metrology, geophysics and medicine, see the reviews [1, 2]. The SQUID has been the topic of various extensive theoretical and experimental studies. Yet, a number of open problems of this setup still remain to be resolved. A prominent example may be the efficiency of the SQUID as a thermodynamical machine converting the input energy into its other forms. It is the subject of this paper.

We study an asymmetric SQUID driven by an external current and analyze the charge transport and voltage induced across the device. The asymmetric SQUID is modeled as a ratchet far from equilibrium, i.e. as a classical Brownian particle moving in a spatially periodic potential with broken reflection symmetry and driven by a time-dependent force. In this mechanical analogy, the voltage across the SQUID corresponds to the particle velocity. The most basic measure for characterizing the motion of the Brownian particle is its long time average velocity $\langle v \rangle$. However, alone it does not give any information on quality of transport process. Is it effective or ineffective? To answer this question, we need to consider its other attributes. One of them are *fluctuations* of the velocity around its average value which in the long time regime are represented by the variance $\sigma_v^2 = \langle v^2 \rangle - \langle v \rangle^2$. Then, typically the instantaneous velocity $v(t)$ takes values within the interval of standard deviation, $v(t) \in [\langle v \rangle - \sigma_v, \langle v \rangle + \sigma_v]$. Note that if fluctuations are large, i.e. if $\sigma_v > |\langle v \rangle|$, then it is possible that the particle moves for some time in the direction opposite to its average velocity $\langle v \rangle$, spread of velocities is large and overall transport is not effective. The next feature which is important in answering the question about the quality of transport phenomenon is related to the ratio of energy input into the system and its energetic output. How much of the energy input is converted into directed motion of the particle and how much of it is wasted by spreading out into environment and dissipated as heat? A proper quantifier to characterize this aspect of transport is the *efficiency* of the system.

By using the correspondence between the SQUID and the mechanical ratchet system, we study three measures for evaluation of transport quality: average voltage, its fluctuations and the efficiency of the SQUID. In the previous paper [3] we analyzed the average voltage in this setup for wide parameter regimes: covering the overdamped to moderate damping regime up to its fully underdamped regime. We found the intriguing features of a negative absolute and differential conductance, repeated voltage reversals, noise induced voltage reversals and solely thermal noise-induced ratchet voltage. We identified a set of parameters for which the ratchet effect is most pronounced and showed how the direction of transport can be controlled by tailoring the external magnetic flux. The main emphasis of that work laid on formulating and exploring conditions that are necessary for the generation and control of transport [4, 5], its direction,

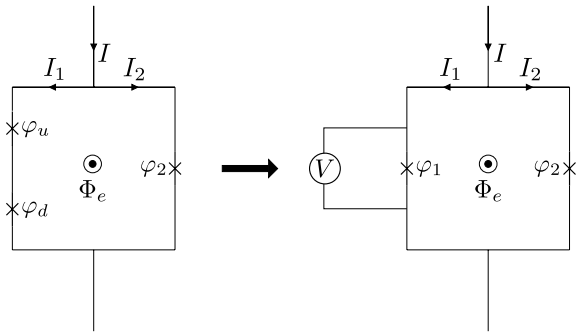

Figure 1. Schematic asymmetric SQUID composed of three Josephson junctions and the equivalent circuit composed of two junctions. The Josephson phase difference is $\varphi_1 = \varphi_u + \varphi_d$, the externally applied current is I, the current through the left and right arms is I_1 and I_2, respectively. The external magnetic flux is Φ_e and the instantaneous voltage across the SQUID is $V = V(t)$. The long time average voltage $\langle V \rangle$ across the SQUID is expressed by the relation $\langle V \rangle = \hbar \langle \dot{\varphi}_1 \rangle / 2e = \hbar \langle \dot{\varphi}_2 \rangle / 2e$.

magnitude as well as its dependence on system parameters. However, apart from these well investigated questions other important features concerning the quality of transport [6, 7, 8] have remained unanswered. Therefore in this paper we concentrate on this topic and connection between the directed transport expressed in terms of the dc voltage, its fluctuation characteristics and energetics of the SQUID.

Theoretical aspects considered in the paper concern not only our specific SQUID ratchet but a much wider class of systems and problems. There are many experiments on a number of ratchet systems [9], in particular superconducting ratchets [10], a part of which can be controlled by an external magnetic field [11, 12, 13, 14] as well as theoretical studies of such systems driven by harmonic and biharmonic external currents [15, 16, 17, 18, 19]. However, the efficiency of transport has not been analyzed in the above-cited papers.

The structure of the paper is as follows. In Sec. II, we recall the model of a SQUID rocking ratchet which is composed of three resistively and capacitively shunted Josephson junctions. In Sec. III we define mean values of arbitrary state functions in the long time regime. Then in Secs. IV-VI, the quantities characterizing the quality of the transport such as the voltage fluctuations, the energy balance and the (Stokes) efficiency are introduced, respectively. In Sec. 7 we elaborate on key aspects of transport efficiency in the system: starting from the power delivered by the externally applied current, covering the tailoring of the Stokes efficiency of the device, up to presentation of the regime for which thermal noise enhances the efficiency and discussion about the impact of variation of the external magnetic flux on the efficiency of the SQUID. Finally, the last section provides a summary.

2. Model of the SQUID ratchet

The asymmetric SQUID [10, 21, 22, 23, 24] is presented in Fig. 1. It is a loop with two resistively and capacitively shunted Josephson junctions [25] in the left arm and one in the right arm. The crosses denote the junctions and $\varphi_k \equiv \varphi_k(t)$ $(k = u, d, 1, 2)$ are the phase differences across them. Each junction is characterized by the capacitance C_k, resistance R_k and critical Josephson supercurrent J_k, respectively.

The SQUID is threaded by an external magnetic flux Φ_e and driven by an external current $I = I(t)$ which is composed of the static dc current I_0 and the ac component of amplitude A and angular frequency Ω, namely

$$I(t) = I_0 + A\cos(\Omega t). \tag{1}$$

To reduce a number of parameters of the model, we consider a special case when two junctions in the left arm are identical, i.e. $J_u = J_d \equiv J_1, R_u = R_d \equiv R_1/2, C_u = C_d \equiv 2C_1$. In some regimes [3], two junctions in a series can be considered as one for which the supercurrent-phase relation takes the form $J_1 \sin(\varphi_1/2)$, where $\varphi_1 = \varphi_u + \varphi_d$. This result is also derived in Ref. [26] for an effective double-well structure described in terms of a double-barrier potential (cf. Eq. (23) therein).

The total magnetic flux Φ piercing the loop is a sum of the external flux Φ_e and the flux due to the flow of currents,

$$\Phi = \Phi_e + Li, \tag{2}$$

where L is the loop inductance and $i \equiv i(t)$ is the circulating current which tends to screen the magnetic flux. In the "dispersive" operating mode of the SQUID [27], i.e. when the condition $|Li| \ll \Phi_0$ holds true ($\Phi_0 = h/2e$ is the flux quantum), the phase $\varphi \equiv \varphi_1$ obeys the Stewart-McCumber type equation of the form [3]

$$\frac{\hbar}{2e}C\ddot{\varphi} + \frac{\hbar}{2e}\frac{1}{R}\dot{\varphi} + J(\varphi) = I(t) + \sqrt{\frac{2k_BT}{R}}\,\xi(t), \tag{3}$$

where the effective supercurrent $J(\varphi)$ reads

$$J(\varphi) = J_1 \sin\left(\frac{\varphi}{2}\right) + J_2 \sin(\varphi + \tilde{\Phi}_e). \tag{4}$$

The parameters are: $C = C_1 + C_2$, $R^{-1} = R_1^{-1} + R_2^{-1}$, k_B is the Boltzmann constant, T is temperature of the system and $\tilde{\Phi}_e = 2\pi\Phi_e/\Phi_0$ is the dimensionless external magnetic flux. Thermal fluctuations are modeled by δ-correlated Gaussian white noise $\xi(t)$ of zero mean and unit intensity

$$\langle \xi(t) \rangle = 0, \quad \langle \xi(t)\xi(s) \rangle = \delta(t - s). \tag{5}$$

The Stewart-McCumber equation (3) has the form of a Langevin equation and describes a non-Markovian stochastic process for the phase φ. In the extended space $\{\varphi, \dot{\varphi}\}$, it has the Markovian property and all well known methods can be applied to analyze it.

Eq. (3) can be interpreted in the framework of a model of a classical Brownian particle. It helps develop the intuition and interpretation. In the one-to-one correspondence, the particle position x translates to the phase φ, the particle velocity

$v = \dot{x}$ to the voltage $V \propto \dot{\varphi}$, the conservative force to the supercurrent $J(\varphi)$, the external force to the current $I(t)$, the mass m to the capacitance $m \propto C$ and the friction coefficient γ to the normal conductance $\gamma \propto G = 1/R$. It is important to note that the friction γ is not proportional to the normal resistance R (as one could expect in the case of electrical circuits) but to the inverse of R. The reason is that plasma oscillations of the junction are more damped if more normal electrons couple to the oscillating condensate (i.e. when G is greater). The voltage accelerates normal electrons and their kinetic energy is dissipated into heat. Thus the plasma oscillations converts into heat with a rate proportional to the conductance G [28].

3. Asymptotic mean values

The main characteristics of the system are the current-voltage curves in the long time regime. It can be shown that for the external current (1), they can be extracted from the relation for the averaged voltage $\langle V \rangle$ developed across the SQUID [3]

$$\langle V \rangle = \frac{\hbar}{2e} \langle \dot{\varphi}_1 \rangle = \frac{\hbar}{2e} \langle \dot{\varphi}_2 \rangle, \tag{6}$$

where $\dot{\varphi}_1$ can be obtained from the Stewart-McCumber equation (3) for the phase $\varphi = \varphi_1$. The above relation holds true when the average is only over the period $T = 2\pi/\Omega$ of the ac current. It is also valid in the long time regime when the averaging is performed over initial conditions and all realizations of thermal fluctuations. Below we present a precise definition of this procedure.

It is convenient to rewrite Eq. (3) for the phase φ and the voltage $V \equiv V(t) = (\hbar/2e)\dot{\varphi}$ in the Ito form

$$d\varphi = \frac{2e}{\hbar} V dt, \tag{7}$$

$$dV = \frac{1}{C}\left[-\frac{1}{R}V - J(\varphi) + I(t)\right] dt + \frac{1}{C}\sqrt{\frac{2k_B T}{R}}\, dW(t), \tag{8}$$

where $dW(t) = \xi(t)dt$ is the differential of the Wiener process of zero mean and the second moment $\langle dW(t) dW(t) \rangle = dt$. The pair $\{\varphi, V\}$ form a Markovian process and its probability density $P = P(\varphi, V, t)$ obeys the Fokker-Planck equation

$$\frac{\partial P}{\partial t} = -\frac{2e}{\hbar} V \frac{\partial}{\partial \varphi} P + \frac{1}{C}\frac{\partial}{\partial V}\left[\frac{1}{R}V + J(\varphi) - I(t)\right] P + \frac{k_B T}{RC^2}\frac{\partial^2}{\partial V^2} P \tag{9}$$

with the initial condition $P(\varphi, V, 0) = p(\varphi, V)$, where a given probability density $p(\varphi, V)$ describes the initial distribution of the phase $\varphi(0)$ and voltage $V(0)$.

For any state function $f(\varphi, V)$, its mean value $\langle f(\varphi, V) \rangle_t$ at time t is calculated from the relation

$$\langle f(\varphi, V) \rangle_t = \int_0^{2\pi} d\varphi \int_{-\infty}^{\infty} dV\, f(\varphi, V) P(\varphi, V, t). \tag{10}$$

Because the system is driven by the time-periodic current $I(t)$, the probability density $P(\varphi, V, t)$ approaches for long time the asymptotic *periodic* form $P_{as}(\varphi, V, t)$, namely

[29, 30]

$$P_{as}(\varphi, V, t) = \sum_{n=-\infty}^{\infty} W_n(\varphi, V) e^{in\Omega t}, \tag{11}$$

where the Fourier coefficients $W_n(\varphi, V)$ are solutions of the differential equations obtained from the Fokker-Planck Eq. (9). The time-dependent asymptotic mean value

$$\langle f(\varphi, V)\rangle_t^{as} = \int_0^{2\pi} d\varphi \int_{-\infty}^{\infty} dV\, f(\varphi, V) P_{as}(\varphi, V, t) \tag{12}$$

is also a periodic function of time. If we are interested in its *time-independent* form, the time averaging over the additional period $T = 2\pi/\Omega$ of the ac current has to be performed

$$\begin{aligned} \langle f(\varphi, V)\rangle &= \frac{\Omega}{2\pi} \int_t^{t+2\pi/\Omega} \langle f(\varphi, V)\rangle_u^{as}\, du \\ &= \lim_{t\to\infty} \frac{\Omega}{2\pi} \int_t^{t+2\pi/\Omega} \langle f(\varphi, V)\rangle_u\, du. \end{aligned} \tag{13}$$

In a particular case, when $f(\varphi, V) = V$, we get the time-independent asymptotic mean voltage $\langle V\rangle$. Similarly, when $f(\varphi, V) = V^k (k = 2, 3, ...)$, we obtain the stationary statistical moments of the voltage $\langle V^k\rangle$.

4. Fluctuations of voltage

The asymptotic average voltage $\langle V\rangle$ calculated according to the prescription (13) is the most important transport characteristics of the system. The magnitude of the instantaneous voltage $V(t)$ can be much larger than its mean value. Moreover, the fluctuations of voltage in the long time regime can also be large. They are described by the voltage variance

$$\sigma_V^2 = \langle V^2\rangle - \langle V\rangle^2. \tag{14}$$

The voltage typically ranges within the interval of several standard deviations

$$V(t) \in [\langle V\rangle - n\sigma_V, \langle V\rangle + n\sigma_V], \quad n = 1, 2, ... \tag{15}$$

If the standard deviation σ_V is large, i.e. when $\sigma_V > |\langle V\rangle|$, the voltage $V(t)$ can spread far from its average value and even assume the sign opposite to it. It is a case for protein motors in biological cells where the instantaneous velocity changes direction very rapidly and its absolute value is several orders of magnitude larger than the average velocity [31].

5. Energetics of the SQUID

The SQUID is a device which converts input energy into its other forms. It is provided by the external current $I(t)$ and the energy flow is determined by the equation of motion

(3). In the mechanical interpretation, the kinetic energy of the particle corresponds to the energy stored in the system of capacitance C, namely

$$E_C \equiv E_C(V(t)) = \frac{1}{2}CV^2(t). \tag{16}$$

The particle potential energy translates to the Josephson energy accumulated in the junction when the supercurrent flows through it

$$\begin{aligned} E_J \equiv E_J(\varphi(t)) &= \int_0^t J(\varphi(u))V(u)du \\ &= \frac{\hbar}{2e}\int_0^t J(\varphi(u))\dot{\varphi}(u)du = \frac{\hbar}{2e}\int_0^{\varphi(t)} J(\phi)d\phi \\ &= -\frac{\hbar}{2e}\left\{2J_1\cos\left[\frac{\varphi(t)}{2}\right] + J_2\cos[\varphi(t)+\tilde{\Phi}_e]\right\} + const. \end{aligned} \tag{17}$$

The sum

$$E \equiv E_C + E_J \tag{18}$$

is the total energy of the system. Its balance can be obtained from Eqs. (7)-(8). For this purpose we apply the Ito differential calculus to both functions $E_C(V)$ and $E_J(\varphi)$

$$\begin{aligned} dE_C &= \frac{dE_C}{dV}dV + \frac{1}{2}\frac{d^2E_C}{dV^2}dVdV + ... \\ &= \left[-\frac{1}{R}V^2 - J(\varphi)V + I(t)V + \frac{k_BT}{RC}\right]dt + \sqrt{\frac{2k_BT}{R}}\,VdW(t), \end{aligned} \tag{19}$$

$$dE_J = \frac{dE_J}{d\varphi}d\varphi = J(\varphi)Vdt. \tag{20}$$

Next, for both sides of the above equations, we calculate the mean values. Exploiting the Ito martingale property we find the average value of the term $\langle VdW(t)\rangle_t = 0$ and obtain the energy balance equation in the form [6, 32]

$$\frac{d}{dt}\langle E\rangle_t = -\frac{1}{R}\langle V^2\rangle_t + I(t)\langle V\rangle_t + \frac{k_BT}{RC} \tag{21}$$

$$= -\frac{1}{R}\left[\langle V^2\rangle_t - \langle V^2\rangle_{eq}\right] + I(t)\langle V\rangle_t, \tag{22}$$

where $\langle\cdot\rangle_t$ denotes a mean value at time t according to the prescription (10). In the right hand side of this equation there are three components, each of them is related to the separate process responsible for the energy change. Let us point out that the first term in Eq. (21) is always negative whereas the third is positive. The former describes the rate of energy loss due to dissipation and the latter refers to the energy provided by thermal equilibrium fluctuations. According to the equipartition theorem, in the thermodynamical equilibrium, when $I(t) = 0$, the relation $\langle CV^2/2\rangle_{eq} = k_BT/2$ holds true. It is utilized in Eq. (21) to get (22). The second term in (21) characterizes the change of energy caused by the external current $I(t)$.

Now, we perform the final averaging of Eq. (21) according to the prescription (13). Since in the long time regime the average values are periodic function of time, the left

hand side vanishes

$$\int_t^{t+2\pi/\Omega} \frac{d}{dt}\langle E\rangle_u \, du = \frac{C}{2}[\langle V^2(t+2\pi/\Omega)\rangle - \langle V^2(t)\rangle] + [\langle E_J(\varphi(t+2\pi/\Omega))\rangle - \langle E_J(\varphi(t))\rangle] = 0. \tag{23}$$

As a consequence, in the stationary regime the mean power $\mathcal{P}_{in}$ delivered to the system by the external current $I(t)$ over the period T is expressed by the relation [32]

$$\mathcal{P}_{in} = \langle I(t)V\rangle = \frac{1}{R}\langle V^2\rangle - \frac{k_B T}{RC} = \frac{1}{R}\left[\langle V^2\rangle - \langle V^2\rangle_{eq}\right]. \tag{24}$$

From the above equation it follows that the amount of the energy input to the SQUID from the external driving $I(t)$ depends not only on the current itself (i.e. on I_0, A, Ω) but also on properties and parameters of the device: its temperature T, the resistance R and the capacitance C. In contrast, the energy supplied by thermal fluctuations does not depend on the external current but only on T, R and C.

6. Efficiency of the SQUID

A generic definition of the efficiency of a device converting energy is a ratio between the output (work, power) and the input (power) energy. Depending on the choice of input and output, different definitions of the efficiency characterize various aspects of energy conversion in the device. To explain the problem, we use the mechanical interpretation of (3). Then the average voltage $\langle V\rangle$ corresponds to the velocity of the Brownian particle or the *Brownian motor*. The thermodynamic efficiency is defined as a ratio of the work done by the motor to the energy input. If the particle is working against a constant force (load) i_0 then in stationary state the efficiency is defined as follows

$$\eta_0 = \frac{i_0\langle V\rangle}{\mathcal{P}_{in}}. \tag{25}$$

In the considered case, there is no a load and the Brownian motor does not transport external objects. It works against the friction "force"

$$F_R = \frac{\hbar}{2e}\frac{1}{R}\dot{\varphi}. \tag{26}$$

(By the way, it has not the unit of Newton but if the above formula is again multiplied by the factor $\hbar/2e$ then it has the correct physical unit.) When the external force $I(t)$ is switched off, the velocity of the motor is damped to zero and the system tends to thermodynamical equilibrium. Because the motor works against the friction force, we can utilize its mean value to get another definition of efficiency, namely

$$\eta_S = \frac{\langle F_R\rangle\langle V\rangle}{\mathcal{P}_{in}} = \frac{\langle V\rangle^2}{R\mathcal{P}_{in}} = \frac{\langle V\rangle^2}{\langle V^2\rangle - \langle V^2\rangle_{eq}} = \frac{\langle V\rangle^2}{\langle V\rangle^2 + \sigma_V^2 - k_B T/C}. \tag{27}$$

This quantity is called the *Stokes efficiency* [33, 31, 34]. Let us note that it depends explicitly on mass C of the Brownian particle and and only implicitly on the friction coefficient R via the Langevin equation (3).

It should be mentioned that (27) is not the rate of the work done by the motor on its surroundings (viscous medium). Moreover, it is not a mean power $\mathcal{P}_R$ to overcome the friction force which correct form reads

$$\mathcal{P}_R = \langle F_R V \rangle = \frac{\langle V^2 \rangle}{R}. \tag{28}$$

However, this expression cannot be put as a numerator in the definition of the efficiency because there are regimes where the mean velocity is extremely small (numerically zero), $\langle V \rangle \approx 0$ but $\langle V^2 \rangle \neq 0$ and the efficiency could be large even though the particle does not move on average in one direction. It is the main reason why the Stokes efficiency is more adequate is such cases as considered in the paper.

Another possible definition of the efficiency is based on the remark that what we observe in the long time regime is the average velocity. Therefore we can introduce "kinetic power" as the "kinetic energy" of the particle per the period T,

$$\mathcal{P}_k = \frac{C\langle V \rangle^2}{2T}. \tag{29}$$

One should note that it is not exactly proper definition of the kinetic power as it should be proportional to $\langle V^2 \rangle$ instead of $\langle V \rangle^2$. However, we replaced it with the latter for the reason explained before. Nevertheless, it is still a measure of performance of the motor. If the average velocity increases then $\mathcal{P}_k$ also grows. We can insert it as a numerator in (25) and then we get the *kinetic efficiency*

$$\eta_k = \frac{\mathcal{P}_k}{\mathcal{P}_{in}} = \frac{RC}{2T} \frac{\langle V \rangle^2}{\langle V^2 \rangle - \langle V^2 \rangle_{eq}} = \frac{\tau_r}{2T} \eta_S. \tag{30}$$

This quantifier can be used only when the time-periodic force is switched on. Then qualitatively, it is similar to the Stokes efficiency. However, the dependence on the mass C, the friction coefficient R and the period T is different. Both the Stokes efficiency and the kinetic efficiency are consistent with our intuition: a decrease of fluctuations σ_V^2 leads to a smaller input power and hence to an increase of the efficiency. Consequently, the transport is optimized in regimes that *maximize* the directed velocity and *minimize* its fluctuations. Because the kinetic efficiency is proportional to the Stokes efficiency, below we analyze only the last one.

7. The results

7.1. Dimensionless model

There are several dimensionless forms of Eq. (3) in dependence of the choice of scaling time. In this system there are four characteristic frequencies: plasma frequency $\omega_p^2 = 2eJ_1/\hbar C$, the characteristic frequency of the junction $\omega_c = 2eRJ_1/\hbar$, the frequency $\omega_r = 1/RC$ related to the relaxation time and the frequency Ω of the ac current. There are three independent characteristic time scales related to these frequencies (note that

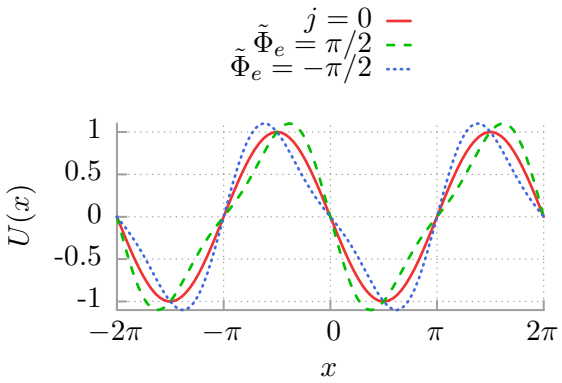

Figure 2. The potential (33) for the symmetric case $j = 0$ (solid red line) in comparison with the ratchet potential for $j = 1/2$ and two values of the external magnetic flux $\tilde{\Phi}_e = \pi/2$ (dashed green line) and $\tilde{\Phi}_e = -\pi/2$ (dotted blue line).

$\omega_p^2 = \omega_c\omega_r$). Here, we follow [20] and define the new phase x and the dimensionless time $\hat{t}$ as

$$x = \frac{\varphi + \pi}{2}, \quad s = \frac{t}{\tau_c}, \quad \tau_c = \frac{\hbar}{eRJ_l}. \tag{31}$$

Then (3) takes the dimensionless form

$$\tilde{C}\ddot{x}(s) + \dot{x}(s) = -U'(x(s)) + F + a\cos(\omega s) + \sqrt{2D}\,\hat{\xi}(s), \tag{32}$$

where the dot and prime denotes a differentiation over the dimensionless time s and the phase x, respectively. We introduced a spatially periodic potential $U(x)$ of period 2π of the following form [20]

$$U(x) = -\sin(x) - \frac{j}{2}\sin(2x + \tilde{\Phi}_e - \pi/2). \tag{33}$$

This potential is reflection-symmetric if there exists x_0 such that $U(x_0 + x) = U(x_0 - x)$ for any x. If $j \neq 0$, it is generally asymmetric and its reflection symmetry is broken, see Fig. 2. We classify this characteristics as a ratchet potential. However, even for $j \neq 0$ there are certain values of the external flux $\tilde{\Phi}_e$ for which it is still symmetric. The dimensionless capacitance $\tilde{C}$ is the ratio between two characteristic time scales $\tilde{C} = \tau_r/\tau_c$, where the relaxation time is $\tau_r = RC$. Other re-scaled parameters are $j = J_2/J_1$, $F = I_0/J_1$, $a = A/J_1$ and $\omega = \Omega\tau_c$. The rescaled zero-mean Gaussian white noise $\hat{\xi}(s)$ has the auto-correlation function $\langle\hat{\xi}(s)\hat{\xi}(u)\rangle = \delta(s-u)$ and its intensity $D = ek_BT/\hbar J_1$ is the quotient of the thermal and the Josephson coupling energy. The dimensionless voltage $v(t) = \dot{x}(s) = V(t)/RJ_1$ and therefore the physical average voltage $\langle V\rangle$ is given by the relation

$$\langle V\rangle = RJ_1\langle v\rangle. \tag{34}$$

In particular, after such a scaling procedure the dimensionless input power P_{in} is expressed as

$$P_{in} = \langle v^2\rangle - D/\tilde{C} \tag{35}$$

and consequently, the Stokes efficiency reads

$$\eta_S = \frac{\langle v\rangle^2}{\langle v\rangle^2 + \sigma_v^2 - D/\tilde{C}} = \frac{\langle v\rangle^2}{\langle v^2\rangle - D/\tilde{C}}. \tag{36}$$

The key feature for the occurrence of the directed transport $\langle v\rangle \neq 0$ is the symmetry breaking. This is the case when either the dc current $F \neq 0$ or the reflection symmetry of the potential $U(x)$ is broken.

The system described by (32) becomes deterministic when the thermal noise intensity D is set to zero. Even in this case it exhibits complex dynamics including chaotic regimes [35, 36]. The application of noise generally smooths out its characteristic response function. There are two classes of states of the driven system dynamics: the locked states, in which the phase stays inside finite number of potential wells and the running states for which it runs over the potential barriers. The latter are crucial for the occurrence of the transport. They can be either chaotic (diffusive) or regular.

7.2. Details of simulations

The Fokker-Planck equation (9) corresponding to the Langevin equation (3) cannot be solved by use of closed analytical forms. Therefore, in order to obtain the relevant transport characteristics we have to resort to comprehensive numerical simulations of the driven Langevin dynamics. We have integrated (32) by employing a weak version of the stochastic second order predictor corrector algorithm [37] with a time step typically set to about $10^{-3}\cdot 2\pi/\omega$. Since (32) is a second-order differential equation, we have to specify two initial conditions $x(0)$ and $\dot{x}(0)$. Moreover, because for some regimes the system may be non ergodic in order to avoid the dependence of the presented results on the specific selection of initial conditions we have chosen phases $x(0)$ and dimensionless voltages $\dot{x}(0)$ equally distributed over interval $[0, 2\pi]$ and $[-2, 2]$, respectively. All quantities of interest were ensemble-averaged over $10^3 - 10^4$ different trajectories which evolved over $10^3 - 10^4$ periods of the external ac driving. Numerical calculations were done by use of a CUDA environment implemented on a modern desktop GPU. This scheme allowed for a speed-up of a factor of the order 10^3 times as compared to a common present-day CPU method [38, 39]. Part of our so obtained results are presented next.

7.3. Power delivered by external current

Let us begin analysis of the SQUID efficiency by looking at the power P_{in} delivered by the external current $I(t)$. Notably, it depends implicitly not only on the parameters of the applied external current (F, a, ω) but also on the quantities characterizing the device like the capacitance $\tilde{C}$. We have found that generally the input power (35) tends to increase for larger values of the dc current F and ac driving amplitude a. The dependence on the frequency ω is more complex. However, in most cases P_{in} is relatively large when ω is small. It is because very fast oscillation of the driving current cannot induce neither the average voltage $\langle v\rangle$ nor $\langle v^2\rangle$. In panel (a) of Fig. 3 we show the

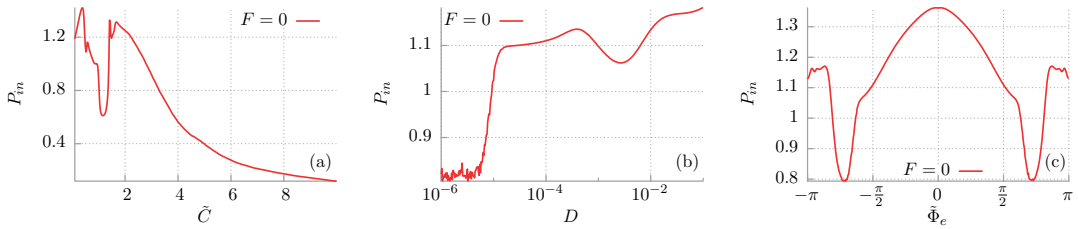

Figure 3. The power (24) delivered by the external current $I(t)$ is presented in the dimensionless form (35) as a function of the dimensionless capacitance $\tilde{C}$, the thermal noise intensity D and the external magnetic flux $\tilde{\Phi}_e$ in panels (a)-(c), respectively. Other parameters read: $a = 1.9$, $\omega = 0.6$, $j = 1/2$. In panel (a): $D = 9.7 \cdot 10^{-5}$ and $\tilde{\Phi}_e = \pi/2$. In panel (b): $\tilde{C} = 0.645$ and $\tilde{\Phi}_e = \pi/2$. In panel (c): $\tilde{C} = 0.645$ and $D = 9.7 \cdot 10^{-5}$.

representative dependence of the input power P_{in} on the dimensionless capacitance $\tilde{C}$ of the SQUID. One can observe that P_{in} is maximal for the overdamped or close to damped regime and decreases when $\tilde{C}$ grows. Since in the mechanical framework the capacitance $\tilde{C}$ translates to the mass of the Brownian particle it is intuitively clear that when the inertial term becomes large then the device needs more power to response equivalently. Perhaps the most surprising is the fact that P_{in} depends explicitly on the thermal noise intensity D, i.e. on temperature of the system. Typically, it decreases for increasing D. However, there are also regimes for which P_{in} is enhanced by thermal noise. In panel (b) of Fig. 3 we exemplify this situation. Indeed, for a wide interval of temperature the input power is almost monotonically increasing function of the noise intensity D. Finally, the influence of the constant external magnetic flux $\tilde{\Phi}_e$ on P_{in} is depicted in the last panel. It is remarkable that one can tune the input power P_{in} by changing the external magnetic flux. The reader should note that for the presented regime it is maximal when $\tilde{\Phi}_e = 0$, i.e. potential $U(x)$ is reflection symmetric. In such a case there is no average voltage drop $\langle v \rangle = 0$ across the device when additionally the dc current F vanishes. It follows that large input power P_{in} does not necessarily translate into the efficient directed transport.

7.4. Tailoring Stokes efficiency

The system described by Eq. (32) has a 7-dimensional parameter space $\{\tilde{C}, a, \omega, F, j, \tilde{\Phi}_e, D\}$. We set $F = 0$ and check how it depends on the remaining system parameters. We limit our considerations to positive a because the system (32) is symmetric under changes of sign of a. Depending on the magnitude of the dimensionless capacitance $\tilde{C}$ of the device it can operate in three distinct regimes: overdamped ($\tilde{C} \to 0$), damped (moderate $\tilde{C}$) and underdamped ($\tilde{C} \to \infty$). We note that the conditions that are necessary for the generation and control of the direction of transport have been extensively studied in these regimes in our recent work [3]. Since very fast oscillation of the driving current cannot induce the average voltage $\langle v \rangle$ it is sufficient to limit our considerations to low and moderate ac driving

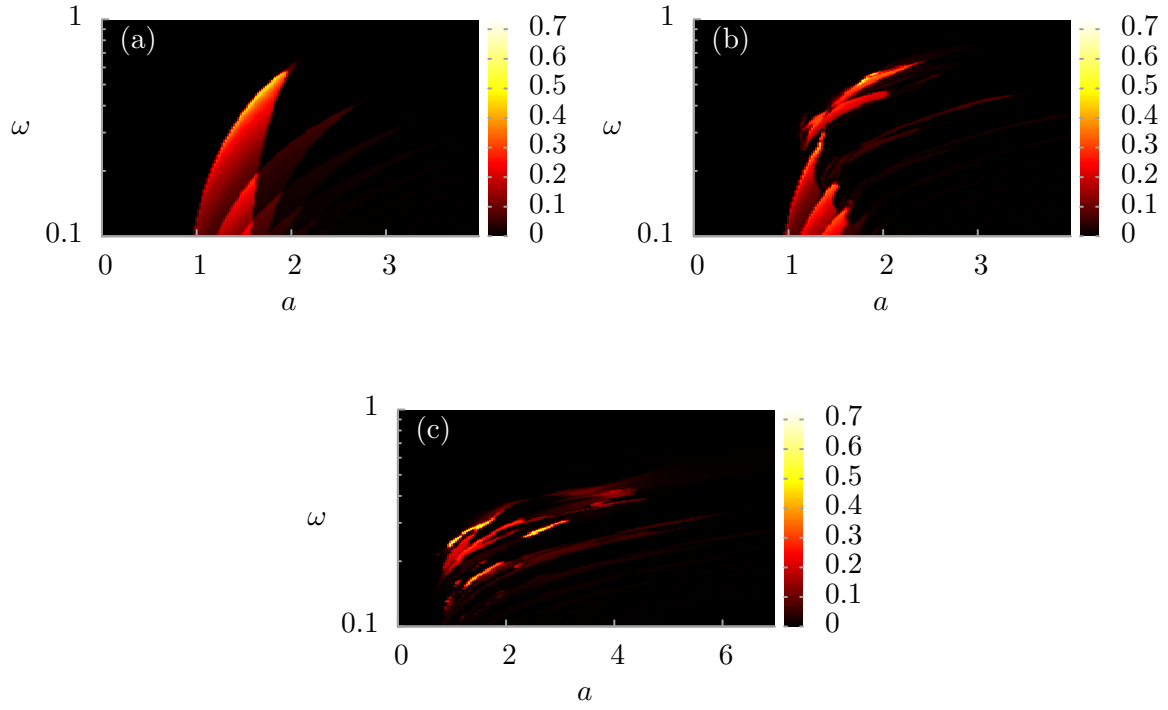

Figure 4. The Stokes efficiency η_S defined by Eq. (27) in the parameter plane $\{a, \omega\}$ of the ac current for three distinct regimes: overdamped ($\tilde{C} = 0.2$), moderate damping ($\tilde{C} = 2$) and underdamped ($\tilde{C} = 10$) in panels (a), (b) and (c), respectively. The remaining parameters are: $F = 0$, $D = 10^{-5}$, $j = 1/2$ and $\tilde{\Phi}_e = \pi/2$.

frequencies ω. We have performed scans of the following area of the parameter space $\tilde{C} \times a \times \omega \in [0.1; 10] \times [0; 10] \times [0.1; 1]$ at a resolution of 200 points per dimension to determine the general behavior of the system. The results are depicted in Fig. 4.

We can see that regardless of the regime in which the device operates its Stokes efficiency η_S is zero or negligibly small for $a < 1$ and high frequencies ω. This is due to the fact that the rocking mechanism is either too weak or too fast to induce finite average voltage $\langle v \rangle$. The areas of non-zero efficiency η_S have a striped structure. For a given amplitude a, the ratchet behavior generally tends to disappear as the frequency ω grows. On the other hand, for a given frequency, there is optimum amplitude a that maximize the Stokes efficiency. The increase of the capacitance $\tilde{C}$ causes blurring of the regions for which the efficiency is nonzero. Moreover, this tendency is often accompanied by its reduction. Consequently, the studied device operates best in the overdamped or close to damped regimes.

7.5. Optimal regime

We have explored the parameter space of the system (32) and we have been able to detect a regime for which the efficiency η_S is *globally maximal*. It is in the vicinity of the point

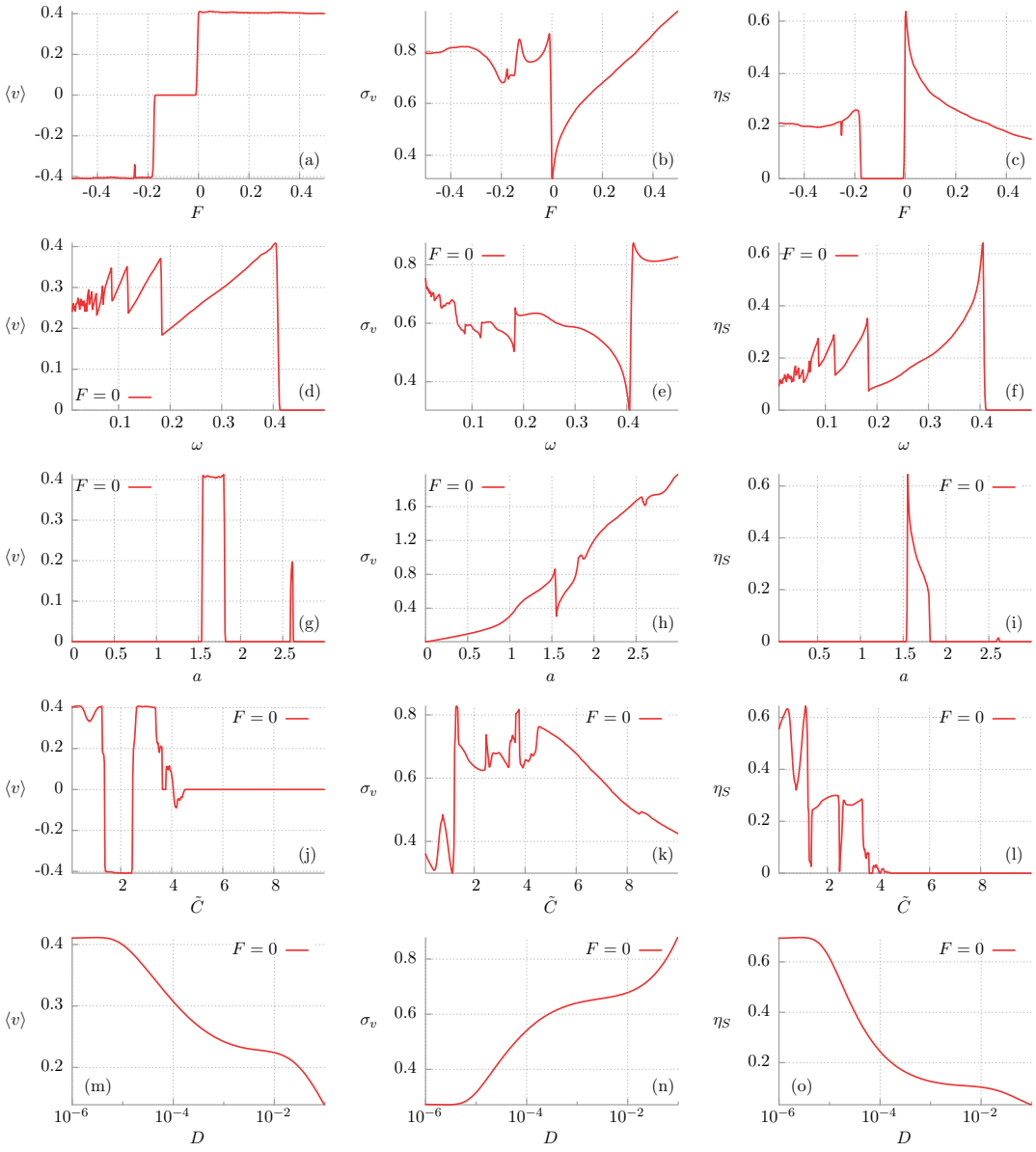

Figure 5. Optimal regime for the Stokes efficiency of the transport occurring in (32). The dependence of the average voltage $\langle v\rangle$, its fluctuations σ_v and finally the Stokes efficiency η_S on the static dc-bias F, frequency ω, amplitude a, capacitance $\tilde{C}$ and thermal noise intensity D is presented in panels (a)-(o). Parameters are: $F = 0$, $\omega = 0.406$, $a = 1.55$, $\tilde{C} = 0.496$, $D = 10^{-5}$, $j = 1/2$ and $\tilde{\Phi}_e = \pi/2$.

$\{\tilde{C}, a, \omega\} = \{0.496, 1.55, 0.406\}$. All relevant transport characteristics, i.e. the average voltage $\langle v\rangle$, its fluctuations σ_v and the efficiency η_S corresponding to neighborhood of this set of parameters are presented in Fig. 5.

Let us begin with the dependence of the transport characteristics on the dc current F. It is depicted in Fig. 5(a)-(c) for small values of $F \in (-0.5, 0.5)$. Panel (a) presents the current-voltage curve. In the low temperature limit ($D = 10^{-5}$) the average voltage is almost quantized at values $n\omega$, $n = 0, \pm 1, ...$ For a symmetric potential, these plateaus

correspond to standard Shapiro steps [27]. However, in our case also steps at half integer multiplies of ω can be observed. This is due to the deviation of $U(x)$ from a simple $\sin x$ form, which is the sole case for which steps lie only at integer values of $n\omega$ [20]. However, in both the symmetric and asymmetric cases a proper amount of noise is sufficient to wipe out their evident structure [40]. This Shapiro-like current-voltage curve is characteristic for the device operating in the low temperature limit of overdamped or damped regimes. Panel (b) of the same Fig. 5 presents the dependence of the voltage fluctuations σ_v on the dc current F. It is rather complicated non-linear and non-monotonic function of F without any immediately obvious relation to the average voltage of panel (a). However, the most important observation is that the voltage fluctuations are minimal for $F = 0$. This fact is of fundamental importance for the influence of F on η_S. In Fig. 5(c) we can see that η_S is locally maximal for $F = 0$. For large values of F (not shown here) the mean voltage is an almost linear function of F and the efficiency approaches the value 1. It support the statement in Ref. [31] that when the Stokes efficiency is close to 1, the driving resembles the constant force.

The role of the frequency ω of the ac current is illustrated in Fig. 5(d)-(f). Panel (d) presents the dependence of the average voltage $\langle v\rangle$ on ω. In the adiabatic limit $\omega \to 0$ it undergoes rapid oscillations. This behavior has its reflection in the influence of the frequency on the voltage fluctuations σ_v (see Fig. 5(e)). According to the previous statement very fast oscillations of the driving current cannot induce the non-zero average voltage. Therefore for sufficiently high frequency there is no transport and as a consequence the Stokes efficiency η_S is zero. However, a strong peak of efficiency is observed for moderate value of $\omega = 0.406$. It is associated with the fact that for this frequency the average voltage $\langle v\rangle$ is maximal and simultaneously its fluctuations σ_v are minimal.

The impact of the amplitude a of the ac current is shown in Fig. 5(g)-(i), respectively. In particular, the resonance-like behavior is observed in the dependence of the average voltage $\langle v\rangle$ on the amplitude a (see Fig. 5(g)). Apart from two clearly visible peaks there is almost imperceptible small directed transport. This fact has critical impact on the functional dependence of the efficiency η_S. It is proportional to $\langle v\rangle^2$ so it vanishes too when the device response is zero. The influence of variation of the amplitude a on the voltage fluctuations σ_v is depicted in panel (h). It is almost linearly increasing function of a. Only one evident deviation from this trend can be noted, i.e. a local minimum around $a = 1.55$ corresponding to the first high peak in Fig. 5(g). It should be stressed that there is no any contradiction with the dependence of the average voltage since $\langle v\rangle = 0$ does not necessarily mean $\langle v^2\rangle = 0$ and therefore σ_v can at the same time assume nonzero value.

The dependence of all relevant transport characteristics on the capacitance $\tilde{C}$ is very complicated as shown in Fig. 5(j)-(l). The first panel of this group shows the average voltage versus the capacitance $\tilde{C}$. We note the important feature of the voltage reversal [35, 41]: starting from zero, the voltage changes its sign from positive to negative and again in the opposite direction as $\tilde{C}$ grows. Therefore the capacitance can serve

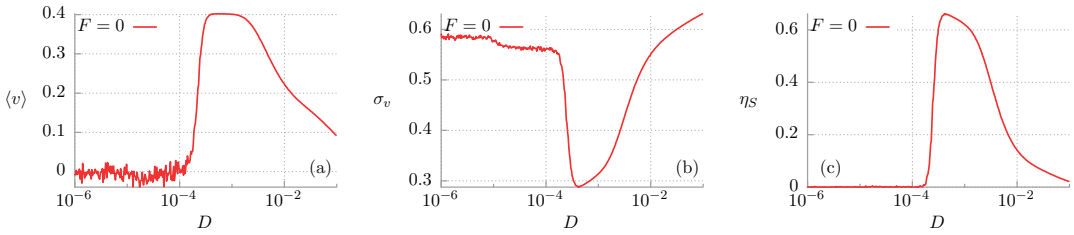

Figure 6. Noise enhanced Stokes efficiency. The dependence of the average voltage $\langle v \rangle$, its fluctuations σ_v and finally the efficiency η_S on thermal noise intensity D is presented in panels (a)-(c), respectively. Parameters read: $a = 1.899$, $\omega = 0.403$, $\tilde{C} = 6$, $j = 1/2$ and $\tilde{\Phi}_e = \pi/2$.

as a parameter to manipulate the direction of transport processes. The efficiency η_S is maximal close to the border between the overdamped and damped regimes. It is (almost) zero in the underdamped limit which corresponds to large capacitance $\tilde{C} \to \infty$. This is a consequence of the fact that for this regime the average voltage $\langle v \rangle$ vanishes or is negligibly small.

The last three panels of Fig. 5 depict the influence of the thermal noise intensity D on all previously studied quantities. An increase of the noise intensity D leads to both monotonic decrease of the induced average voltage $\langle v \rangle$ and increase of its fluctuations σ_v. Consequently, the efficiency is the best in the low temperature regime when the deterministic dynamics of the system (32) plays a crucial role.

7.6. Noise enhanced Stokes efficiency

We have found the opposite scenario when thermal noise enhances the efficiency. This perhaps surprising effect is exemplified in Fig. 6. Panel (c) presents the dependence of the efficiency η_S on D. Evidently, in some intervals of D, the increase of temperature causes the increase of η_S. There is also optimal value of temperature or equivalently the thermal noise intensity $D \approx 0.0004$ for which the efficiency takes its maximum. Moreover, in this case the ratchet mechanism is solely activated by thermal equilibrium fluctuations as for low noise intensity no rectification can be observed. This statement is confirmed in the functional dependence of the average voltage $\langle v \rangle$ which is presented in panel (a). It is also remarkable that in this regime an increase of thermal noise intensity D leads to a decrease of voltage fluctuations σ_v.

7.7. Impact of external magnetic flux

As it was shown before, the efficiency can be tuned in several ways. However, it seems that from the experimental point of view the simplest method is to vary the external constant magnetic flux $\tilde{\Phi}_e$. The dependence of the average voltage $\langle v \rangle$, its fluctuations σ_v and the efficiency on the external magnetic flux $\tilde{\Phi}_e$ in the previously presented regime for which thermal noise induces the ratchet effect (cf. Fig. 6) is depicted in Fig. 7. From the symmetry considerations of (32) it follows that for an arbitrary integer number n, the

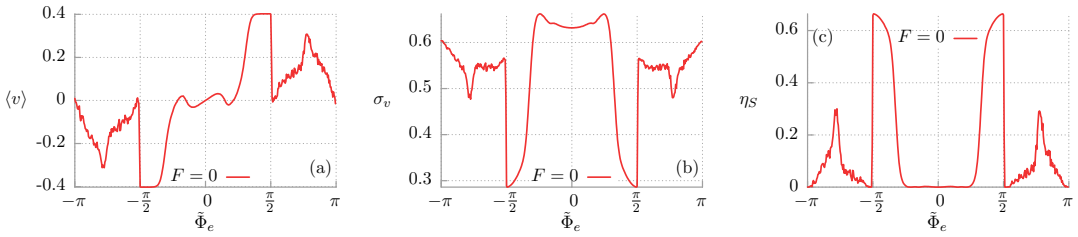

Figure 7. Impact of the external magnetic flux on the average voltage $\langle v \rangle$, its fluctuations σ_v and finally the efficiency η_S is presented in panels (a)-(c) for the noise intensity $D = 0.0004$ which corresponds to the maximum in Fig. 6(c). Other parameters are the same as in Fig. 6.

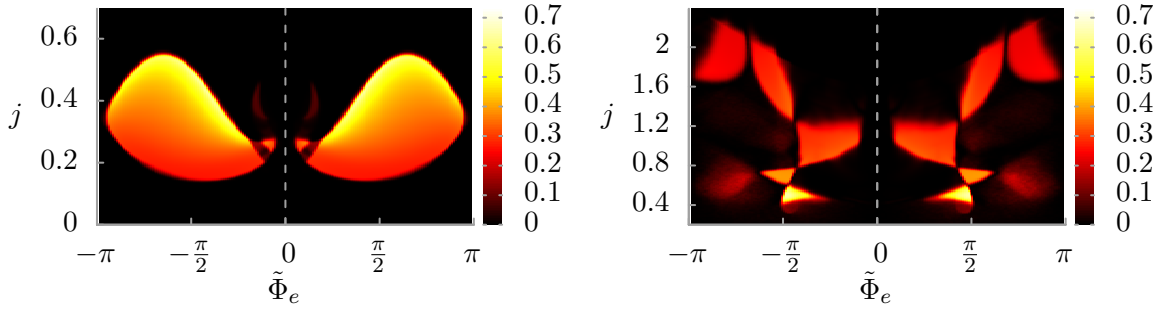

Figure 8. The Stokes efficiency of the rocked SQUID in the parameter plane $\{\tilde{\Phi}_e, j\}$. The left panel corresponds to the optimal regime as in Fig. 5 and the remaining parameters are the same as there. The right panel presents the regime depicted in Fig. 6 with $D = 0.0004$.

transformation $\tilde{\Phi}_e \to 2\pi n - \tilde{\Phi}_e$ reverses the sign of the average voltage $\langle v \rangle \to -\langle v \rangle$. This fact can be directly observed in panel (a) of Fig. 7. However, this is not the case for the voltage fluctuations σ_v, where they are symmetric around $\tilde{\Phi}_e = 0$. A careful inspection of panel (b) reveals that one can reduce magnitude of σ_v by nearly two times just by correct adjustment of the external magnetic flux. This fact has further consequences in the dependence of the efficiency which is depicted in panel (c). It can be slightly tuned by a small variation of the external magnetic flux.

In Fig. 8 we present how the Stokes efficiency behaves in the parameter plane $\{\tilde{\Phi}_e, j\}$ that specifies the form of the spatially periodic potential $U(x)$. For both sufficiently small and large j it vanishes completely. One can observe that for a given external magnetic flux $\tilde{\Phi}_e$ the Stokes efficiency generally tends to increase as the parameter j grows. On the contrary, for a given j there is an optimal value of the external magnetic flux $\tilde{\Phi}_e$ for which the Stokes efficiency is maximal. We note that for two presented regimes, the set structure of the non-zero efficiency in the parameters plane $\{\tilde{\Phi}_e, j\}$ is radically different. The left panel looks like butterfly wings and the right is similar to a rocking horse.

8. Summary

In this paper, we comprehensively studied the Stokes efficiency of the asymmetric SQUID in the case of the non-zero capacitance of all Josephson junctions and in presence of thermal noise. It allowed to analyze transport properties in the system for the entire scale of regimes: starting from overdamped, by damped and finally underdamped one. We focused on the connection between the directed transport characterized by the voltage across the SQUID and its efficiency. In particular, we examined voltage fluctuations and energetic performance of the device. We derived the expression for the power delivered by externally applied current and discuss its dependence on the system parameters. Apart from the expected influence of the current parameters I_0, A and Ω it also depends on the thermal noise intensity D, i.e. on temperature of the system.

We have found that regions of low efficiency of the SQUID dominates in the parameter space. However, we have identified remarkable and distinct regimes of high efficiency $\eta_S \approx 0.65$. It turns out that the device operates best in the overdamped or close to damped regimes. Moreover, with the help of the computational power of modern GPU supercomputers we have identified the tailored set of parameters for which the efficiency η_S is globally maximal and for this regime we discussed impact of variation of almost all system parameters on the relevant transport quantities. In particular, it follows that thermal fluctuations often have destructive influence on the energetic performance of the device. Moreover, we were able to detect also the regime for which thermal noise enhances the efficiency by inducing the large average voltage and minimizing its variance. Last but not least, we discussed in detail the impact of the external magnetic flux $\tilde{\Phi}_e$ on the performance and effectiveness of the SQUID.

Our results can readily be experimentally verified with an accessible setup consisting of three resistively and capacitively shunted Josephson junctions formed in an asymmetric SQUID device. Some partial transport characteristics like voltage have been experimentally studied in the overdamped regime [10, 24]. However, the underdamped regime has not been tested and the efficiency has not been measured which makes our study a challenge for experimentalists.

Acknowledgments

This work was supported in part by the MNiSW program Diamond Grant (J. S.) and NCN Grant DEC-2013/09/B/ST3/01659 (J. Ł.).

References

[1] Fagaly R L 2006 *Rev. Sci. Instrum.* **77** 101101
[2] Hämäläinen M, Hari R, Ilmoniemi R J, Knuutila J, Lounasmaa O V 1993 *Rev. Mod. Phys.* **65** 413
[3] Spiechowicz J, Hänggi P and Łuczka J 2014 *Phys. Rev. B* **90** 054520
[4] Hänggi P, Marchesoni F, Nori F 2005 *Ann. Phys. (Leipzig)* **14** 51
[5] Hänggi P, Marchesoni F 2009 *Rev. Mod. Phys.* **81** 387

[6] Machura Ł, Kostur M, Talkner P, Łuczka J, Marchesoni F and Hänggi P 2004 *Phys. Rev. E* **70** 061105
[7] Machura Ł, Kostur M, Marchesoni F, Talkner P, Hänggi P and Łuczka J 2005 *J. Phys. Condens. Matter* **17** 3741
[8] Machura Ł, Kostur M, Marchesoni F, Talkner P, Hänggi P and Łuczka J 2005 *J. Phys. Condens. Matter* **18** 4111
[9] Bogunovic L, Eichhorn R, Regtmeier J, Anselmetti D and Reimann P 2012 *Soft Matter* **8** 3900 and Refs. therein
[10] Sterck A, Kleiner R and Koelle D 2005 *Phys. Rev. Lett.* **95** 177006
[11] Villegas J E, Savel'ev S, Nori F, Gonzalez E M, Anguita J V, Garcia R, Vicent J L 2003 *Science* **302** 1188
[12] Togawa Y, Harada K, Kasai H, Matsuda T, Nori F, Maeda A, Tonomura A 2005 *Phys. Rev. Lett.* **95** 087002
[13] Cole D, Bending S J, Savel'ev S, Tamegai T and Nori F 2006 *Europhys. Lett.* **76** 1151
[14] Ooi S, Savel'ev S, Gaifullin M B, Mochiku T, Hirata K and Nori F 2007 *Phys. Rev. Lett.* **99** 207003
[15] Savel'ev S, Marchesoni F, Hänggi P, Nori F 2004 *Phys. Rev. E* **70** 066109
[16] Savel'ev S, Marchesoni F, Hänggi P and Nori F 2004 *Eur. Phys. J. B* **40** 403
[17] Savel'ev S, Marchesoni F, Hänggi P and Nori F 2004 *Europhys. Lett.* **67** 179
[18] Zhu B, Marchesoni F, Nori F 2004 *Phys. Rev. Lett.* **92** 180602
[19] Zhu B, Marchesoni F, Moschchalkov V V, Nori F 2003 *Phys. Rev. B* **68** 014514
[20] Zapata I, Bartussek R, Sols F and Hänggi P 1996 *Phys. Rev. Lett.* **77** 2292
[21] Weiss S, Koelle D, Müller J, Gross R and Barthel K 2000 *Europhys. Lett.* **51** 499
[22] Sterck A, Weiss S and Koelle D 2002 *Appl. Phys. A* **75** 253
[23] Berger J 2004 *Phys. Rev. B* **70** 024524
[24] Sterck A, Koelle D and Kleiner R 2009 *Phys. Rev. Lett.* **103** 047001
[25] Josephson B D 1962 *Phys. Lett.* **1** 251
[26] Zapata I and Sols F 1996 *Phys. Rev. B* **53** 6693
[27] Barone A and Paterno G 1982 *Physics and Applications of the Josephson Effect* (John Wiley & Sons, New York)
[28] Bezryadin A 2012 *Superconductivity in Nanowires: Fabrication and Quantum Transport* (Wiley-VCH, Weinheim).
[29] Jung P and Hänggi P 1990 *Phys. Rev. A* **41** 2977
[30] Jung P 1993 *Phys. Rep.* **234** 175
[31] Oster G and Wang H 2003 *M. Schliwa (ed.), Molecular Motors* (Viley-VCH, Weinheim)
[32] Jung P and Marchesoni F 2011 *Chaos* **21** 047516
[33] Wang H and Oster G 2002 *Europhys. Lett.* **57** 134
[34] Wang H 2009 *Appl. Math. Lett.* **22** 76
[35] Jung P, Kissner J G and Hänggi P 1996 *Phys. Rev. Lett.* **76** 3436
[36] Mateos J L 2000 *Phys. Rev. Lett.* **84** 258
[37] Platen E and Bruti-Liberati N 2010 *Numerical Solution of Stochastic Differential Equations with Jumps in Finance* (Springer)
[38] Januszewski M and Kostur M 2009 *Comp. Phys. Commun.* **181** 183
[39] Spiechowicz J, Kostur M and Machura Ł 2014 *arXiv*: **1409.4923**
[40] Kautz R L 1996 *Rep. Prog. Phys.* **59** 935
[41] Kostur M and Łuczka J 2001 *Phys. Rev. E* **63** 021101

Josephson phase diffusion in the superconducting quantum interference device ratchet

Jakub Spiechowicz[1] and Jerzy Łuczka[1,2,a)]
[1]*Institute of Physics, University of Silesia, 40-007 Katowice, Poland*
[2]*Silesian Center for Education and Interdisciplinary Research, University of Silesia, 41-500 Chorzów, Poland*

(Received 19 February 2015; accepted 4 May 2015; published online 18 May 2015)

We study diffusion of the Josephson phase in the asymmetric superconducting quantum interference device (SQUID) subjected to a time-periodic current and pierced by an external magnetic flux. We analyze a relation between phase diffusion and quality of transport characterized by the dc voltage across the SQUID and efficiency of the device. In doing so, we concentrate on the previously reported regime [J. Spiechowicz and J. Łuczka, New J. Phys. **17**, 023054 (2015)] for which efficiency of the SQUID attains a global maximum. For long times, the mean-square displacement of the phase is a linear function of time, meaning that diffusion is normal. Its coefficient is small indicating rather regular phase evolution. However, it can be magnified *several times* by tailoring experimentally accessible parameters like amplitudes of the ac current or external magnetic flux. Finally, we prove that in the deterministic limit this regime is essentially *non-chaotic* and possesses an unexpected simplicity of attractors. © *2015 AIP Publishing LLC*.
[http://dx.doi.org/10.1063/1.4921211]

A Superconducting quantum interference device (SQUID) is one of the most important elements of apparatuses of research laboratories worldwide. It exhibits a wide variety of phenomena and has been successfully used for testing the fundamentals of quantum mechanics, quantum information, and chaotic phenomena in classical physics. In the semiclassical regime, dynamics of the Josephson phase in the SQUID can be visualized as a Brownian particle moving in a periodic potential. This correspondence has allowed to study the transport properties of the SQUID by applying methods of Langevin equation. Earlier research in this field has been concentrated on the influence of thermal noise and external driving on current-voltage characteristics. The present paper studies diffusion of the Josephson phase. We consider a special type of the SQUID which operates as a Brownian ratchet. In particular, we analyze the phase diffusion in the regime for which the efficiency of the SQUID is globally maximal.

I. INTRODUCTION

The SQUIDs[1] are elements of ultrasensitive electric and magnetic measurement systems. They are also exploited in a number of commercial applications in industrial metrology, geophysical systems, and medicine as a noninvasive technique for investigating the human body.[2,3] In terms of the Stewart-McCumber model,[4,5] both the dynamics of the Josephson phase in the SQUID and the position of a Brownian particle can be described by similar Langevin equation.[6] Therefore, time evolution of the Josephson phase is analogous to a random motion of a Brownian particle in a spatially periodic potential. While prior studies have mostly been focused on the current-voltage characteristics, diffusion of the Josephson phase, i.e., its mean-square displacement, has not been intensively analyzed. There are only several papers closely or loosely related to this latter subject.[7–11]

In this work, we study diffusion of the Josephson phase in the asymmetric SQUID[12–18] which is composed of three capacitively and resistively shunted Josephson junctions. Two junctions are collocated in series in one half-piece of the ring and the third junction is disposed in the other half of the ring. The SQUID is driven by a time-periodic current and subjected to an external constant magnetic flux. Its dynamics is extremely rich and complex even in the deterministic case, involving harmonic, subharmonic, quasiperiodic, and chaotic trajectories. At non-zero temperature, thermal fluctuations lead to diffusive behaviour with random escape events among possibly coexisting attractors and with the system typically exploring its whole phase space. Due to a multi-dimensionality of the parameter space describing the model, it would be extremely difficult to perform a complete analysis of diffusion process of the Josephson phase in such a setup. Therefore, we consider it only in the previously reported regime[19] for which the Stokes efficiency of the SQUID attains its global maximum.

The paper is structured as follows. In Sec. II, we present a model of the asymmetric SQUID in terms of the Langevin equation for the Josephson phase. Next, we define several quantifiers characterizing the quality of transport process occurring in this setup. Among them are those that relate directly to an asymptotic long time stationary average voltage drop like its variance and the Stokes efficiency of the SQUID. However, we also study in this context those connected with the realization of stochastic motion of the Josephson phase like its mean squared displacement and a diffusion coefficient. We also combine these complementary quantities into the so called Péclet number. In Sec. IV, we

a)Electronic mail: jerzy.luczka@us.edu.pl

present results based on the comprehensive numerical simulation of the studied system in a regime for which the transport efficiency is globally maximal. In particular, we demonstrate a possibility of steering of diffusive behaviour of the phase by tuning the experimentally accessible parameters like the amplitude of ac current applied to the system or the external magnetic flux. It turns out that the diffusion coefficient can be significantly enhanced by small variation of these quantities. Moreover, we establish a clear relation between the directed transport, its efficiency, and the diffusive motion of the Josephson phase. It is very important that the regime of globally maximal transport quality measured by the Stokes efficiency is also effective in the sense that phase motion is ordered and regular. Finally, Sec. V provides summary and conclusions.

II. MODEL OF THE ASYMMETRIC SQUID

The asymmetric SQUID[12–18] is presented in Fig. 1. It is formed by a superconducting loop with two resistively and capacitively shunted Josephson junctions[20] in the left arm and only one in the right arm. The crosses denote the junctions and $\varphi_k \equiv \varphi_k(t)$ $(k = u, d, 1, 2)$ are the phase differences across them. Each junction is characterized by the capacitance C_k, resistance R_k, and critical Josephson current J_k, respectively. To reduce a number of parameters of the model, we consider only a special case when two junctions in the left arm are identical, i.e., $J_u = J_d \equiv J_1$, $R_u = R_d \equiv R_1/2$, and $C_u = C_d \equiv 2C_1$. In some regimes,[21] they can be considered as one for which the supercurrent-phase relation takes the form $J_1 \sin(\varphi_1/2)$, where $\varphi_1 = \varphi_u + \varphi_d$. Additionally, the SQUID is threaded by an external magnetic flux Φ_e. As a consequence, the effective potential experienced by the phase φ_1 forms a ratchet structure.[22] The device is driven by an external current $I = I(t)$ which is composed of the static dc current I_0 and the ac component of amplitude A and angular frequency Ω, namely,

$$I(t) = I_0 + A\cos(\Omega t). \tag{1}$$

The Langevin equation for the phase $\varphi \equiv \varphi_1$ is of the form[21]

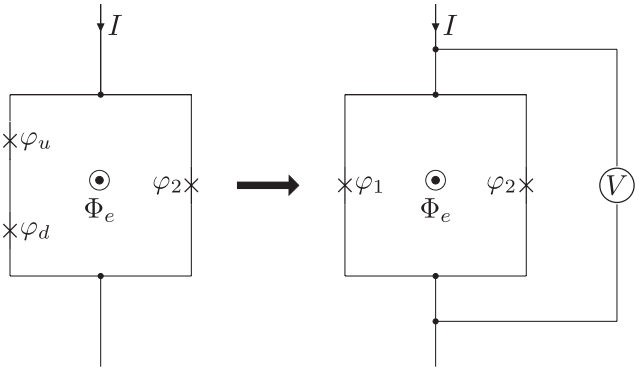

FIG. 1. Schematic asymmetric SQUID composed of three Josephson junctions and the equivalent circuit built from two junctions. The Josephson phase difference is $\varphi_1 = \varphi_u + \varphi_d$, the externally applied current is I, the external magnetic flux is Φ_e, and the instantaneous voltage across the SQUID is $V = V(t)$.

$$\frac{\hbar}{2e}C\ddot{\varphi} + \frac{\hbar}{2e}\frac{1}{R}\dot{\varphi} + J(\varphi) = I(t) + \sqrt{\frac{2k_BT}{R}}\xi(t), \tag{2}$$

where the effective supercurrent $J(\varphi)$ reads

$$J(\varphi) = J_1 \sin\left(\frac{\varphi}{2}\right) + J_2 \sin\left(\varphi + \tilde{\Phi}_e\right). \tag{3}$$

The parameters are $C = C_1 + C_2$, $R^{-1} = R_1^{-1} + R_2^{-1}$, k_B is the Boltzmann constant, T is temperature of the system, and $\tilde{\Phi}_e = 2\pi\Phi_e/\Phi_0$ is the dimensionless external magnetic flux. Thermal fluctuations are modelled by δ-correlated Gaussian white noise $\xi(t)$ of the statistics

$$\langle \xi(t) \rangle = 0, \quad \langle \xi(t)\xi(s) \rangle = \delta(t-s). \tag{4}$$

The average voltage across the device can be calculated from the relation

$$\langle V \rangle = (\hbar/2e)\langle \dot{\varphi}_1 \rangle = (\hbar/2e)\langle \dot{\varphi}_2 \rangle, \tag{5}$$

where the averaging is over the period $2\pi/\Omega$ of the ac current. This relation is also valid in the long time regime when additionally averaging is performed over initial conditions and all realizations of thermal noise.

It is useful to interpret Eq. (2) in the mechanical framework as a model of the inertial Brownian particle subjected to the conservative force $J(\varphi)$ and propelled by the time dependent driving $I(t)$. In this correspondence, the particle position x translates to the phase φ, its velocity $v = \dot{x}$ to the voltage V, the conservative force to the supercurrent $J(\varphi)$, the external force to the current $I(t)$, the mass m to the capacitance C, and the friction coefficient γ to the normal conductance $G = 1/R$.

In our recent paper,[21] we analyzed conditions that are necessary for generation and control of the voltage drop across the device. In particular, we focused on the direction and magnitude of transport as well as its dependence on the system parameters. We found the intriguing features of a negative absolute and differential conductance,[23–25] repeated voltage reversals,[26] and noise induced voltage reversals.[27] We showed how the direction of transport can be controlled by the applied magnetic field. Moreover, very recently[19] important aspects concerning the quality of transport occurring in this system have been addressed. We analyzed fluctuations of the voltage and energetics of the device.[28–32] It turned out that the power delivered by the external current depends not only on its amplitude and frequency but also on thermal noise and the external magnetic field.[33] We explored a set of the system parameters to reveal a regime where the voltage rectification efficiency is globally maximal. We detected the surprising feature of the thermal noise enhanced efficiency[34] and showed how the efficiency of the device can be tuned by adjusting the external magnetic flux. However, apart from these well investigated problems there are still some questions about the transport properties of the system which should be imposed and answered. One important example might be a diffusion process[7–11] of the Josephson phase. Therefore, in this paper we focus on the connection between the directed transport quantified by the averaged voltage $\langle V \rangle$,

its quality measured by the efficiency η of the device, and diffusion of the Josephson phase φ.

III. TRANSPORT QUANTIFIERS

It is convenient to convert Eq. (2) into its dimensionless form. There are several forms of such an equation depending on time scaling. Here, we follow Ref. 12 and define the new phase x and the dimensionless time $\hat{t}$ as

$$x = \frac{\varphi + \pi}{2}, \quad \hat{t} = \frac{t}{\tau_c}, \quad \tau_c = \frac{\hbar}{eRJ_1}. \tag{6}$$

In these new variables, Eq. (2) reads

$$\tilde{C}\ddot{x}(\hat{t}) + \dot{x}(\hat{t}) = -U'(x(\hat{t})) + F + a\cos(\omega\hat{t}) + \sqrt{2D}\,\hat{\xi}(\hat{t}), \tag{7}$$

where the dot and prime denotes a differentiation with respect to the dimensionless time $\hat{t}$ and the phase x, respectively. The dimensionless capacitance $\tilde{C}$ is the ratio between two characteristic time scales $\tilde{C} = \tau_r/\tau_c$, where the relaxation time is $\tau_r = RC$. Other re-scaled parameters are $F = I_0/J_1$, $a = A/J_1$, and $\omega = \Omega\tau_c$. The periodic potential $U(x)$ of period 2π takes the form[21]

$$U(x) = -\sin(x) - \frac{j}{2}\sin\left(2x + \tilde{\Phi}_e - \pi/2\right), \tag{8}$$

where $j = J_2/J_1$. This potential is symmetric if there exists x_0 such that $U(x_0 + x) = U(x_0 - x)$ for any x. If $j \neq 0$, it is generally asymmetric and is called a ratchet type, see Fig. 2. However, even for $j \neq 0$ there are certain values of the external flux $\tilde{\Phi}_e$ for which it is still symmetric. The rescaled zero-mean Gaussian white noise $\hat{\xi}(\hat{t})$ has the auto-correlation function $\langle\hat{\xi}(\hat{t})\hat{\xi}(\hat{s})\rangle = \delta(\hat{t} - \hat{s})$ and its intensity $D = ek_BT/\hbar J_1$ is the quotient of the thermal and the Josephson coupling energy. From now on, we will use only the dimensionless quantities and therefore we skip all hats appearing in (7).

There are several quantifiers characterizing transport properties of the system. The most important are the current-voltage curves in the asymptotic limit of long times when all effects due to initial conditions and transient processes have quiet down. They can be obtained from Eq. (5), the dimensionless form of which reads[35]

$$\langle v\rangle = \lim_{t\to\infty}\frac{\omega}{2\pi}\int_t^{t+2\pi/\omega}\mathbb{E}[\dot{x}(s)]\,ds, \tag{9}$$

where $\mathbb{E}[\dot{x}(s)]$ denotes averaging over initial conditions and all realizations of thermal noise. The stationary dimensional voltage is then given as

$$\langle V\rangle = RJ_1\langle v\rangle. \tag{10}$$

The long time average voltage $\langle v\rangle$ represents the basic transport measure. However, there are other transport quantifiers like the *voltage variance*

$$\sigma_v^2 = \langle v^2\rangle - \langle v\rangle^2, \tag{11}$$

which describes voltage fluctuations around its average value $\langle v\rangle$. The voltage drop $v(t)$ across the SQUID typically ranges within the interval of standard deviations

$$v(t) \in [\langle v\rangle - \sigma_v, \langle v\rangle + \sigma_v]. \tag{12}$$

It means that when $\sigma_v > |\langle v\rangle|$ the instantaneous voltage $v(t)$ may assume the opposite sign to the average voltage $\langle v\rangle$ and transport in not effective.

Next, we can introduce a measure for the efficiency of the SQUID in terms of the rectification of thermal fluctuations. It is defined as the ratio between the energetic output and the input power $\langle[F + A\cos(\omega t)]v(t)\rangle$. This quantity follows from an energy balance of the underlying Langevin equation (7) and corresponds to the well known *Stokes efficiency*[28,36,37]

$$\eta = \frac{\langle v\rangle^2}{\langle v\rangle^2 + \sigma_v^2 - D/\tilde{C}} = \frac{\langle v\rangle^2}{\langle v^2\rangle - D/\tilde{C}}. \tag{13}$$

One should note that this definition yields a non vanishing rectification efficiency even when there is no external static current, $F = 0$. Furthermore, it follows that this result is accordant with our intuition: a decrease of the voltage variance σ_v^2 leads to an increase of the rectification efficiency. Consequently, to optimize the effectiveness of the device one should seek for regimes that *maximize* the directed voltage and *minimize* its fluctuations.

The next quantifier characterizing transport is related to spread of trajectories of the stochastic phase $x(t)$. It is the mean square displacement[38] of the phase defined as

$$\langle\Delta x^2(t)\rangle = \langle[x(t) - \langle x(t)\rangle]^2\rangle = \langle x^2(t)\rangle - \langle x(t)\rangle^2.$$

One can expect that in the long time regime it grows according to a power law[38]

$$\langle\Delta x^2(t)\rangle_\xi \sim 2D_x t^\alpha, \tag{14}$$

where the constant prefactor D_x is sometimes called a diffusion coefficient and the exponent α characterizes a type of diffusion:[38–40] subdiffusion for $0 < \alpha < 1$, normal diffusion for $\alpha = 1$ and superdiffusion for $\alpha > 1$. Another special case

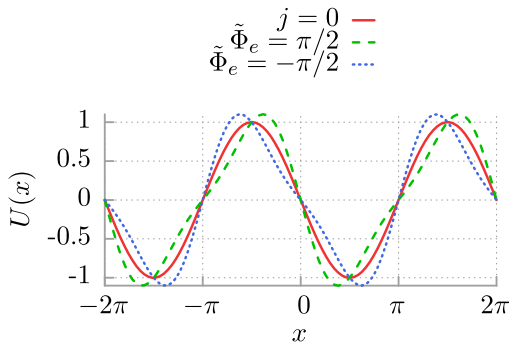

FIG. 2. The potential (8) for the symmetric case $j = 0$ (solid red line) in comparison with the ratchet potential for $j = 1/2$ and two values of the external magnetic flux $\tilde{\Phi}_e = \pi/2$ (dashed green line) and $\tilde{\Phi}_e = -\pi/2$ (dotted blue line).

is ballistic diffusion for $\alpha = 2$. When $\alpha = 1$, the diffusion coefficient can be determined as

$$D_x = \lim_{t\to\infty} D_x(t) = \lim_{t\to\infty} \frac{\langle \Delta x^2(t)\rangle}{2t}. \tag{15}$$

Otherwise the above definition is not constructive because such a quantity is either zero (subdiffusion) or diverges to infinity (superdiffusion). The diffusion coefficient measures the spreading of trajectories $x(t)$ around its mean value $\langle x(t)\rangle$, see Fig. 3. Intuitively, when it is small then the spread of trajectories is small and transport is more optimal.

Another way of introducing the diffusion coefficient is based on the generalized Green-Kubo response theory.[29,30,41] The asymptotic long time voltage autocorrelation function

$$C(t,\tau) = \langle \Delta v(t)\Delta v(t+\tau)\rangle, \quad \Delta v(t) = v(t) - \langle v(t)\rangle \tag{16}$$

can be obtained experimentally. Due to presence of the periodic driving of frequency ω this function is periodic with respect to the first argument[35]

$$C(t,\tau) = C(t+\mathsf{T},\tau), \tag{17}$$

where $\mathsf{T} = 2\pi/\omega$ is a rescaled period of the ac current. Therefore, we introduce the time average of the autocorrelation function $C(t,\tau)$, namely,

$$\mathcal{C}(\tau) = \frac{1}{\mathsf{T}}\int_0^{\mathsf{T}} dt\, C(t,\tau). \tag{18}$$

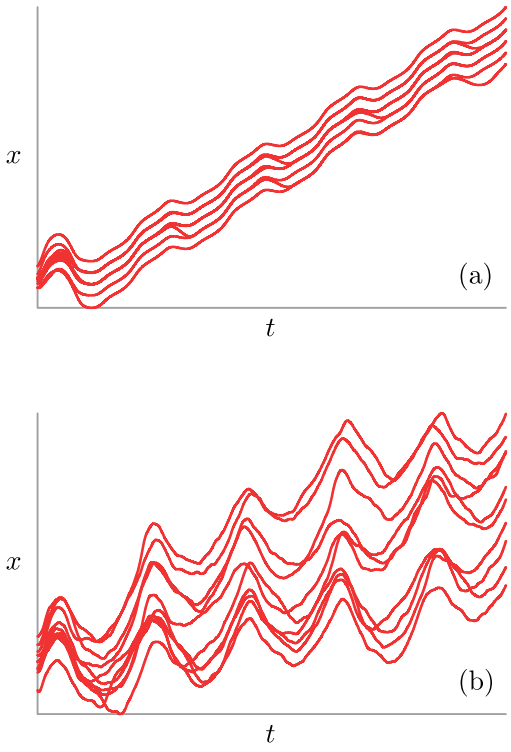

FIG. 3. Two sets of illustrative trajectories of the phase motion $x(t)$ across the asymmetric SQUID device. Parameters are $\tilde{C} = 0.496$, $a = 1.55$, $\omega = 0.406$, $\tilde{\Phi}_e = \pi/2$, $j = 0.5$. In (a) and (b), the thermal noise intensity is set to $D = 10^{-5}$ and $D = 0.1$, respectively. A distinct different diffusive behaviour is observed.

The diffusion process is characterized by the low frequency part of the power spectrum of the voltage fluctuations[38]

$$\chi(s) = \frac{1}{2}\int_{-\infty}^{+\infty} d\tau\, e^{is\tau}\mathcal{C}(\tau) \sim s^{1-\alpha}. \tag{19}$$

The diffusion coefficient is connected with the above equation via the relation[38]

$$D_x = \chi(0) = \frac{1}{2}\int_{-\infty}^{+\infty} d\tau\, \mathcal{C}(\tau). \tag{20}$$

Formulas (19) and (20) are particularly important from the experimental point of view as they allow for convenient measurement of both the nature of diffusion and if needed also its coefficient.

Finally, the ratio $D_x/2\pi$ can be considered as a velocity describing the normal phase diffusion over one period of the potential $U(x)$. Its relation to the average voltage $\langle v\rangle$ determines the dimensionless Péclet number defined as[29,30,32]

$$Pe = \frac{2\pi|\langle v\rangle|}{D_x}. \tag{21}$$

A large Péclet number indicates a motion of mainly regular nature. If it is small then random or chaotic influences dominate the dynamics.

IV. REGIME OF GLOBALLY MAXIMAL EFFICIENCY: NORMAL DIFFUSION

We have integrated the Langevin equation (7) by employing a weak version of the stochastic second order predictor corrector algorithm[42] with a time step typically set to about $10^{-3} \cdot 2\pi/\omega$. Since Eq. (7) is a second-order differential equation, we have to specify two initial conditions $x(0)$ and $\dot{x}(0)$. We have chosen phases $x(0)$ and dimensionless voltages $\dot{x}(0)$ equally distributed over interval $[0, 2\pi]$ and $[-2, 2]$, respectively. All quantities of interest were ensemble-averaged over 10^3–10^4 different trajectories which evolved over 10^3–10^4 periods of the external ac driving. Numerical calculations were done by use of a CUDA environment implemented on a modern desktop GPU. This scheme allowed for a speed-up of a factor of the order 10^3 times as compared to a common present-day CPU method.[43,44]

The system described by Eq. (7) has a 7-dimensional parameter space $\{\tilde{C}, a, \omega, F, j, \tilde{\Phi}_e, D\}$. Below, we study a nontrivial ratchet effect by putting the dc current $F = 0$. We have performed scans of the parameter space at a high resolution to determine the general behaviour of the system. The conditions that are necessary for the generation and control of the direction of transport in the SQUID have been extensively studied in these regimes in our previous work.[21] Moreover, very recently we also reported a regime for which the rectification efficiency η is globally maximal.[19] In this regime, the capacitance is $\tilde{C} \approx 0.496$, the amplitude of the ac current reads $a \approx 1.55$, and its is frequency $\omega \approx 0.406$. Let us now focus on the connection between the voltage drop $\langle v\rangle$, its

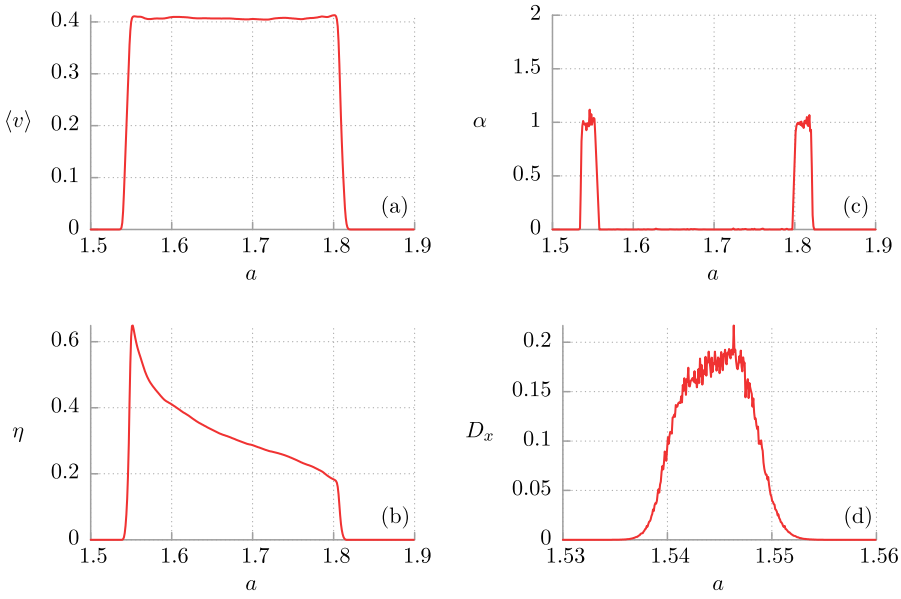

FIG. 4. Impact of the ac current amplitude a on transport characteristics. (a) The dc voltage drop $\langle v\rangle$ across the SQUID, (b) the Stokes efficiency η, (c) phenomenological power exponent α describing a type of phase diffusion, and (d) the diffusion coefficient D_x in the regime when $\alpha \approx 1$. Other parameters correspond to the regime for which the rectification efficiency η takes its globally maximal value, namely, $\tilde{C} = 0.496$, $a = 1.55$, $\omega = 0.406$, $D = 10^{-5}$, $\tilde{\Phi}_e = \pi/2$, $j = 0.5$, and $F = 0$.

rectification efficiency η, and the phase diffusion process across the SQUID in this prominent regime.

In Fig. 4, we present influence of the ac driving amplitude a on all characteristics describing quality of the transport process observed in the SQUID. In particular, panel (a) shows the dc voltage drop $\langle v\rangle$ across the device. There is a finite window of the parameter a for which the directed transport of about equal phase velocity $\langle v\rangle$ is observed. When a is smaller than $a \approx 1.53$ then the rocking mechanism is too weak to induce the non-negligible voltage drop. Similar situation can be discovered for the amplitudes greater than $a \approx 1.82$. These facts have their further consequences in the dependence of the Stokes efficiency η on the ac driving amplitude a. Since this quantity is proportional to $\langle v\rangle^2$ it vanishes when there is no directed transport, see panel (b) of the same figure. The most intriguing feature of this plot is emergence of the rapid maximum for $a \approx 1.55$. It is caused by the evident local minimum of the voltage fluctuations σ_v in the vicinity of this point. We refer the reader to Ref. 19 for a detailed study on this effect. Panel (c) depicts the phenomenological power exponent α characterizing the diffusion process as a function of the ac driving amplitude a. It was computed from the slopes of time evolution of the mean squared displacement $\langle \Delta x^2(t)\rangle$. Surprisingly, apart from two clearly visible intervals of the ac driving amplitude where $\alpha \approx 1$ there is no phase diffusion. Especially, it is noteworthy that a wide window of a can be observed where there is a finite dc voltage drop $\langle v\rangle \neq 0$ and simultaneously the power exponent vanishes $\alpha = 0$, yielding in a directed and non-diffusive transport across the device. In the neighbourhood of the maximal efficiency for $a \approx 1.55$, the exponent α is guaranteed to be unity. In consequence, the phase diffusion is normal, the diffusion coefficient D_x has well established physical interpretation and can be conveniently computed by use of the formula (15). Its variation is shown in Fig. 4(d). The most important finding is that transport in this regime is essentially stochastic. However, the diffusion coefficient is small $D_x \approx 0.05$. Moreover, it is seen that one can change the magnitude of D_x by adjusting the ac current amplitude a. In particular, a small change of a is accompanied by multiple increase of the diffusion coefficient D_x, thus leading to the phenomenon of diffusion enhancement.[45–47]

To gain insight into the nature of the phase diffusion process, we have computed the corresponding deterministic ($D = 0$) dc voltage bifurcation diagram. In Fig. 5, we show the asymptotic long time voltage $\langle v\rangle_{\mathsf{T}}$ averaged over the period $\mathsf{T} = 2\pi/\omega$ of the external ac driving for 1024 different initial conditions $x(0)$ and $\dot{x}(0)$ randomly sampled from the intervals $[0, 2\pi]$ and $[-2, 2]$, respectively. Therefore, all existing attractors are plotted at a given value of control parameter a. This figure reveals an unexpected simplicity of the phase space dynamics. The most important observation is that the system described by Eq. (7) is non-chaotic in the analyzed regime of the parameters. Moreover, there are regions for which only a single period one attractor exists, meaning that eventually all initial conditions evolve to it. Thus, each trajectory undergoes the same kind of motion resulting in the power exponent $\alpha = 0$ (cf. Fig. 4(c)). Moreover, there are also intervals where several attractors

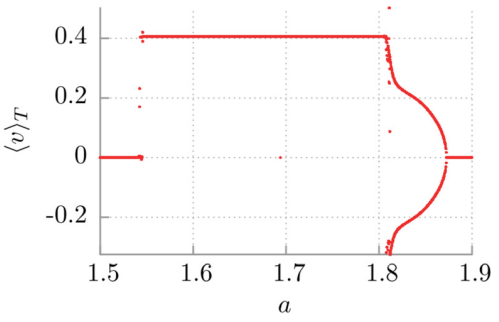

FIG. 5. The dc voltage bifurcation diagram in the deterministic limit $D = 0$ as a function of the ac driving amplitude a. The remaining parameters are given in Fig. 4.

coexist. This, in fact, is enough to observe the phenomenon of *deterministic diffusion*.[8–10,38] At sufficiently high temperature, the system will be typically ergodic with thermal fluctuations enabling stochastic escape events among coexisting deterministic separate attractors. In particular, transitions between neighbouring periodic solutions give rise to diffusive directed transport.

Let us now briefly discuss an influence of the external magnetic flux $\tilde{\Phi}_e$ on all previously introduced transport measures. From the symmetry considerations of Eq. (7), it follows that for an arbitrary integer number n, the transformation $\tilde{\Phi}_e \to 2\pi n - \tilde{\Phi}_e$ reverses the sign of the average voltage $\langle v \rangle \to -\langle v \rangle$. This fact can be directly observed in Fig. 6(a). There are two intervals where the average voltage drop assumes non-zero values which differ only with the direction of transport. Since the external magnetic flux alters the effective potential experienced by the phase x we conclude that in order to detect the average voltage one must tune it to a given rocking mechanism in the form of the ac driving of the amplitude a and the frequency ω. Similar to the previously discussed case, this fact is reflected in the dependence of the Stokes efficiency η on the external magnetic flux $\tilde{\Phi}_e$. A careful inspection of panel (b) reveals that one can tune the effectiveness of voltage rectification just by correct adjustment of the external magnetic flux. The next plot depicts impact of the external magnetic flux $\tilde{\Phi}_e$ on the exponent α. Regions where the transport is non-diffusive dominate this parameter space. It is associated with existence of a single period one attractor describing either the running or locked solution of (7) as it was in the previous case. Still, there are also intervals where the diffusive motion of the phase x can be observed with $\alpha \approx 1$. In particular, panel (d) presents the dependence of the diffusion coefficient D_x on the external magnetic flux $\tilde{\Phi}_e$ for such a scenario: One can conveniently manipulate the phase diffusion by change of the external magnetic flux. This way of control of the diffusion process is very convenient from the experimental point of view.

We now focus on the influence of inertia described by the capacitance $\tilde{C}$ of the SQUID on the phase diffusion, see Fig. 7. Panels (a) and (c) depict the average voltage drop $\langle v \rangle$ across the device and the Stokes efficiency η as a function of the capacitance $\tilde{C}$. They are non-monotonic functions similar in shape but without any immediately obvious relation to each other. However, the most important observation is that in the vicinity of a point corresponding to the maximum transport efficiency η also the voltage drop $\langle v \rangle$ is large. Notably, it lies closely to the border between overdamped $\tilde{C} \to 0$ and damped $\tilde{C} \approx 1$ regime. In panel (b), fluctuations of the phase velocity are depicted. One can notice an evident correlation, when velocity fluctuations are maximal, the efficiency is minimal. The next two panels present the diffusive behaviour as a function of the same parameter. In panel (d), one can see that the transport is essentially diffusive $\alpha \approx 1$ for entire interval of the inertial term variance. The last plot depicts the diffusion constant D_x versus the capacitance $\tilde{C}$ of the device. In the overdamped limit, the transport is rather regular as the diffusion coefficient is very small. On the contrary, an increase of inertia is accompanied by simultaneous grow of the phase diffusion with a sharp increase in the vicinity $\tilde{C} \approx 0.78$. One can observe that when the average voltage $\langle v \rangle$ and Stokes efficiency η are locally minimal and velocity fluctuations are maximal then the diffusion coefficient D_x takes its maximum. Consequently, the transport is highly irregular and not optimal. Therefore, we validate that quantities characterizing the phase diffusion in the device are somehow complementary to those usually used in order to describe the quality of transport. They give additional information which often corresponds well with the one measured by the voltage fluctuations (11) or the efficiency (13). It is intriguing to find a deeper reason of the sharp increase of D_x in the vicinity $\tilde{C} \approx 0.78$. In Fig. 8, we present the dc voltage bifurcation diagram in the deterministic limit $D = 0$ as a function of the capacitance $\tilde{C}$ of the SQUID. In the vicinity of $\tilde{C} \approx 0.78$, a cascade of bifurcations is observed and a transition to chaos takes place. Due to this fact, the phase

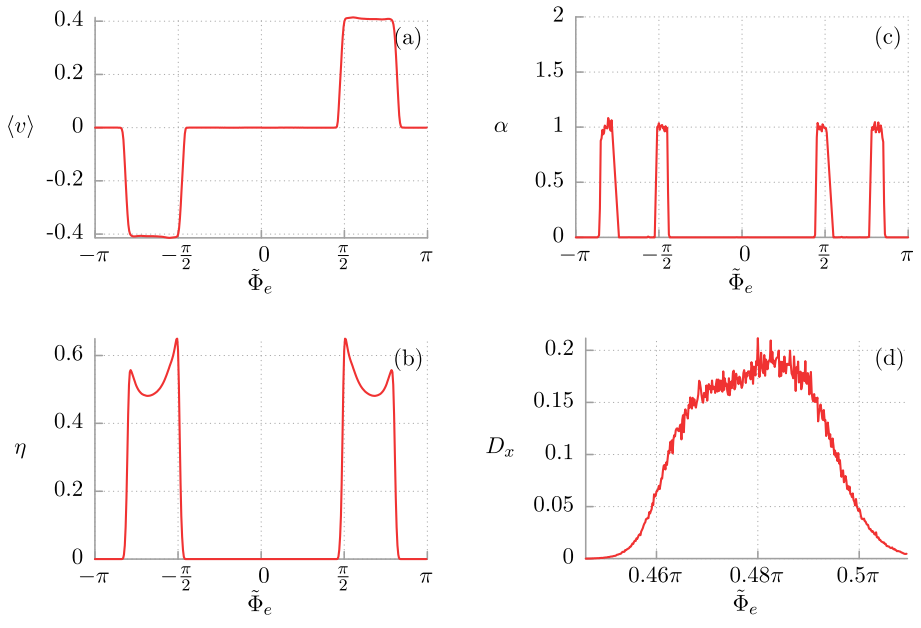

FIG. 6. Impact of variation of the external magnetic flux $\tilde{\Phi}_e$ on relevant characteristics in the form of: (a) the directed transport measured as the dc voltage drop $\langle v \rangle$ across the SQUID, (b) the Stokes efficiency η, (c) phenomenological power exponent α describing phase diffusion in this setup and finally (d) the normal diffusion coefficient D_x. Other parameters are the same as in Fig. 4.

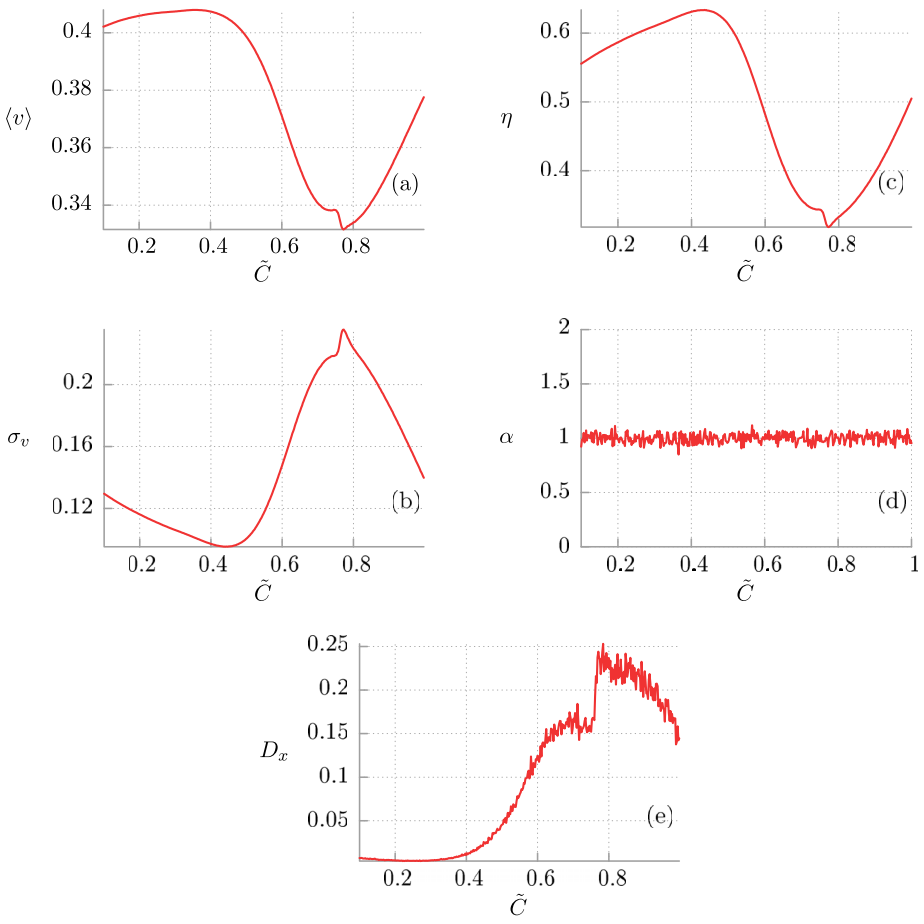

FIG. 7. Influence of variation of the capacitance $\tilde{C}$ on relevant characteristics in the form of: (a) the directed transport measured as the dc voltage drop $\langle v\rangle$ across the SQUID, (b) the voltage fluctuations σ_v, (c) the Stokes efficiency η, (d) phenomenological power exponent α describing phase diffusion in this setup, and finally (e) the normal diffusion coefficient D_x. Other parameters are the same as in Fig. 4.

diffusion can be observed even in the purely deterministic regime and the diffusion coefficient rapidly increases.

Finally, we examine the influence of thermal fluctuations on the phase diffusion process. The relevant panels comparing all discussed quantities are presented in Fig. 9. One can see that an increase of the thermal fluctuation intensity D leads to monotonic decrease of both the average voltage drop $\langle v\rangle$ across the SQUID and its voltage rectification efficiency η. Therefore, we conclude that it is a regime for which impact of thermal fluctuations is destructive. It is confirmed in the last two panels of this figure where the phase diffusion process is studied. Not unexpectedly, the system is diffusive for the entire range of thermal fluctuation intensity D. It is because thermal noise activates stochastic transitions between

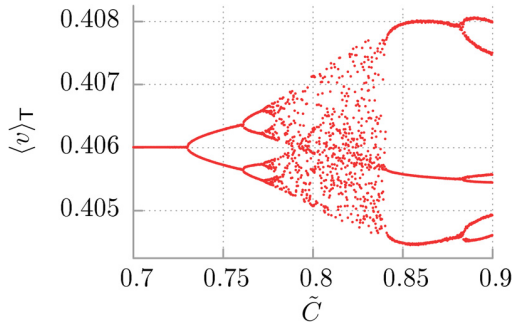

FIG. 8. The dc voltage bifurcation diagram in the deterministic limit $D=0$ as a function of the capacitance $\tilde{C}$ of the SQUID. The remaining parameters are given in Fig. 4.

coexisting deterministic disjoint attractors. Moreover, in the last panel we can see that when the temperature grows the transport becomes more and more diffusive as the diffusion coefficient D_x monotonically increases.

We collect part of our results by presenting the dependence of the dimensionless Péclet number on the SQUID capacitance $\tilde{C}$ and the thermal noise intensity D. The corresponding panels can be found in Fig. 10. In the first one, the reader can observe clear separation between the overdamped $\tilde{C}\to 0$ and underdamped $\tilde{C}\approx 1$ regimes. In the former case, the Péclet number is large indicating the transport of predominantly regular nature. Contrary, in the latter one it is small saying that the phase motion is chaotic or diffusive. Having in mind that this particular regime is essentially non-chaotic, we conclude that in region of a parameter space transport is diffusive. This fact supports our previous statement on that subject. Moreover, the most important remark is that the Péclet number corresponding to the point $\tilde{C}=0.496$ of globally maximal Stokes efficiency η is relatively large being evidence of the diffusive but still highly regular transport. In panel (b) of the same figure, we can observe a fast monotonic decay of the Péclet number with increasing temperature of the system. Therefore, in this regime thermal fluctuations have destructive impact on all transport quantifiers, starting from the average voltage $\langle v\rangle$, by the Stokes efficiency η of the SQUID, and finally up to irregularity of the phase motion reflected in the large diffusion coefficient D_x.

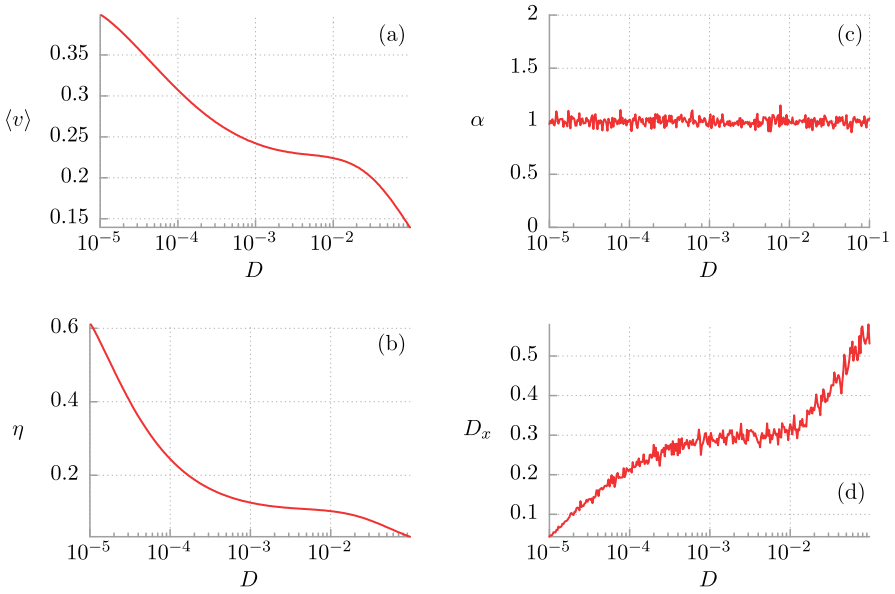

FIG. 9. (a) The directed transport measured as the dc voltage drop $\langle v \rangle$ across the SQUID, (b) the Stokes efficiency η, (c) phenomenological power exponent α describing phase diffusion in this setup, and finally (d) the normal diffusion coefficient D_x presented as a function of thermal noise intensity D. Other parameters are the same as in Fig. 4.

V. SUMMARY

We have studied diffusion process of the Josephson phase in the asymmetric SQUID system. Our analysis has been restricted to the regime of the maximal Stokes efficiency of the device and found normal diffusion with the exponent $\alpha \approx 1$. We have searched a neighbourhood of this point in the parameter space to check robustness of the observed behaviour in domains $\{a, \Phi_e, \tilde{C}, D\}$. When the amplitude a of ac current is changed two windows of normal diffusion are detected (Fig. 4(c)). In turn when the applied magnetic field is varied, four intervals of normal phase motion are observed (Fig. 6(c)). These areas are interrupted by windows where the exponent $\alpha = 0$ and there is no diffusion. The dependence on the capacitance $\tilde{C}$ and intensity D of thermal fluctuations is robust. The exponent $\alpha \approx 1$ for overdamped and damped case $\tilde{C} < 1$ (Fig. 7(d)) as well as for rescaled temperature D which can change several orders of magnitude (Fig. 8(c)).

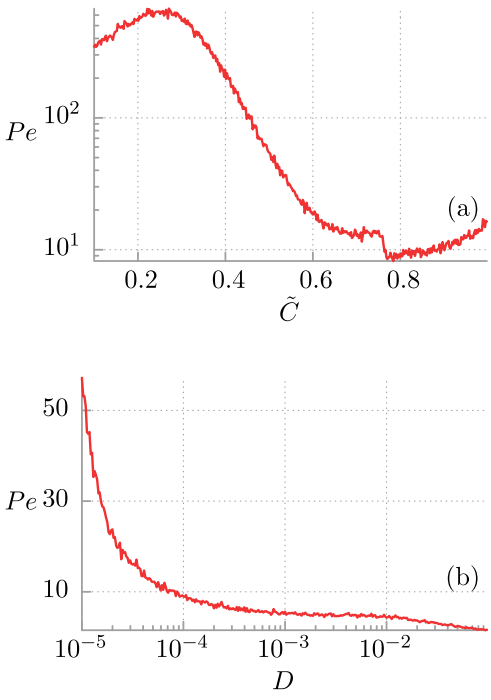

FIG. 10. The dimensionless Péclet number is presented as a function of the capacitance $\tilde{C}$ of the SQUID and the thermal noise intensity D in (a) and (b), respectively. Other parameters are listed in Fig. 4.

We have presented the possibility of convenient manipulation of the diffusion coefficient D_x by tuning the experimentally accessible parameters of the setup like the ac driving amplitude a or the external magnetic flux $\tilde{\Phi}_e$. Surprisingly, by doing it one can change its value several times. This lead us to the phenomenon of *diffusion enhancement*.

Last but not least, we have found that the regime of maximal Stokes efficiency is essentially *non-chaotic*. Regions where only a single period one attractor exists dominate the parameter space in the vicinity of this prominent area. Consequently, the phase motion is there non-diffusive. However, there are also intervals where due to the coexistence of several deterministic separate attractors the phase diffusion process can be observed. Then, sufficiently large thermal fluctuations enable stochastic transitions between them resulting in the diffusive directed transport. Overall, thermal noise has destructive impact on all presented quantities measuring the quality of transport in the system, starting from the average voltage $\langle v \rangle$ and ending on the diffusion coefficient D_x. It is remarkable that the non-diffusive or regular nature of the phase motion across the device is detected mainly in the overdamped regime $\tilde{C} \to 0$. Contrary, when the inertial term is increasing then the transport becomes more and more diffusive.

Finally, an interesting question concerns a possibility of observing the *anomalous phase diffusion*[38,39] in this setup. This question has been answered in the positive for the case of the extremely underdamped (Hamiltonian) symmetric SQUID device in the deterministic limit.[10] Our case is much more complicated, however, with the help of the computational power of modern GPU computers it should still be doable. This additional aspect is on our agenda for a potential future research.

The results described above may be helpful for further understanding of nontrivial response of nonlinear dynamics to external driving. They can readily be experimentally verified with an accessible setup consisting of three resistively and capacitively shunted Josephson junctions formed in an asymmetric SQUID device. Having in mind the mechanical interpretation of the studied model our research may also have potential applications for particle mixing, homogenization, selection, or separation tasks.[48]

ACKNOWLEDGMENTS

This work was supported in part by the MNiSW program "Diamond Grant" (J.S.) and NCN grant DEC-2013/09/B/ST3/01659 (J.Ł.).

[1]*The SQUID Handbook: Fundamentals and Technology of SQUIDs and SQUID Systems*, edited by J. Clarke and A. I. Braginski (Wiley-VCH, Weinheim, 2004), Vol. I; J. Clarke and A. I. Braginski, *The SQUID Handbook: Applications of SQUIDs and SQUID Systems* (Wiley-VCH, Weinheim, 2006), Vol. II.
[2]R. L. Fagaly, Rev. Sci. Instrum. **77**, 101101 (2006).
[3]M. Hämäläinen, R. Hari, R. J. Ilmoniemi, J. Knuutila, and O. V. Lounasmaa, Rev. Mod. Phys. **65**, 413 (1993).
[4]W. C. Stewart, Appl. Phys. Lett. **12**, 277 (1968).
[5]D. E. McCumber, J. Appl. Phys. **39**, 3113 (1968).
[6]R. L. Kautz, Rep. Prog. Phys. **59**, 935 (1996).
[7]H. Gang, A. Daffertshofer, and H. Haken, Phys. Rev. Lett. **76**, 4874 (1996).
[8]J. A. Blackburn and N. Gronbech-Jensen, Phys. Rev. E **53**, 3068 (1996).
[9]R. Harish, S. Rajasekar, and K. P. N. Murthy, Phys. Rev. E **65**, 046214 (2002).
[10]K. Tanimoto, K. Kato, and K. Nakamura, Phys. Rev. B **66**, 012507 (2002).
[11]W. Guo, L. C. Du, and D. C. Mei, J. Stat. Mech. **2014**, P04025.
[12]I. Zapata, R. Bartussek, F. Sols, and P. Hänggi, Phys. Rev. Lett. **77**, 2292 (1996).
[13]S. Weiss, D. Koelle, J. Müller, R. Gross, and K. Barthel, Europhys. Lett. **51**, 499 (2000).
[14]A. Sterck, S. Weiss, and D. Koelle, Appl. Phys. A **75**, 253 (2002).
[15]J. Berger, Phys. Rev. B **70**, 024524 (2004).
[16]A. Sterck, R. Kleiner, and D. Koelle, Phys. Rev. Lett. **95**, 177006 (2005).
[17]S. Savel'ev, A. L. Rakhmanov, and F. Nori, Phys. Rev. E **72**, 056136 (2005).
[18]A. Sterck, D. Koelle, and R. Kleiner, Phys. Rev. Lett. **103**, 047001 (2009).
[19]J. Spiechowicz and J. Łuczka, New. J. Phys. **17**, 023054 (2015).
[20]B. D. Josephson, Phys. Lett. **1**, 251 (1962).
[21]J. Spiechowicz, P. Hänggi, and J. Łuczka, Phys. Rev. B **90**, 054520 (2014).
[22]P. Hänggi and F. Marchesoni, Rev. Mod. Phys. **81**, 387 (2009).
[23]Ł. Machura, M. Kostur, P. Talkner, J. Łuczka, and P. Hänggi, Phys. Rev. Lett. **98**, 40601 (2007).
[24]D. Speer, R. Eichhorn, and P. Reimann, Europhys. Lett. **79**, 10005 (2007).
[25]M. Kostur, Ł. Machura, P. Talkner, P. Hänggi, and J. Łuczka, Phys. Rev. B **77**, 104509 (2008).
[26]M. Kostur and J. Łuczka, Phys. Rev. E **63**, 021101 (2001).
[27]J. Kula, T. Czernik, and J. Łuczka, Phys. Rev. Lett. **80**, 1377 (1998).
[28]Ł. Machura, M. Kostur, P. Talkner, J. Łuczka, F. Marchesoni, and P. Hänggi, Phys. Rev. E **70**, 061105 (2004).
[29]Ł. Machura, M. Kostur, F. Marchesoni, P. Talkner, P. Hänggi, and J. Łuczka, J. Phys.: Condens. Matter **17**, S3741 (2005).
[30]Ł. Machura, M. Kostur, F. Marchesoni, P. Talkner, P. Hänggi, and J. Łuczka, J. Phys.: Condens. Matter **18**, 4111 (2006).
[31]M. Kostur, Ł. Machura, P. Hänggi, J. Łuczka, and P. Talkner, Physica A **371**, 20 (2006).
[32]Ł. Machura, M. Kostur, P. Talkner, P. Hänggi, and J. Łuczka, Physica E **42**, 590 (2010).
[33]P. Jung and F. Marchesoni, Chaos **21**, 047516 (2011).
[34]J. Spiechowicz, P. Hänggi, and J. Łuczka, Phys. Rev. E **90**, 032104 (2014).
[35]P. Jung, Phys. Rep. **234**, 175 (1993).
[36]H. Wang and G. Oster, Europhys. Lett. **57**, 134 (2002).
[37]H. Wang, Appl. Math. Lett. **22**, 79 (2009).
[38]R. Klages, G. Radons, and I. M. Sokolov, *Anomalous Transport: Foundations and Applications* (Wiley-VCH, Weinheim, 2008).
[39]R. Metzler and J. Klafter, Phys. Rep. **339**, 1 (2000).
[40]J. P. Bouchaud, Phys. Rep. **195**, 127 (1990).
[41]R. Kubo, Rep. Prog. Phys. **29**, 255 (1966).
[42]E. Platen and N. Bruti-Liberati, *Numerical Solution of Stochastic Differential Equations with Jumps in Finance* (Springer, New York, 2010).
[43]M. Januszewski and M. Kostur, Comput. Phys. Commun. **181**, 183 (2010).
[44]J. Spiechowicz, M. Kostur, and Ł. Machura, Comput. Phys. Commun. **191**, 140 (2015).
[45]G. Constantini and F. Marchesoni, Europhys. Lett. **48**, 491 (1999).
[46]P. Reimann, C. Van den Broeck, H. Linke, P. Hänggi, J. M. Rubi, and A. Pérez-Madrid, Phys. Rev. Lett. **87**, 010602 (2001).
[47]P. Reimann, C. Van den Broeck, H. Linke, P. Hänggi, J. M. Rubi, and A. Pérez-Madrid, Phys. Rev. E **65**, 031104 (2002).
[48]T. M. Squires and S. R. Quake, Rev. Mod. Phys. **77**, 977 (2005).

Diffusion anomalies in ac-driven Brownian ratchets

Jakub Spiechowicz[1] and Jerzy Łuczka[1,2,*]
[1]*Institute of Physics, University of Silesia, 40-007 Katowice, Poland*
[2]*Silesian Center for Education and Interdisciplinary Research, University of Silesia, 41-500 Chorzów, Poland*
(Received 31 March 2015; published 4 June 2015)

We study diffusion in ratchet systems. As a particular experimental realization we consider an asymmetric SQUID subjected to an external ac current and a constant magnetic flux. We analyze mean-square displacement of the Josephson phase and find that within selected parameter regimes it evolves in three distinct stages: initially as superdiffusion, next as subdiffusion, and finally as normal diffusion in the asymptotic long-time limit. We show how crossover times that separates these stages can be *controlled by temperature and an external magnetic flux*. The first two stages can last many orders longer than characteristic time scales of the system, thus being comfortably detectable experimentally. The origin of abnormal behavior is noticeable related to the ratchet form of the potential revealing an *entirely new mechanism of emergence of anomalous diffusion*. Moreover, a normal diffusion coefficient exhibits nonmonotonic dependence on temperature leading to an intriguing phenomenon of *thermal noise suppressed diffusion*. The proposed setup for experimental verification of our findings provides a new and promising *testing ground* for investigating anomalies in diffusion phenomena.

DOI: 10.1103/PhysRevE.91.062104 PACS number(s): 05.40.Ca, 05.10.Gg, 05.60.−k

I. INTRODUCTION

The theory of Brownian motion has played a guiding role in the development of statistical physics. It provides a link between the microscopic dynamics and the observable macroscopic phenomena such as diffusion. The latter has been in the research spotlight already for over 100 years [1]. One century after pioneering Einstein's work it remains both a fundamental open issue and a continuous source of developments for many areas of science. Recent prominent examples include stochastic resonance [2], ratchet effects [3], enhancement of diffusion [4] or efficiency [5], to name but a few. Due to universal character of diffusion and its ubiquitous presence both in classical and quantum systems as well as in molecular biology it is still a subject of intensive studies. In recent years its anomalous character has been one of the main research topics in various fields [6–9]. In particular, diffusion of Brownian particles in deterministic periodic or random potentials, or a combination of both has been investigated [10–13]. Anomalous behavior may not survive until the asymptotic long-time regime; nonetheless, lately its transient nature has been predicted theoretically and observed experimentally [14–17]. In this work we study a model that belongs to an archetypal class of Brownian ratchets [3]. Despite its simplicity it is able to exhibit an extremely rich dynamics and variety of *anomalous transport* features, such as the absolute negative mobility in a linear response regime [18–20], the negative mobility in a nonlinear response regime, and the negative differential mobility [21]. However, here we focus on diffusion anomalies occurring in this system.

Our model consists of four relevant components and can be formulated in terms of (i) a classical inertial Brownian particle of mass M, (ii) moving in a deterministic ratchet potential $U(x) = U(x + L)$ of period L, (iii) driven by an unbiased time-periodic force $a\cos(\omega t)$ of amplitude a and angular frequency ω, and (iv) affected by thermal noise of temperature T. There are examples of experimentally accessible physical systems that can be described by this type of a model. An important representative that comes to mind is transport of ions through nanopores [22], cold atoms in optical lattices [23–25], type II superconducting devices based on motion of Abrikosov vortices [26,27], Josephson vortices [28–30], and a superconducting phase in weak links and SQUIDs [31–33], to give only a few. To maintain a close link with recent experimental research in this field and challenge experimentalists to put our theoretical predictions into a reality check, from now on we stick to a particular realization of a rocking ratchet mechanism, namely the asymmetric SQUID [34,35]. This Josephson-Brownian ratchet offers some advantages over other setups: (i) precise experimental control of applied driving forces here in the form of external currents, (ii) detection of directed motion manifested in a nonzero long-time dc voltage, (iii) access to studies over a wide frequency range of adiabatic and nonadiabatic external perturbations, and finally (iv) both underdamped and overdamped dynamics can be investigated by proper junction fabrication and variation of system parameters. We want to emphasize that our findings are *universal* in the sense that they apply to a broad selection of physical setups and could be observed in a variety of experimental realizations of a rocking ratchet mechanism. In this context, we recommend readers refer to Refs. [36,37], where normal and anomalous diffusion in ac-driven systems of cold atoms in dissipative optical lattices has been studied both experimentally and theoretically. Moreover, in Ref. [37], the survey of previous experiments on anomalous diffusion in such systems is presented.

Our work is organized as follows. In Sec. II we introduce the model and all quantities of interest. Section III contains a detailed description of our results, in particular control of anomalous diffusion by temperature and an external magnetic field as well as explanation of the mechanism that stands behind observed diffusion anomalies. In Sec. IV we discuss temperature dependence of the diffusion coefficient. Finally, Sec. V is devoted to summary and conclusions.

*jerzy.luczka@us.edu.pl

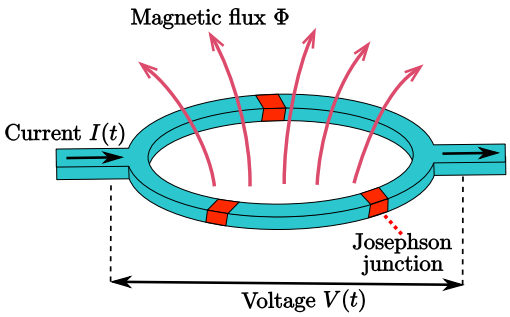

FIG. 1. (Color online) The asymmetric SQUID composed of three Josephson junctions and driven by the external current $I(t)$. The external constant magnetic flux is Φ and the instantaneous voltage across the SQUID is $V(t)$.

II. MODEL

As an exemplary real system we consider a SQUID presented in Fig. 1. It is a loop with three resistively and capacitively shunted Josephson junctions: two identical are placed in one arm, whereas the third is located in the other arm. Additionally, the SQUID is threaded by an external constant magnetic flux Φ and driven by a time-periodic current $I(t)$. There is a one-to-one correspondence between this setup and a classical Brownian particle. The particle position x translates to the phase $\varphi = \varphi_1 + \varphi_2$, where φ_1 and φ_2 are the Josephson phases of two junctions located in the same arm. The particle velocity $v = \dot{x}$ translates to the voltage $V \propto \dot{\varphi}$ across the SQUID, the external force to the current $I(t)$, the particle mass M to the capacitance $M \propto C$, and the friction coefficient γ to the normal conductance $\gamma \propto G = 1/R$. Here we present only the dimensionless form of the Langevin equation governing the phase dynamics. For details we refer the reader to our recent paper [35]. It reads

$$\tilde{C}\ddot{x}(t) + \dot{x}(t) = -U'[x(t)] + a\cos(\omega t) + \sqrt{2Q}\,\xi(t), \quad (1)$$

where the dot and prime denotes a differentiation with respect to the dimensionless time t and the rescaled phase $x = (\varphi + \pi)/2$, respectively. Other dimensionless quantities appearing in this formula are the capacitance $\tilde{C}$ of the device, the amplitude a, and the frequency ω of the external ac current $I(t)$. Johnson-Nyquist thermal noise is modeled by symmetric and unbiased δ-correlated Gaussian white noise $\xi(t)$ of average $\langle\xi(t)\rangle = 0$ and the correlation function $\langle\xi(t)\xi(s)\rangle = \delta(t-s)$. Its intensity $Q \propto k_B T$ is proportional to thermal energy, where T and k_B is the system temperature and the Boltzmann constant, respectively. The spatially periodic potential $U(x)$ of period 2π is in the following form [35]:

$$U(x) = -\sin(x) - \frac{j}{2}\sin(2x + \tilde{\Phi}_e - \pi/2). \quad (2)$$

The parameter $j = J_2/J_1$ is a ratio of critical currents of two junctions in opposite arms and $\tilde{\Phi}_e$ is the dimensionless external constant magnetic flux. If $j \neq 0$ the potential is generally asymmetric and its reflection symmetry is broken; see Fig. 2. However, even when $j \neq 0$ there are certain values of the external magnetic flux $\tilde{\Phi}_e$ for which it is still symmetric.

The most important quantity characterizing diffusion of the phase $x(t)$ is its mean-square displacement (MSD) $\langle\Delta x^2(t)\rangle$,

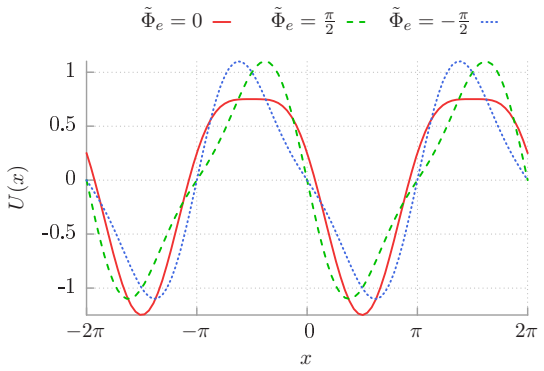

FIG. 2. (Color online) The potential Eq. (2) for $j = 1/2$ in the symmetric case $\tilde{\Phi}_e = 0$ (solid red line) in comparison with the ratchet potential for two values of the external magnetic flux $\tilde{\Phi}_e = \pi/2$ (dashed green line) and $\tilde{\Phi}_e = -\pi/2$ (dotted blue line).

defined as

$$\langle\Delta x^2(t)\rangle = \langle[x(t) - \langle x(t)\rangle]^2\rangle, \quad (3)$$

where $\langle\cdot\rangle$ indicates an average over initial conditions and thermal noise realizations. Although the dynamics may not be normal diffusion at all times, nonetheless a time-dependent diffusion coefficient $D(t)$ can be defined as

$$D(t) = \frac{\langle\Delta x^2(t)\rangle}{2t}. \quad (4)$$

Information on the diffusive process is also contained in the slope of the MSD, which can be obtained from the power-law fitting [38]:

$$\langle\Delta x^2(t)\rangle \sim t^{\alpha}. \quad (5)$$

The exponent α characterizes a type of diffusion. Normal diffusion is for $\alpha = 1$. There are two distinct regimes of *anomalous diffusion*: subdiffusion for $0 < \alpha < 1$ and superdiffusion for $\alpha > 1$. In the former case the MSD increases over time slower and in the latter case faster than the rate of normal diffusion. Another special case is ballistic diffusion when $\alpha = 2$. When the value of α is guaranteed to be unity, the time-independent diffusion coefficient D can be determined as

$$D = \lim_{t\to\infty} D(t). \quad (6)$$

Otherwise the above definition is not constructive because D is either zero (subdiffusion) or diverges to infinity (superdiffusion). In the case of SQUID, the phase diffusion can be investigated experimentally via measurement of the power spectrum of voltage fluctuations [38–40].

III. RESULTS

The Fokker-Planck equation corresponding to the Langevin Eq. (1) cannot be solved by use of any known analytical methods [41]. Moreover, even in the deterministic limit of vanishing thermal noise intensity $Q = 0$, this system exhibits very complex dynamics, including chaotic regimes [42,43]. Therefore, In order to investigate the diffusion process we have carried out comprehensive numerical simulations of the driven Langevin dynamics determined by Eq. (1). All numerical

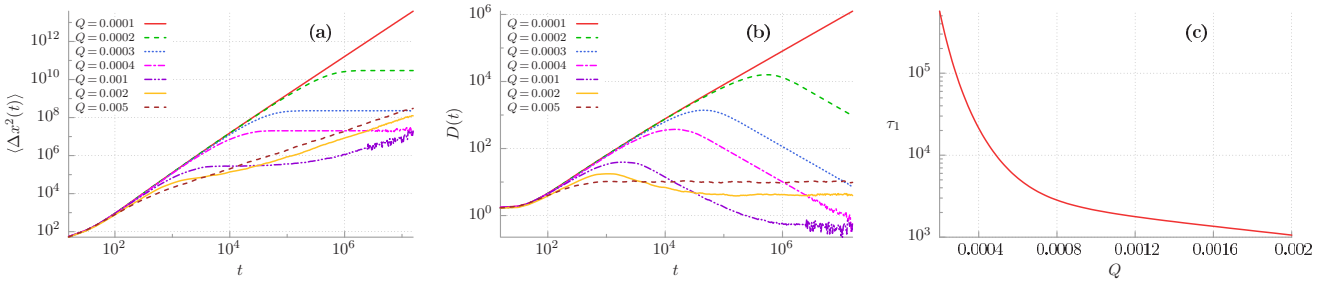

FIG. 3. (Color online) Impact of temperature $Q \propto T$ on the diffusion process. (a) The mean-square displacement $\langle \Delta x^2(t) \rangle$ of the Josephson phase. (b) The diffusion coefficient $D(t)$. (c) The crossover time τ_1 separating superdiffusion and subdiffusion stages. Parameters are $\tilde{C} = 6$, $a = 1.899$, $\omega = 0.403$, $\tilde{\Phi}_e = \pi/2$, and $j = 0.5$.

calculations were done by use of a CUDA environment implemented on a modern desktop GPU. This proceeding allowed for a speedup of a factor of the order of 10^3 as compared to a common present-day CPU method. For up-to-date review of this scheme we refer the reader to Ref. [44].

The system described by Eq. (1) has a six-dimensional parameter space $\{\tilde{C}, a, \omega, j, \tilde{\Phi}_e, Q\}$, which is too large to analyze numerically in a systematic fashion, even with the help of our innovative computational methods. We therefore have decided to focus our attention on the effect of temperature $Q \propto T$ and the impact of the external constant magnetic flux $\tilde{\Phi}_e$ in the remarkable regime of the thermal noise enhanced rectification efficiency of the SQUID studied in detail in Ref. [45]. Unless stated otherwise, this case corresponds to the following set of parameters $\{\tilde{C}, a, \omega, j, \tilde{\Phi}_e, Q\} = \{6, 1.899, 0.403, 0.5, \pi/2, 0.0004\}$.

A. Control of anomalous diffusion regimes by temperature

In Figs. 3(a) and 3(b) we show time evolution of the MSD $\langle \Delta x^2(t) \rangle$ and the diffusion coefficient $D(t)$, respectively, for selected values of the noise intensity $Q \propto T$. Especially in the latter the reader may easily distinguish between the type of diffusion: superdiffusion occurs in the interval where $D(t)$ increases, the case of decreasing $D(t)$ corresponds to subdiffusion, and for nonvarying $D(t)$ normal diffusion takes place. In the low-temperature limit the lifetime of superdiffusion is extremely long; see the case of $Q = 0.0001$ in Fig. 3(b). It might lead one incorrectly to conclude that this anomalous diffusion regime occurs in the stationary regime. This statement is true only in the deterministic case when formally $Q = 0$. However, in such a case the considered SQUID model is not correct. The deflection from the early superdiffusive behavior can expressively be noted as temperature increases. The evolution can be divided into three time domains: the early period of superdiffusion τ_1, the intermediate interval τ_2 where subdiffusion is developed, and the asymptotic long-time regime where normal diffusion occurs. The crossover times τ_1 and τ_2 separating these domains can be *controlled by temperature*. For example, when $Q = 0.0004$, $\tau_1 \approx 1.52 \times 10^4$, and $\tau_2 \approx 0.9985 \times 10^7$. If temperature is increased to $Q = 0.002$, the crossover times are reduced to $\tau_1 \approx 10^3$ and $\tau_2 \approx 0.99 \times 10^5$. In Fig. 3(c) of the same figure we present the dependence of the crossover time τ_1 separating super- and subdiffusion on temperature $Q \propto T$. It is remarkable that superdiffusion lifetime τ_1 changes nearly three orders of magnitude when the thermal noise intensity Q varies in the interval $(0.0002, 0.002)$. For higher temperatures the phase motion is initially superdiffusive and next normal diffusion takes place, as, e.g., in the case $Q = 0.005$ in Fig. 3(b).

B. Control of anomalous diffusion regimes by external magnetic field

From the experimental point of view it is more convenient to manipulate transport properties of the SQUID by the external magnetic flux $\tilde{\Phi}_e$. In Fig. 4, its impact on the diffusion process is illustrated. In some regimes, two crossover times τ_1 and τ_2 are identified and their magnitudes can be *changed by variation of the external magnetic flux* $\tilde{\Phi}_e$. For example, when $\tilde{\Phi}_e = 0.73\pi$, the superdiffusion lifetime is $\tau_1 \approx 1.56 \times 10^7$, while for $\tilde{\Phi}_e = 0.492\pi$ it is $\tau_1 \approx 1.8 \times 10^3$, i.e., four orders shorter.

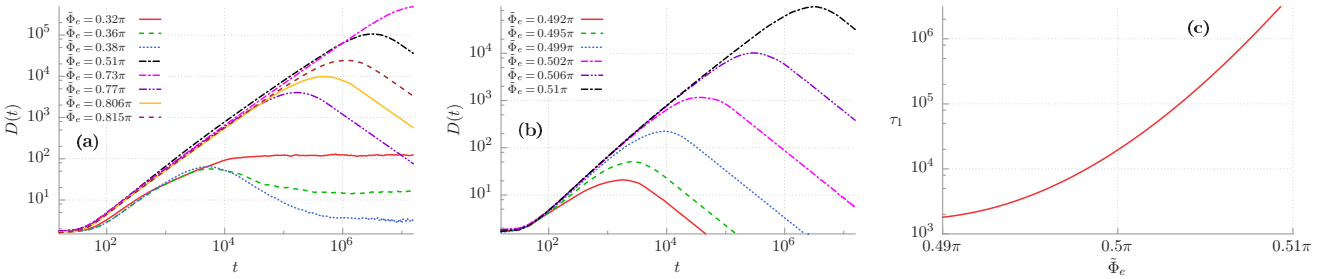

FIG. 4. (Color online) Control of diffusion by the external magnetic flux $\tilde{\Phi}_e$. (a) The diffusion coefficient $D(t)$ for selected values of the flux $\tilde{\Phi}_e$. (b) Sensitivity of the diffusion coefficient $D(t)$ in the vicinity of the magnetic flux $\tilde{\Phi}_e = \pi/2$. (c) The crossover time τ_1 as a function of $\tilde{\Phi}_e$ in the vicinity of $\tilde{\Phi}_e = \pi/2$. Note the colossal increase of order 10^3 in the crossover time τ_1 when the magnetic flux changes in the small interval $(0.49\pi, 0.51\pi)$. Other parameters are the same as described in the legend of Fig. 3 except $Q = 0.0004$.

However, in contrast to the case when temperature Q is varied the dependence of the crossover times τ_1 and τ_2 on $\tilde{\Phi}_e$ is nonmonotonic. It can be concluded from Fig. 4(a). Moreover, for some intervals of the magnetic flux these times are extremely sensitive to small changes of $\tilde{\Phi}_e$. This situation is exemplified in Figs. 4(b) and 4(c): small changes of order 10^{-2} in $\tilde{\Phi}_e$ are accompanied by the giant increase of order 10^3 in the crossover time τ_1. For our particular parameter regime the crossover time τ_2 is often so long that its numerical estimation may be controversial due to surely limited stability of the utilized algorithms leading to uncontrolled propagation of roundoff and truncation errors [44]. Therefore, we do not present its dependence on temperature or the external magnetic flux.

C. Comment on the power exponent

Let us now ask a complementary question, how the power exponent α defined by the relation Eq. (5) depends on temperature and the external magnetic flux. This exponent was fitted from time evolution of the MSD $\langle \Delta x^2(t) \rangle$ over $\approx 10^5$ dimensionless time units at a number of Q and $\tilde{\Phi}_e$ values. The results are presented in Fig. 5. Figure 5(a) depicts the dependence of α on temperature Q for two different potential profiles $U(x)$, namely *symmetric* ($\tilde{\Phi}_e = 0$) and *ratchet* ($\tilde{\Phi}_e = \pi/2$). In the low-temperature limit the crucial role of the potential asymmetry for the emergence of anomalous diffusion is observed. When potential is reflection symmetric, then $\alpha \approx 0$ and there is no diffusion at all. Contrary, for the ratchet case, $\alpha = 2$ and diffusion is ballistic, indicating the wavelike phase motion and revealing an *entirely new mechanism responsible for anomalous diffusion*. This one should be clearly distinguished from the well known one that appears in disordered systems [10–13]. The latter form of the potential manifests also in the fact that there is a finite window of temperature for which the motion is super and subdiffusive. One can alter the regime of diffusion in the SQUID by proper adjustment of thermal noise intensity Q. In the high-temperature limit, diffusion is normal regardless of the potential symmetry. This observation agrees with our naive intuition since then the impact of both the conservative $U'(x)$ and the time-dependent $a\cos(\omega t)$ forces is negligible in comparison to thermal noise. In Fig. 5(b) the same quantity is presented as a function of the external magnetic flux $\tilde{\Phi}_e$ for two selected temperatures Q. The unique feature is the ability to control the type of phase diffusion covering normal and anomalous regimes: from subdiffusion to superdiffusion and finally the ballistic motion just by experimentally doable variation of $\tilde{\Phi}_e$. Moreover, in agreement with our previous statement we note that the phase diffusion regime is very sensitive to changes of this parameter and observe the rapid variability of α in the vicinity of $\tilde{\Phi}_e = 0$ and $\tilde{\Phi}_e = \pi/2$.

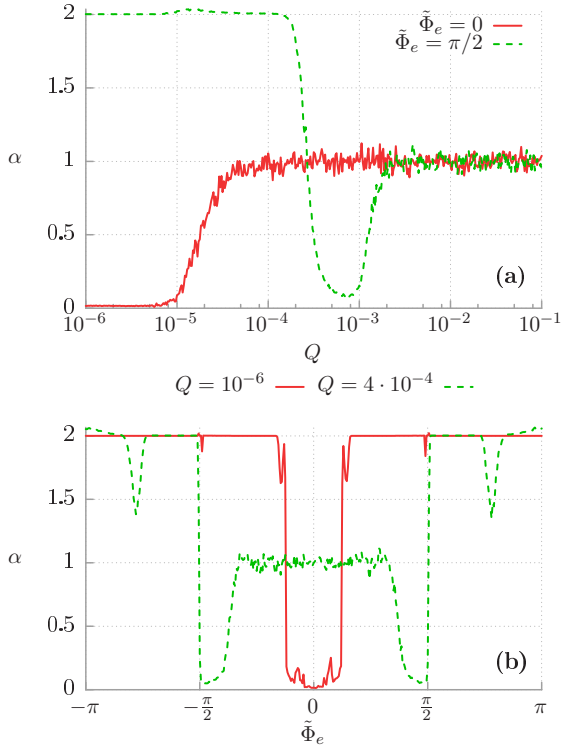

FIG. 5. (Color online) The power exponent α in dependence on temperature $Q \propto T$ and the external magnetic flux $\tilde{\Phi}_e$. Parameters are the same as described in the legend of Fig. 3.

D. Mechanism for transient anomalous diffusion

To gain insight into the origin of transient anomalous diffusion, let us consider the deterministic limit of vanishing thermal noise intensity $Q \to 0$ and study the structure of basins of attraction for the asymptotic long-time phase velocity $v = \dot{x}$ averaged over the period of the external ac driving, to be specific,

$$\langle v \rangle = \lim_{t\to\infty} \frac{\omega}{2\pi} \int_t^{t+2\pi/\omega} ds\, \dot{x}(s). \tag{7}$$

The result is shown in the upper panel of Fig. 6. There exist only three attractors: the running state with either positive or negative phase velocity $\langle v \rangle = \pm 0.4$ (marked by red and blue color, respectively) or the locked state $\langle v \rangle = 0$ when the phase motion is limited to a finite number of potential well (green color). The examples of corresponding trajectories are depicted in the bottom panel of the same figure together with the ensemble averaged temporal evolution of the phase across the device. This unexpected simplicity of attractors is crucial for the occurrence of the ballistic transport. In particular, qualitatively, due to the existence of two counterpropagating solutions with equal constant velocity $\langle v \rangle = 0.4$ the contribution of the average trajectory $\langle x(t) \rangle$ to the mean-square displacement $\langle \Delta x^2(t) \rangle$ is vanishingly small in comparison to its second moment $\langle x^2(t) \rangle$, see the bottom panel of Fig. 6. As a consequence the mean-square displacement is proportional to time in the second power $\langle \Delta x^2(t) \rangle \sim t^2$. The application of thermal noise generally smooths out the complex structure of boundaries demarcating the coexisting attractors. In a qualitative picture, if temperature starts to increase the phase is kicked out of its deterministic trajectory at random time and its mean value corresponds to the crossover time τ_1. When temperature grows τ_1 decreases what is exposed in Fig. 3. Moreover, stochastic escape events among attractors give rise to other forms of the anomalous diffusion [13].

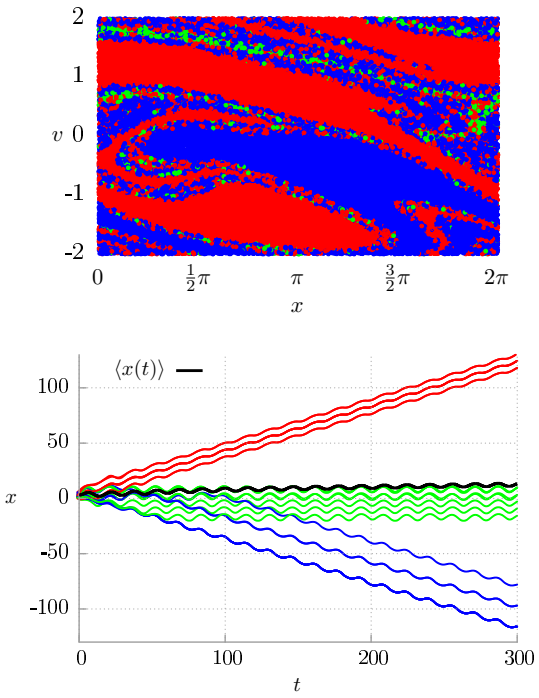

FIG. 6. (Color online) Basins of attraction for the asymptotic long-time phase velocity $\langle v\rangle$ averaged over the period of the external ac driving $a\cos\omega t$ are presented in the upper panel: $\langle v\rangle = 0.4$ (red), $\langle v\rangle = -0.4$ (blue) and locked states $\langle v\rangle = 0$ (green). The bottom one depicts a number of sample realizations of the phase motion together with its ensemble averaged trajectory. Parameters are the same as described in the legend of Fig. 3 except the thermal noise intensity, which is fixed to zero $Q = 0$.

IV. TEMPERATURE SUPPRESSED DIFFUSION

Last but not least, let us analyze the diffusion coefficient D in the normal diffusion regime. This scenario surely takes place in the limiting case of relatively high temperature $Q > 0.002$ since in such a case for times longer than $\approx 10^5$ the diffusion coefficient D does not change with time [see Figs. 3(b) and 5(a)]. Then it has a well-established physical interpretation and can be conveniently computed by use of Eq. (6). In Fig. 7 we present its dependence on temperature, $Q \propto T$. The striking feature is its nonlinear and nonmonotonic behavior. For low temperature, D initially increases as Q grows, passes through its local maximum, and next starts to decrease reaching its local minimum at some characteristic temperature Q_c. For temperatures higher than Q_c the diffusion coefficient is a monotonically increasing function of Q. This *temperature suppressed diffusion* phenomenon is in clear contrast with the Einstein relation $D \propto T$ as well as with the other known formulas as, e.g., for a Brownian particle moving in periodic potentials [46,47] and in tilted periodic potentials (under additional presence of an external constant force) [4,48].

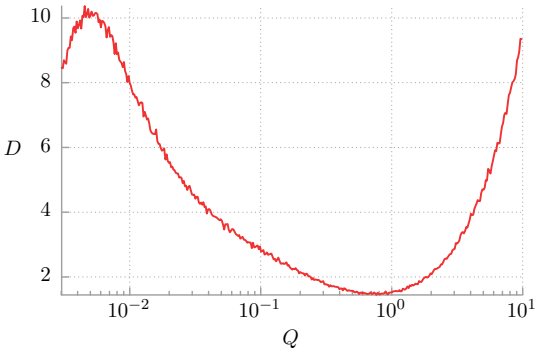

FIG. 7. (Color online) The diffusion coefficient D versus the thermal noise intensity Q in the high-temperature limit. Other parameters are the same as described in the legend of Fig. 3.

V. SUMMARY

In this work we have investigated diffusion processes in the archetypal model of an inertial Brownian ratchet. As a particular realization we picked the asymmetric SQUID device driven by the time-periodic current and pierced by the external constant magnetic flux. We have found selected parameter regimes for which the MSD of the Josephson phase evolves in three distinct stages: initially as superdiffusion, next as subdiffusion, and finally as normal diffusion in the asymptotic long-time limit. We have shown that crossover times separating these three stages can be controlled by temperature and the external magnetic flux. The latter parameter is especially useful for this purpose as these times are particularly sensitive to its changes. Despite the fact that these abnormal processes have only transient nature, they last many order longer than characteristic time scales of the system and thus they are comfortably detectable experimentally. Moreover, we have studied the origin of the discussed anomalous diffusion behavior and revealed the entirely new mechanism of its emergence, which is based on breaking of reflection symmetry of the potential. This effect is particularly evident for low-temperature regimes and should be clearly contrasted with the one that operates in disordered systems. In particular, in the deterministic limit of vanishing thermal noise the origin of the ballistic phase diffusion lies in the existence of two counterpropagating attractors. Finally, we have studied also the opposite limiting scenario of high thermal noise intensity and presented new manifest of the fascinating interplay between nonlinearity and thermal fluctuations, namely the phenomenon of noise-suppressed diffusion.

Our findings can be corroborated experimentally with a wealth of physical systems outlined in the introduction. One of the most promising setups for this purpose is the asymmetric SQUID device, which has already been constructed [32,33]. It is due to its good experimental control as well as easy detection of the discussed diffusion behavior in the power spectrum of the voltage fluctuations. Such an experiment will probably not be as spectacular as those based on the single particle tracking technique [49–51]; however, probably it will be much easier to perform and therefore we think that our work may suggest a completely new *testing ground* for investigating anomalies in diffusion phenomena.

ACKNOWLEDGMENT

This work was supported by the MNiSW program Diamond Grant (J.S.) and NCN Grant No. DEC-2013/09/B/ST3/01659 (J.L.)

[1] P. Hänggi and F. Marchesoni, Chaos **15**, 026101 (2005).
[2] L. Gammaitoni, P. Hänggi, P. Jung, and F. Marchesoni, Rev. Mod. Phys. **70**, 223 (1998).
[3] P. Hänggi and F. Marchesoni, Rev. Mod. Phys. **81**, 387 (2009).
[4] P. Reimann, C. Van den Broeck, H. Linke, P. Hänggi, J. M. Rubi, and A. Pérez-Madrid, Phys. Rev. Lett. **87**, 010602 (2001).
[5] J. Spiechowicz, P. Hänggi, and J. Łuczka, Phys. Rev. E **90**, 032104 (2014).
[6] R. Metzler and J. Klafter, Phys. Rep. **339**, 1 (2000).
[7] J. Klafter and I. M. Sokolov, Phys. World **18**, 29 (2005).
[8] R. Metzler, J. H. Jeon, A. Cherstvy, and E. Barkai, Phys. Chem. Chem. Phys. **16**, 24128 (2014).
[9] V. Zaburdaev, S. Denisov, and J. Klafter, arXiv:1410.5100.
[10] J. M. Sancho, A. M. Lacasta, K. Lindenberg, I. M. Sokolov, and A. H. Romero, Phys. Rev. Lett. **92**, 250601 (2004).
[11] M. Khoury, A. M. Lacasta, J. M. Sancho, and K. Lindenberg, Phys. Rev. Lett. **106**, 090602 (2011).
[12] M. S. Simon, J. M. Sancho, and K. Lindenberg, Phys. Rev. E **88**, 062105 (2013).
[13] M. S. Simon, J. M. Sancho, and K. Lindenberg, Eur. Phys. J. B **87**, 201 (2014).
[14] I. Bronstein, Y. Israel, E. Kepten, S. Mai, Y. Shav-Tal, E. Barkai, and Y. Garini, Phys. Rev. Lett. **103**, 018102 (2009).
[15] R. D. L. Hanes and S. U. Egelhaaf, J. Phys. Condens. Matter **24**, 464116 (2012).
[16] R. D. L. Hanes, C. Dalle-Ferrier, M. Schmiedeberg, M. C. Jenkins, and S. U. Egelhaaf, Soft Matter **8**, 2714 (2012).
[17] R. D. L. Hanes, M. Schmiedeberg, and S. U. Egelhaaf, Phys. Rev. E **88**, 062133 (2013).
[18] L. Machura, M. Kostur, P. Talkner, J. Łuczka, and P. Hänggi, Phys. Rev. Lett. **98**, 040601 (2007).
[19] D. Speer, R. Eichhorn, and P. Reimann, Europhys. Lett. **79**, 10005 (2007).
[20] J. Nagel, D. Speer, T. Gaber, A. Sterck, R. Eichhorn, P. Reimann, K. Ilin, M. Siegel, D. Koelle, and R. Kleiner, Phys. Rev. Lett. **100**, 217001 (2008).
[21] M. Kostur, Ł. Machura, P. Talkner, P. Hänggi, and J. Łuczka, Phys. Rev. B **77**, 104509 (2008).
[22] R. Karnik, C. Duan, K. Castelino, H. Dalguji, and A. Majumdar, Nano Lett. **7**, 547 (2007).
[23] R. Gommers, S. Bergamini, and F. Renzoni, Phys. Rev. Lett. **95**, 073003 (2005).
[24] A. V. Arzola, K. Volke-Sepúlveda, and J. L. Mateos, Phys. Rev. Lett. **106**, 168104 (2011).
[25] S. Denisov, S. Flach, and P. Hänggi, Phys. Rep. **538**, 77 (2014).
[26] C. S. Lee, B. Jankó, I. Derényi, and A. L. Barabási, Nature **400**, 337 (1999).
[27] J. E. Villegas, S. Savel'ev, F. Nori, E. M. Gonzalez, J. V. Anguita, R. Arcia, and J. L. Vincent, Science **302**, 1188 (2003).
[28] A. V. Ustinov, C. Coqui, A. Kemp, Y. Zolotaryuk, and M. Salerno, Phys. Rev. Lett. **93**, 087001 (2004).
[29] M. Beck, E. Goldobin, M. Neuhaus, M. Siegel, R. Kleiner, and D. Koelle, Phys. Rev. Lett. **95**, 090603 (2005).
[30] M. Knufinke, K. Ilin, M. Siegel, D. Koelle, R. Kleiner, and E. Goldobin, Phys. Rev. E **85**, 011122 (2012).
[31] S. Weiss, D. Koelle, J. Müller, R. Gross, and K. Barthel, Europhys. Lett. **51**, 499 (2000).
[32] A. Sterck, R. Kleiner, and D. Koelle, Phys. Rev. Lett. **95**, 177006 (2005).
[33] A. Sterck, D. Koelle, and R. Kleiner, Phys. Rev. Lett. **103**, 047001 (2009).
[34] I. Zapata, R. Bartussek, F. Sols, and P. Hänggi, Phys. Rev. Lett. **77**, 2292 (1996).
[35] J. Spiechowicz, P. Hänggi, and J. Łuczka, Phys. Rev. B **90**, 054520 (2014).
[36] A. Wickenbrock, P. C. Holz, N. A. Abdul Wahab, P. Phoonthong, D. Cubero, and F. Renzoni, Phys. Rev. Lett. **108**, 020603 (2012).
[37] E. Lutz and F. Renzoni, Nat. Phys. **9**, 615 (2013).
[38] R. Klages, G. Radons, and I. M. Sokolov, *Anomalous Transport: Foundations and Applications* (Wiley-VCH, Weinheim, 2008).
[39] T. Geisel, J. Nierwetberg, and A. Zacherl, Phys. Rev. Lett. **54**, 616 (1985).
[40] R. Ishizaki, S. Kuroki, H. Tominaga, N. Mori, and H. Mori, Prog. Theor. Phys. **109**, 169 (2003).
[41] P. Jung, Phys. Rep. **234**, 175 (1993).
[42] P. Jung, J. G. Kissner, and P. Hänggi, Phys. Rev. Lett. **76**, 3436 (1996).
[43] J. L. Mateos, Phys. Rev. Lett. **84**, 258 (2000).
[44] J. Spiechowicz, M. Kostur, and Ł. Machura, Comput. Phys. Commun. **191**, 140 (2015).
[45] J. Spiechowicz and J. Łuczka, New J. Phys. **17**, 023054 (2015).
[46] S. Lifson and J. L. Jackson, J. Chem. Phys. **36**, 2410 (1962).
[47] R. Festa and E. Galleani d'Agliano, Physica A **90**, 229 (1978).
[48] B. Lindner, M. Kostur, and L. Schimansky-Geier, Fluct. Noise Lett. **01**, R25 (2001).
[49] S. Burov, J. H. Jeon, R. Metzler, and E. Barkai, Phys. Chem. Chem. Phys. **13**, 1800 (2011).
[50] J. H. Jeon, V. Tejedor, S. Burov, E. Barkai, Ch. Selhuber-Unkel, K. Berg-Sorensen, L. Oddershede, and R. Metzler, Phys. Rev. Lett. **106**, 048103 (2011).
[51] E. Barkai, Y. Garini, and R. Metzler, Phys. Today **65**(8), 29 (2012).